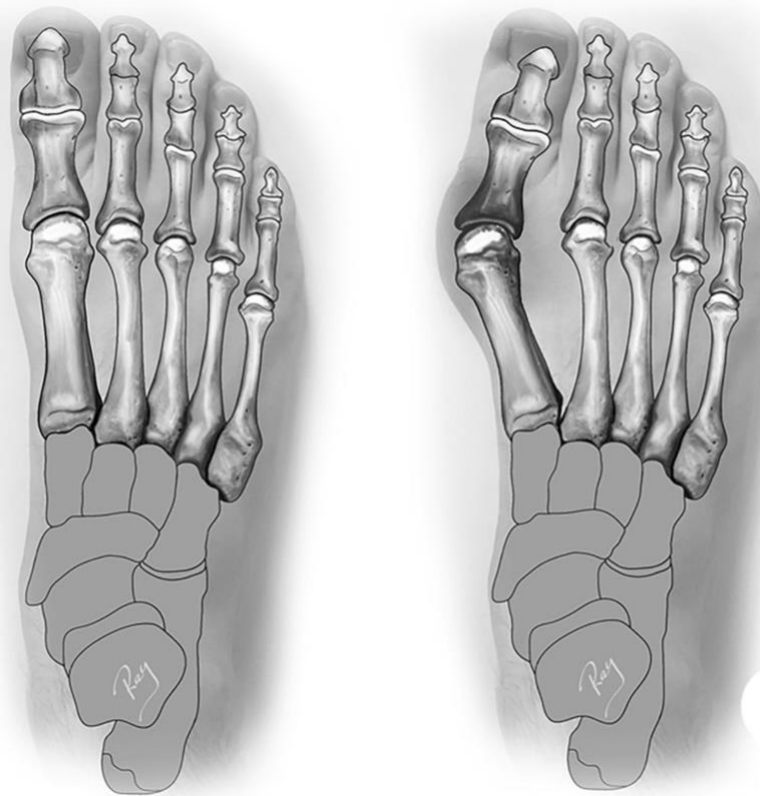


Towards the optimization of surgical hallux valgus corrections

S.M. Krakers



University of Twente
Orthopedisch Centrum Oost Nederland
Technical Medicine – Master Thesis
Sanne Krakkers

Towards the Optimization of Surgical
Hallux Valgus Corrections

September, 2023



**UNIVERSITY
OF TWENTE.**

Examination committee:

Chair

Medical supervisor

Technical supervisor

Process supervisor

Additional member

External member

prof.dr.ir. G.J.M. Tuijthof

dr. A. Peters

prof.dr.ir. G.J.M. Tuijthof

drs. A.G. Lovink

dr. J. Olde Heuvel

B. Wermelink MSc

Preface

Dear reader,

I have spent the last year of my Master Technical Medicine at Orthopedisch Centrum Oost Nederland (OCON) in Hengelo. I started here by doing a short internship in June 2022 which was a great experience. That is why I was thrilled to be able to complete my graduation internship at OCON. This master thesis titled “Towards the Optimization of Surgical Hallux Valgus Corrections” marks the end of my six years of being a student, and the start of my professional life.

I want to express my gratitude to everyone who supported me during my graduation internship. I want to thank my supervisors for their input, constructive feedback, and support during this period. I have learned a lot from each of you. I am also very grateful for the medical staff of the orthopedic department; with your help I have been able to develop myself clinically and I felt very welcome. In addition, thanks to the people of Team Research, you were always willing to help, and I also want to thank you for a very pleasant time. My thanks also go to the fellow students at OCON. Not only did they support me over the course of my graduation internship, but they also made my period at OCON very enjoyable. Finally, I want to express my gratitude to my family and friends for their unconditional support.

I enjoyed my year at OCON and learned to integrate the clinical and technical part of the Technical Medicine Master. I eagerly anticipate what the future holds.

Sanne Krakers
Hengelo, September 2023

Table of Contents

PREFACE	5
TABLE OF CONTENTS	7
CHAPTER 1: GENERAL INTRODUCTION	9
1.1 BACKGROUND.....	9
1.2 REFERENCES	14
CHAPTER 2: FLUOROSCOPY DURING SURGICAL HALLUX VALGUS CORRECTIONS	17
2.1 ABSTRACT	17
2.2 INTRODUCTION	18
2.3 METHODS	19
2.4 RESULTS	21
2.5 DISCUSSION.....	23
2.6 CONCLUSION	24
2.7 REFERENCES	26
CHAPTER 3: DEVELOPMENT OF A COORDINATE SYSTEM	29
3.1 ABSTRACT	29
3.2 INTRODUCTION	30
3.3 METHODS	30
3.4 RESULTS	36
3.5 DISCUSSION.....	37
3.6 CONCLUSION	38
3.7 REFERENCES	39
CHAPTER 4: CONCEPTS FOR THE 3D QUANTIFICATION OF HALLUX VALGUS	42
4.1 INTRODUCTION	42
4.2 AXIAL PLANE DEFORMITY.....	42
4.3 ROTATIONAL DEFORMITY	44
4.4 FUTURE DIRECTIONS.....	50
4.5 REFERENCES	52
CHAPTER 5: GENERAL DISCUSSION	55
5.1 GENERAL DISCUSSION.....	55
5.2 REFERENCES	58
APPENDIX A: PROTOCOL FOR THE USE OF PERIOPERATIVE FLUOROSCOPY DURING SURGICAL HALLUX VALGUS CORRECTIONS	61
APPENDIX B: DEFINITIONS OF TWO DIFFERENT COORDINATE SYSTEMS	64
APPENDIX C: CS1 AND CS2 OF THE THREE 3D FOOT MODELS WITHOUT A SPLINT	67



Chapter 1

General introduction

Chapter 1: General introduction

1.1 Background

Hallux valgus is the most common forefoot deformity. It is a multiplanar deformity defined by medial angulation and pronation of the first metatarsal and lateral deviation of the proximal phalanx at the first metatarsophalangeal (MTP) joint (Figure 1).¹⁻⁶ The prevalence of hallux valgus increases with age, affecting 23% of adults aged 18 to 65 years and more than 35% in people over 65 years old.^{1,3,7,8} The deformity is more prevalent in females (30%) than in males (13%). Hallux valgus deformity is commonly referred to as bunion. It is associated with increased levels of forefoot pain and can lead to foot malalignment, inability to wear appropriate footwear, loss of function and disability.^{4,7,9} The etiology of hallux valgus is multifactorial and can be divided into extrinsic and intrinsic factors.^{4,10} Extrinsic factors are inadequate footwear and overload, such as long walks and carrying excessive load.^{4,8,10} Intrinsic factors are genetics, ligamentous laxity, metatarsus primus varus, pes planus, functional hallux limitus, sexual dimorphism, age, metatarsal morphology, first-ray hypermobility, and a tight Achilles tendon.^{4,8,10}

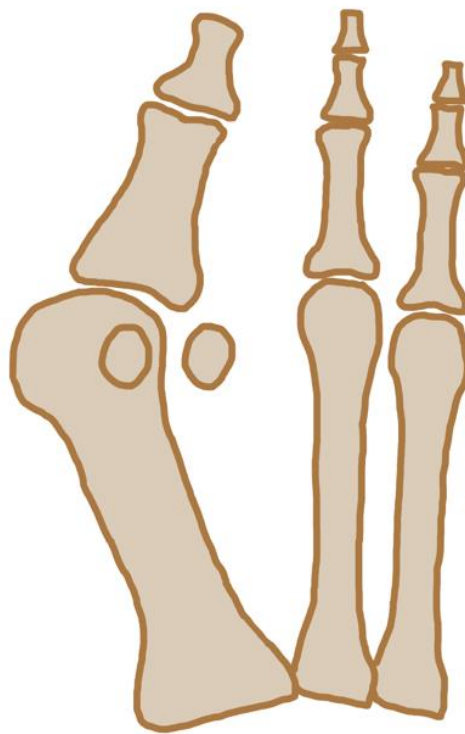


Figure 1. Illustration of the hallux valgus deformity in the anteroposterior view.

Although the pathophysiology of hallux valgus is complex, it is generally accepted that the formation of the deformity occurs in the following steps within years (Figure 2).^{5,10-12} 1) The medial capsule, medial metatarsal sesamoid ligament and medial collateral ligament fail, causing the first metatarsal to drift medially, slipping off the sesamoids. 2) The proximal phalanx moves laterally as it is attached to the sesamoids and the adductor hallucis tendon. 3) The medial sesamoid can erode the cartilage and crista on the plantar surface of the metatarsal head, allowing the metatarsal head to shift more medially. 4) The extensor and flexor hallucis longus tendons shifts laterally to the first MTP joint exaggerating the abduction force on the hallux. 5) As the metatarsal head drops off the sesamoid apparatus, it pronates because of the muscle forces acting across it. 6) Due to the plantar migration of the abductor hallucis tendon, it is unable to correct the hallux valgus deformity. Since the adductor hallucis tendon is laterally attached to the plantar surface, it tends to pull the proximal phalanx into pronation. 7) The pressure exerted by footwear on the prominent medial eminence causes the bursa overlying the medial eminence to thicken.

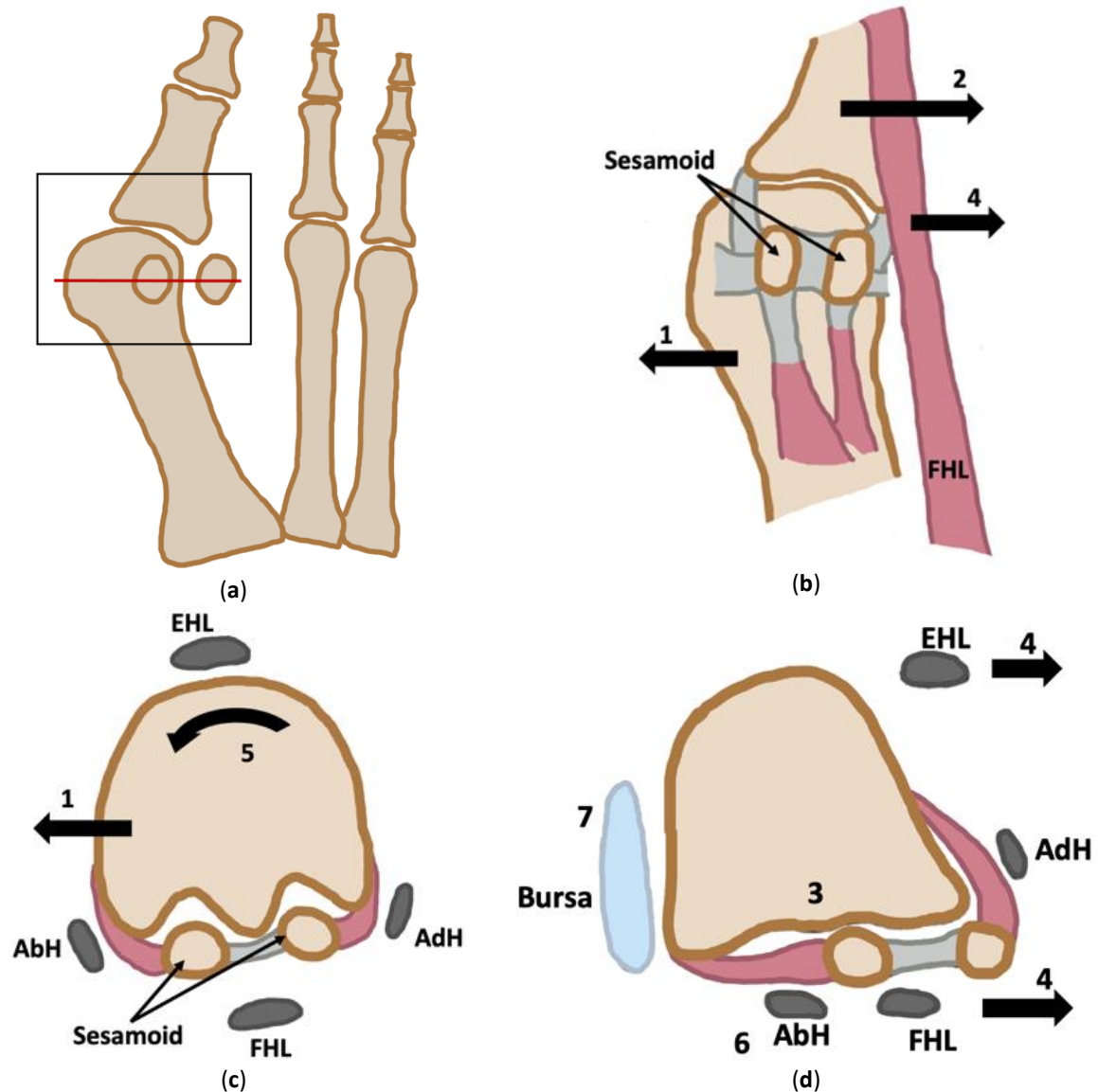


Figure 2. Pathophysiology of hallux valgus adapted from Perera et al.¹⁰ (a) Illustration of hallux valgus in the anteroposterior view. (b) Closer look at the black box in Figure 1a, showing the medial shift of the metatarsal head (1), with the lateral movement of the proximal phalanx (2). The flexor hallucis longus tendon (FHL) shifts laterally (4). (c) Cross-section at the red line in Figure 1a, showing the medial shift of the metatarsal head (1) and the pronation of the metatarsal head (5). (d) Cross-section at the red line in Figure 1a, showing the lateral shift of the abductor hallucis (AbH), adductor hallucis (AdH), flexor hallucis longus (FHL), and extensor hallucis longus (EHL) (4 and 6). Due to the pressure of the medial sesamoid on the crista, the cartilage is eroded, and the crista flattened (3). The bursa overlying the medial eminence thickens because of the pressure exerted by footwear on a prominent medial eminence (7).

Establishing the diagnosis of hallux valgus can typically be done through a physical exam and radiographic two-dimensional (2D) imaging.¹³ Radiographic imaging is performed for multiple purposes during diagnosis and treatment.^{4,5} For diagnosis and to assess the severity of the deformity, weight-bearing lateral and anteroposterior (AP) images of the foot are taken (Figure 3). The lateral images of the foot are used to evaluate the first metatarsal position (elevated or plantar-flexed) and dorsal exostosis/osteophytes.¹³ On the AP images of the foot, various radiographic angles allow assessment of the severity of the hallux valgus deformity.^{4,14} Of which, the Hallux Valgus Angle (HVA) and the Intermetatarsal Angle (IMA) are the most regularly utilized radiographic measurements (Figure 4).^{4,7} A HVA < 15° is considered normal, and angles > 15°, 20°, and 40° representing mild, moderate, and severe deformities.¹⁵ A IMA < 9° is considered normal, and angles > 9°, 11°, and 18° representing mild, moderate, and severe deformities.¹⁵ Based on the severity of the deformity, a treatment plan is made.¹³

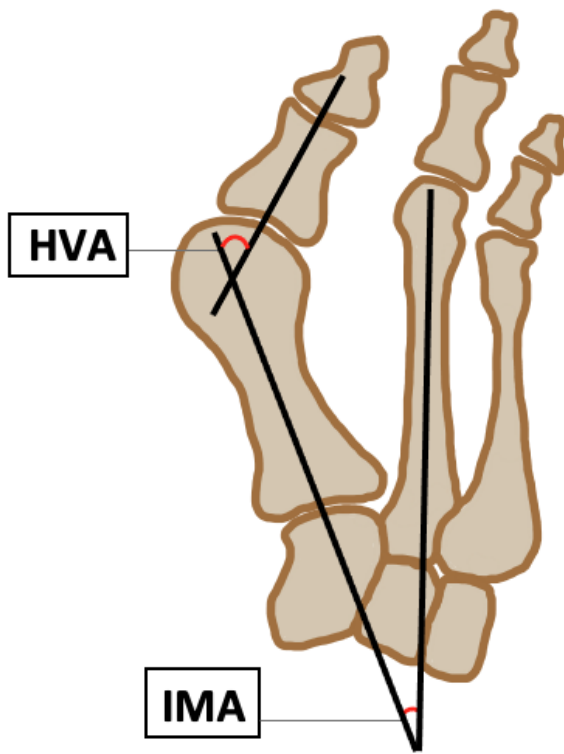


(a)



(b)

Figure 3. (a) Weight-bearing lateral radiographic image of the foot. (b) Weight-bearing anteroposterior radiographic image of the foot.



(a)



(b)

Figure 4. (a) The measured Hallux Valgus Angle (HVA) and Intermetatarsal Angle (IMA). (b) The measured HVA and IMA on anteroposterior radiographic images.

The goal of hallux valgus treatment is to relieve pain and improve function of the foot.⁷ Conservative treatment, including footwear modifications and insoles, should be started first.¹⁶⁻¹⁸ However, conservative management is not curative and is followed by surgery if pain persists.¹ There are more than 100 surgical procedures for the correction of hallux valgus, such as osteotomies, tarsal-metatarsal arthrodesis (Lapidus), and soft tissue procedures.^{7,19} A Chevron osteotomy, Scarf osteotomy, opening wedge osteotomy, and Akin proximal phalanx osteotomy are some of the numerous forms of osteotomies available (Figure 5). The severity of the deformity and the amount of correction needed determine the choice and level of osteotomy (proximal, midshaft, or distal).¹⁷ Proximal osteotomies (e.g. proximal Chevron and proximal wedge osteotomy) are used for more severe deformities with a high IMA ($\geq 14^\circ$).^{17,19-21} Midshaft osteotomies (e.g. Scarf osteotomy) are indicated for moderate to severe hallux valgus deformities.^{17,19} Distal osteotomies (e.g. distal Chevron osteotomy and Akin) are used for mild to moderate deformities.^{17,19,20} Tarsal-metatarsal arthrodesis (Lapidus procedure) is indicated for severe hallux valgus deformities, a hypermobile first ray, and a degenerative first tarsometatarsal.^{17,21}

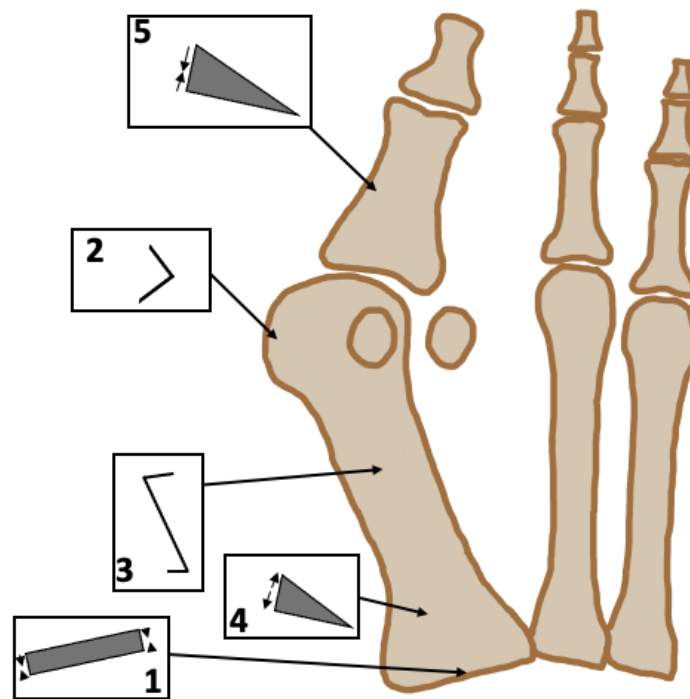


Figure 5. Locations of surgical procedures to treat hallux valgus. 1) Lapidus. 2) Chevron. 3) Scarf. 4) Opening wedge. 5) Akin.

Surgical hallux valgus correction is still somewhat tainted by higher than anticipated rates of suboptimal outcomes.²² As only two-thirds of patients report being completely satisfied with the surgical outcome. Next, the reported incidence of complications, such as the common postoperative complication of recurrent hallux valgus (postoperative HVA $\geq 20^\circ$ and IMA $\geq 12^\circ$), ranges from 10% to 55%.²³⁻²⁵ Most hallux valgus recurrences are caused by surgical factors such as inadequate procedure selection, technical issues including the fixation method, and the performance of the orthopedic surgeon.²⁴

Mini-C-arm fluoroscopy is frequently used perioperatively to assist the orthopedic surgeon in hardware placement and the assessment of the deformity correction to prevent technical issues and supports the performances of the orthopedic surgeon.^{4,7,26-28} During surgical hallux valgus corrections, the objective is to correct the HVA and IMA.²⁹ Correction of these angles decreases the chance of hallux valgus recurrence.³⁰ Since the orthopedic surgeon is perioperatively scrubbed and does not have time for an in-depth analysis of each perioperative image, the degree of correction is visually inspected, giving a visual estimation of the HVA and IMA (Figure 6). Based on this visual information, the correction may be surgically altered, and the perioperative fluoroscopy repeated to verify if the desired correction is achieved. This process requires repeatable and consistent perioperative images that correlate with the postoperative fluoroscopic images to visualize the achieved correction accurately. To achieve consistent perioperative fluoroscopic images, the rotational and linear movements of a mini-C-arm must be efficiently and properly positioned.²⁷ Obtaining fluoroscopic images in a standardized fashion is difficult to achieve during foot and ankle surgery.²⁶ Several factors make it difficult

to get certain views, for example the range of motion at the hip and knee, the weight of the leg, the drapes, and highly complex anatomy of the foot. Repeated image acquisition as the C-arm is positioned through trial-and-error, achieves accurate fluoroscopic images at the expense of time and radiation exposure to the patient and surgical staff.²⁷ To obtain repeatable and consistent perioperative images, reduce the radiation dose and save time, a structured protocol for the use of perioperative fluoroscopy is necessary. This may help to improve the outcomes of the surgical correction of hallux valgus.



Figure 6. Perioperative radiographic image of the foot during surgical hallux valgus corrections.

The surgical procedure is chosen based on the severity of the deformity and the amount of correction needed, which are assessed using 2D radiographs.¹⁷ Standard 2D radiographs use a 2D projection of a 3D structure as a simplified representation of anatomical information in one plane. Since the standard 2D radiographic images are not exactly orthogonal, multiplanar deformities like hallux valgus cannot be adequately analyzed on each anatomical plane separately, causing unintentional corrections in untargeted planes.³¹ As a result, 2D radiographs provide a limited amount of information to aid in the surgical procedure selection.³² Since one procedure does not correct all forms of hallux valgus deformities, adequate procedure selection is a critical issue. The large number of surgical procedures for the treatment of hallux valgus demonstrates how difficult it is to select the adequate surgical procedure and consequently achieve consistently satisfactory, long-term outcomes.^{23,33} Next, it would be beneficial to switch to the 3D analysis of hallux valgus to address the errors induced by 2D analysis. In comparison to conventional surgical procedure selection, a sufficient 3D analysis method could provide more information of the multiplanar nature of hallux valgus.³⁴ This might help to improve the adequate surgical procedure selection of hallux valgus corrections, and consequently achieve more consistently satisfactory, long-term outcomes.

This thesis aims to optimize surgical hallux valgus corrections by 1) obtaining repeatable and consistent perioperative images, and 2) transition the surgical procedure selection based upon a 3D analysis and planning approach. Therefore, a protocol for the use of perioperative fluoroscopy was developed and evaluated (Chapter 2). To enable the transition towards a 3D planning approach, a relevant global coordinate system in the foot was developed (Chapter 3). Concepts of the 3D quantification of hallux valgus for future 3D planning of surgical hallux valgus corrections were elaborated (Chapter 4).

1.2 References

- 1 Jia, J.; Li, J.; Qu, H.; Li, M.; Zhang, S.; Hao, J.; Gao, X.; Meng, X.; Sun, Y.; Hakonarson, H.; Zeng, X.; Xia, Q.; Li, J. New insights into hallux valgus by whole exome sequencing study. *Exp Biol Med (Maywood)*. 2021;246(14):1607-1616, doi:10.1177/15353702211008641.
- 2 Gawande, K.B.; Mungikar, S.; Hotwani, R.; Ingle, S.; Kulkarni, C.A. Prevalence of Hallux Valgus in Normal Individuals. *J. Med. Pharm. Allied Sci.* 2021;10(4):3138-3141, doi:10.22270/jmpas.V10I4.1263.
- 3 Nix, S.; Smith, M.; Vicenzino, B. Prevalence of hallux valgus in the general population: a systematic review and meta-analysis. *J Foot Ankle Res.* 2010;3:1-9, doi:10.1186/1757-1146-3-21.
- 4 Saad, A.; Lyengar, K.P.; Fitzpatrick, J.; Azopardi, C.; Panchal, H.; Botchu, R. The Linear Hallux Valgus Offset– A novel way to measure Hallux Valgus. *J Clin Orthop Trauma.* 2022;30, doi:10.1016/j.jcot.2022.101898.
- 5 Kakwani, M.; Kakwani, R. Current concepts review of hallux valgus. *J. Arthrosc. Jt. Surg.* 2021;8(3):222-230, doi:10.1016/j.jajs.2021.04.006.
- 6 Wagner, P.; Wagner, E. Role of Coronal Plane Malalignment in Hallux Valgus Correction. *Foot Ankle Clin.* 2019;25:69-77, doi:10.1016/j.fcl.2019.10.009.
- 7 Heineman, N.; Liu, G.; Pacicco, T.; Dessouky, R.; Wukich, D.K.; Chhabra, A. Clinical and imaging assessment and treatment of hallux valgus. *Acta Radiol.* 2019;61(1):56-66, doi:10.1177/0284185119847675.
- 8 Ferreyra, M.; Núñez-Samper, M.; Viladot, R.; Ruiz, J.; Isidro, A.; Ibañez, L. What do we know about hallux valgus pathogenesis? Review of the different theories. *J Foot Ankle* 2020;14(3):223-230, doi:10.30795/jfootankle.2020.v14.1202.
- 9 Nix, S.; Vicenzino, B.; Smith, M. Foot pain and functional limitation in healthy adults with hallux valgus: a cross-sectional study. *BMC Musculoskelet Disord.* 2012, doi:10.1186/1471-2474-13-197.
- 10 Perera, A.M.; Mason, L.; Stephens, M.M. The pathogenesis of hallux valgus. *J Bone Joint Surg Am.* 2011;93(17):1650-1661, doi:10.2106/JBJS.H.01630.
- 11 Stephens, M. Pathogenesis of hallux valgus. *Foot Ankle Surg.* 1994;1(1):7-10, doi:10.1016/S1268-7731(05)80050-5.
- 12 Menz, H.; Marshall, M.; Thomas, M.; Rathod-Mistry, T.; Peat, G.; Roddy, E. Incidence and Progression of Hallux Valgus: A Prospective Cohort Study. *Arthritis Care Res (Hoboken)*. 2021, doi:10.1002/acr.24754.
- 13 Kuhn, J.; Alvi, F. Hallux Valgus. StatPearls. Treasure Island (FL). Available online: <https://www.ncbi.nlm.nih.gov/books/NBK553092/> (accessed on 30 June 2023).
- 14 Steadman, J.; Barg, A.; Saltzman, L. First Metatarsal Rotation in Hallux Valgus Deformity. *Foot Ankle Int.* 2021;42(4), doi:10.1177/1071100721997149.
- 15 Piqué-Vidal, C.; Vila, J. A geometric analysis of hallux valgus: correlation with clinical assessment of severity. *J Foot Ankle Res.* 2009, doi:10.1186/1757-1146-2-15.
- 16 Tarantino, D.; Palermi, S.; Sirico, F.; Corrado, B. Hallux valgus deformity: Treatment options, post-operative management, and return to sport. *J. Hum. Sport Exerc.* 2021;16(4):1674-1687, doi:10.14198/jhse.2021.16.Proc4.14.
- 17 Lin, J.; Bustillo, J. Surgical treatment of hallux valgus: a review. *Curr. opin. orthop.* 2007;18(2):112-117, doi:10.1097/BCO.0b013e328082e2b6.
- 18 Wülker, N.; Mittag, F. The Treatment of Hallux Valgus. *Dtsch Arztebl Int.* 2012;109(49), doi:10.3238/arztebl.2012.0857.
- 19 Bertolo, F.; Pautasso, A.; Cuocolo, C.; Invernizzi, D.; Atzori, F. The Endolog technique for moderate to severe hallux valgus treatment: Clinical and radiographic analysis of 194 patients. *Foot Ankle Surg.* 2021;27(1):46-51, doi:10.1016/j.fas.2020.02.001
- 20 Wagner, E.; Ortiz, C. Osteotomy Considerations in Hallux Valgus Treatment Improving the Correction Power. *Foot Ankle Clin.* 2012;17(3):481-498, doi:10.1016/j.fcl.2012.06.007.
- 21 Smyth, N.; Aiyer, A. Introduction: Why Are There so Many Different Surgeries for Hallux Valgus? *Foot Ankle Clin.* 2018;23(2):171-182, doi:10.1016/j.fcl.2018.01.001.
- 22 Fleischer, A.; Yorath, M.; Joseph, R.; Baron, A.; Nordquist, T.; Moore, B.; Robinson, R.; Reilly, C. Impact of podiatry resident experience level in hallux valgus surgery on postoperative outcomes. *J Surg Res.* 2014;189(2):262-267, doi:10.1016/j.jss.2014.03.005.
- 23 Sawah, A.; Zemenova, S.; Haque, R.; Ridley, D.; Abboud, R.; Wang, W.; Harrold, F. Forecasting Posttreatment Outcome of Hallux Valgus Surgery Patients. *Foot Ankle int.* 2021;42(9):1144-1152, doi:10.1177/10711007211002498.

- 24 Trnka, H. Managing Complications of Foot and Ankle Surgery: Hallux Valgus. *Foot Ankle Clin.* 2022;27(2):271-285, doi:10.1016/j.fcl.2021.11.015.
- 25 Ezzatvar, Y.; López-Bueno, L.; Fuentes-Aparicio, L.; Dueñas, L. Prevalence and Predisposing Factors for Recurrence after Hallux Valgus Surgery: A Systematic Review and Meta-Analysis. *J Clin Med.* 2021;10(24), doi:10.3390/jcm10245753.
- 26 Elliot, R.; Saxby, T.; Whitehouse, S. Intraoperative imaging in hallux valgus surgery. *Foot Ankle Surg.* 2012;18(1):19-21, doi:10.1016/j.fas.2011.01.006.
- 27 De Silva, T.; Punnoose, J.; Uneri, A.; Mahesh, M.; Goerres, J.; Jacobsen, M.; Ketcha, M.; Manbachi, A.; Vogt, S.; Kleinszig, G.; Khanna, A.; Wolinsky, J.; Siwerdsen, J.; Osgood, G. Virtual fluoroscopy for intraoperative C-arm positioning and radiation dose reduction. *J Med Imaging (Bellingham).* 2018;5(1), doi:10.1117/1.JMI.5.1.015005.
- 28 Guyonnet, G.; Mulliez, A.; Fessy, M.; Besse, J. Prospective analysis of intraoperative radiation dose in foot and ankle surgery using mini-C-arm fluoroscopy. Continuous series of 1064 procedures. *Orthop Traumatol Surg Res.* 2021;107(6), doi:10.1016/j.otsr.2021.102994.
- 29 Price, A.; Hughes, T.; Kurnik, C.; Kurnik, C.; Gavin, K.; Miller, R. Comparison of Intraoperative Fluoroscopy to Postoperative Weight-Bearing Radiographs Obtained 4 to 6 Weeks After Bunion Repair With A Chevron Osteotomy. *J. Orthop. Res.* 2019;8.
- 30 Pentikainen, I.; Ojala, R.; Ohtonen, P.; Piippo, J.; Leppilahti, J. Preoperative radiological factors correlated to long-term recurrence of hallux valgus following distal chevron osteotomy. *Foot Ankle Int.* 2014;35(12):1262-1267, doi:10.1177/1071100714548703.
- 31 Schweizer, A.; Fürnstahl, P.; Harders, M.; Székely, G.; Nagy, L. Complex Radius Shaft Malunion: Osteotomy with Computer-Assisted Planning. *Hand (N Y).* 2010;5(2):171-178, doi:10.1007/s11552-009-9233-4.
- 32 Welck, M.J.; Al-Khudairi, N. Imaging of Hallux Valgus How to Approach the Deformity. *Foot Ankle Clin.* 2018;23:183-192, doi:10.1016/j.fcl.2018.01.002.
- 33 Surgeons, Foot and Ankle Working Committee; Chinese Association of Orthopaedic Surgeons Orthopaedic Branch; Chinese Association of Orthopaedic. Consensus on Surgical Management of Hallux Valgus from China. *Orthop Surg.* 2015;7(4):291-296, doi:10.1111/os.12207.
- 34 Ozturk, A.M.; Suer, O.; Coban, I.; Ozer, M.A.; Govsa, F. Three-Dimensional Printed Anatomical Models Help in Correcting Foot Alignment in Hallux Valgus Deformities. *Indian J Orthop.* 2020;54:199-209, doi:10.1007/s43465-020-00110-w.

Chapter 2

Fluoroscopy during surgical hallux valgus corrections

Developing a protocol for the use of perioperative fluoroscopy during surgical hallux valgus corrections: a pilot study

Sanne Krakers^{1,2}, Anil Peters², Judith olde Heuvel² and Gabriëlle Tuijthof³

¹Technical Medicine, University of Twente, Enschede, The Netherlands

²Department of Orthopedics, Orthopedisch Centrum Oost Nederland (OCON), Hengelo, The Netherlands

³Department of Biomechanical Engineering, University of Twente, Enschede, The Netherlands

2.1 Abstract

Purpose The hallux valgus deformity is one of the most challenging foot and ankle deformities to correct. During surgical hallux valgus corrections, the objective is to correct the Hallux Valgus Angle (HVA) and Intermetatarsal Angle (IMA) to decrease the chance of hallux valgus recurrence. The orthopedic surgeon can accurately assess the deformity correction by using consistent anteroposterior (AP) imaging at various stages of care. The degree of correction is visually inspected on perioperative fluoroscopic images, giving a visual estimation of the HVA and IMA. This process requires repeatable and consistent perioperative images that correlate with the postoperative fluoroscopic images to visualize the achieved correction accurately. This study developed a protocol and tested its feasibility in a pilot study for the use of perioperative fluoroscopy during surgical hallux valgus corrections to obtain perioperative images that correlate with the postoperative images and fits into the workflow.

Methods An observational study yielded insights on the correlation of the peri- and postoperative fluoroscopic images without the use of a protocol, by using HVA and IMA measurements of twelve patients who underwent a Chevron osteotomy. The mean measured HVA and IMA of the technical physician were compared and paired t-testing was used to assess whether there was a significant difference between the peri- and postoperative fluoroscopic images. An orthopedic foot and ankle surgeon also measured the HVA and IMA to assess the repeatability of the peri- and postoperative fluoroscopic measurements by computing the Intraclass Correlation Coefficients (ICCs) both intra- and inter-observer. Physician-centered experiences with the use of perioperative fluoroscopy were explored through a questionnaire and focus group or interview to reveal the requirements of the protocol. A pilot study was conducted to verify how the developed protocol meets the requirements of safety, efficiency, and effectiveness. The total dose area product (DAP) and time per image acquisition were compared during three surgical hallux valgus corrections without protocol versus three with protocol. The HVA and IMA were measured on both the peri- and postoperative images by a technical physician, and a small consensus meeting was held to test the opinion on the use of the protocol.

Results Results show that the mean peri- ($11.5^\circ \pm 5.9^\circ$) and postoperative ($11.4^\circ \pm 4.5^\circ$) measured HVA were not significantly different ($p = 0.946$). However, a statistically significant increase is measured between the mean postoperative ($6.9^\circ \pm 1.9^\circ$) IMA compared with the perioperative ($5.0^\circ \pm 1.8^\circ$) IMA ($p = 0.008$). The inter- and intraobserver repeatability of the peri- and postoperative fluoroscopic measurements ranged from 0.617 to 0.893 and from 0.778 to 0.960. Based on the information collected from the observational study, questionnaire, focus group, and interviews, the requirements revealed that the use of perioperative fluoroscopy should generate fluoroscopic images that correlate with the postoperative fluoroscopic images, and fit into the workflow of surgical hallux valgus corrections. Not using the protocol resulted in a total DAP ranging from 0.2701 cGy cm² to 0.3585 cGy cm² and a time per image acquisition ranging from 10.3 sec to 13.4 sec. Using the protocol resulted in a total DAP ranging from 0.2046 cGy cm² to 1.5060 cGy cm² and the time per image acquisition ranging from 3.4 to 12 sec.

Conclusion The results suggested that the current perioperative image during surgical hallux valgus corrections does not correlate with the postoperative image. Based on the information collected from this observational study, questionnaire, focus group, and interviews, specific requirements revealed that the use of a protocol should generate fluoroscopic images that correlate with the postoperative fluoroscopic images, and fit into the workflow of surgical hallux valgus corrections. A pilot study suggest that the implementation of the protocol results in the efficient and effective use of perioperative fluoroscopy.

Keywords hallux valgus – mini C-arm – perioperative fluoroscopy – protocol – radiographic angles

2.2 Introduction

Hallux valgus is the most common forefoot deformity, affecting 23% of adults aged 18 to 65 years and more than 35% in people over 65 years old.¹⁻⁴ It is a multiplanar deformity defined by medial angulation and pronation of the first metatarsal and lateral deviation of the proximal phalanx at the first metatarsophalangeal (MTP) joint.^{1,2,5-8} Fluoroscopy is performed for multiple purposes during the diagnosis, treatment, and postoperative evaluation of hallux valgus (Figure 1).^{3,6,7} On pre- and postoperative weight-bearing anteroposterior (AP) images of the foot, various fluoroscopic angles allow assessment of the severity of the deformity.^{6,9} Of which, the Hallux Valgus Angle (HVA) and the Intermetatarsal Angle (IMA) are the most regularly utilized fluoroscopic measurements (Figure 2).^{3,6} The perioperative use of fluoroscopy, using a mini-C-arm, assist the orthopedic surgeon in hardware placement and the assessment of the deformity correction.^{3,6,10}

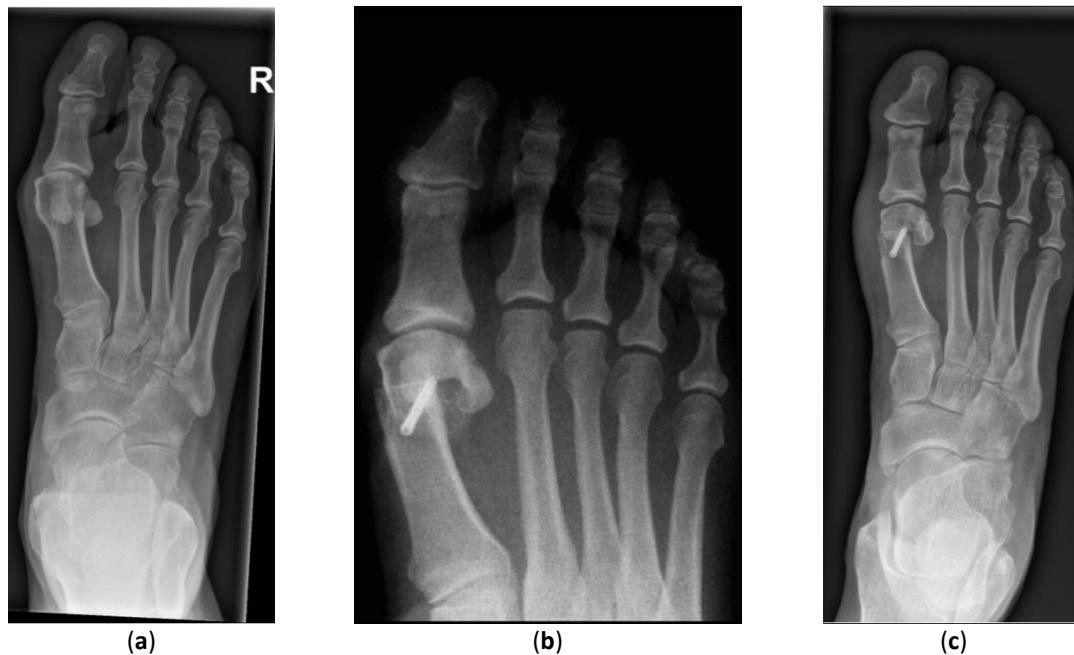


Figure 1. (a) The preoperative fluoroscopic image performed during diagnosis. (b) The perioperative fluoroscopic image performed during treatment. (c) The postoperative fluoroscopic image performed during postoperative evaluation.

The hallux valgus deformity is one of the most challenging foot and ankle deformities to correct, which can lead to an unsatisfactory result.¹¹ The reported incidence of complications, such as the recurrent hallux valgus ranges from 10% to 55%.¹²⁻¹⁴ During surgical hallux valgus corrections, the objective is to correct the HVA and IMA.¹⁵ Correction of these angles decreases the chance of hallux valgus recurrence.¹⁶ The orthopedic surgeon can accurately assess the deformity correction by using consistent AP imaging at various stages of care.¹⁷ However, the orthopedic surgeon is scrubbed and does not have time for an in-depth analysis of each perioperative image, making the utility of perioperative fluoroscopic imaging complicated. The degree of correction is visually inspected on perioperative fluoroscopic images after hardware fixation, giving a visual estimation of the HVA and IMA (Figure 1B). Based on this visual information, the correction may be surgically altered, and the perioperative fluoroscopy repeated to verify if the desired correction is achieved. This process requires repeatable and consistent perioperative images that correlate with the postoperative fluoroscopic images to visualize the achieved correction accurately. To achieve perioperative fluoroscopic images, the rotational and linear movements of a mini-C-arm must be efficiently and properly positioned.^{18,19} Obtaining fluoroscopic images in a standardized fashion is difficult to achieve in foot and ankle surgery.¹⁰ Several factors including the range of motion at the hip and knee, weight of the leg, drapes, and highly complex anatomy of the foot make it difficult to get certain views. Repeated image acquisition as the C-arm is positioned through trial-and-error achieves fluoroscopic images at the expense of time and radiation exposure to the patient and surgical staff.¹⁸ It is desirable to have a standardized method for obtaining perioperative fluoroscopic images that correlate with the postoperative fluoroscopic images to visualize the achieved correction accurately. The purpose of this study is to develop a protocol and test its feasibility in a pilot study for the use of perioperative fluoroscopy during surgical hallux valgus corrections to obtain perioperative images that correlate with the postoperative images and fits into the workflow.

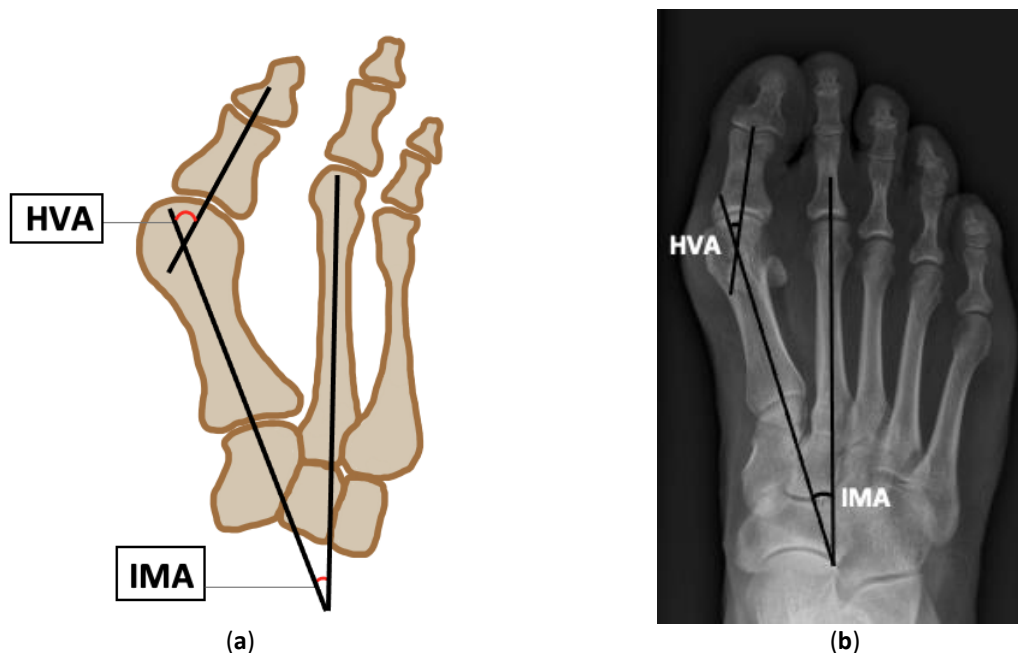


Figure 2. (a) The Hallux Valgus Angle (HVA), as the angle formed by the bisection of the proximal phalanx of the hallux and the line bisecting the shaft of the first metatarsal. The Intermetatarsal Angle (IMA), as the angle formed by the line drawn bisecting the first metatarsal and bisecting the second. (b) The measured HVA and IMA on an anteroposterior fluoroscopic image.

2.3 Methods

2.3.1 Observational study

An observational study was conducted at the OCON Centre for Orthopedic Surgery and Sports Medicine, Hengelo, The Netherlands. This observational study assessed the correlation of the peri- and postoperative fluoroscopic images without the use of a protocol. Inclusion criteria for the observational study were patients with a hallux valgus deformity who underwent a Chevron osteotomy from September 2021 to January 2022 at OCON. Exclusion criteria were the absence of perioperative fluoroscopic AP images and previous surgery for the correction of hallux valgus. Data were anonymized and used for the present study unless patients had opted-out for use of their medical data for research purposes. A total of twelve patients (twelve female) were included. Perioperative fluoroscopic AP images were acquired after final fixation of the Chevron osteotomy using a Hologic Fluoriscan InSight FD mini-C-arm (Hologic, Inc., Marlborough, United States) with the foot positioned by the primary surgeon (Figure 3). Weight-bearing AP images of the foot were acquired six weeks postoperatively. The patients were standing in an upright position with the foot in plantigrade and neutral ankle position, perpendicular to the detector.

To get insight into the correlation of the peri- and postoperative fluoroscopic images without the use of a protocol, the HVA and IMA were measured on both images twice by a technical physician (JiveX Review 5.2.0.22 (Alphatron Medical Systems B.V.)), with an interval of one week. The mean measured HVA and IMA of the technical physician were calculated and compared. To assess whether there was a significant difference between the perioperative fluoroscopic images and the postoperative fluoroscopic images, paired t-testing was used, after confirmation of data normality (SPSS® v28.0.1.0, IBM Corp., Armonk, NY, US). The p-value of interest was 0.05 at the 5% level.

An orthopedic foot and ankle surgeon also measured the HVA and IMA to assess the repeatability of the peri- and postoperative fluoroscopic measurements. This was done to see if it was possible to draw any conclusions about the correlation between the peri- and postoperative images based on the fluoroscopic measurements. Fluoroscopic measurements that remain constant throughout measurements (are highly repeatable) can reveal information about the correlation between peri- and postoperative images. Intraclass Correlation Coefficients (ICCs) were computed both intra- and inter-observer (SPSS® v28.0.1.0, IBM Corp., Armonk, NY, US). 95% CIs were determined in the setting of a two-way random effect model, with absolute agreement of a single measurement. The fluoroscopic measurements were defined as highly repeatable when there is an ICC > 0.90 both intra- and inter-observer.²⁰ The measurements have good repeatability with ICC values between 0.75 and 0.90.

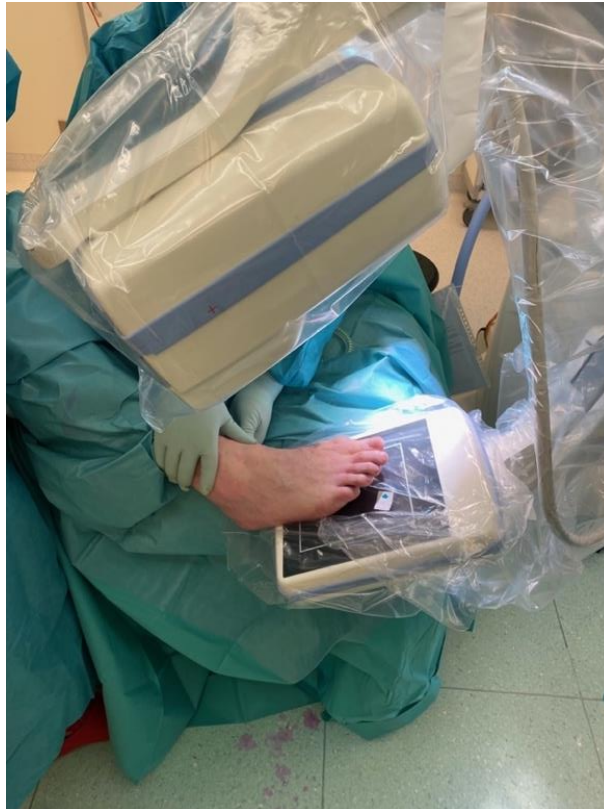


Figure 3. Obtaining the perioperative fluoroscopic images with the foot positioned by the primary surgeon.

2.3.2 Physician-centered experiences

Physician-centered experiences with the use of perioperative fluoroscopy were explored through a questionnaire and semi structured focus group or interview. This revealed the requirements of the protocol to fit the perioperative use of fluoroscopy in the workflow of surgical hallux valgus corrections. All participants were recruited at OCON. A total of six medical professionals (two orthopedic foot and ankle surgeons and four foot and ankle operation assistants) were asked to fill out a questionnaire. The questionnaire contained open questions concerning their experiences with perioperative fluoroscopy, covering the use of perioperative fluoroscopy, their attitude towards operating the mini-C-arm, and their attitude towards communication during mini-C-arm positioning. Next, a scaling question was asked to rate their ability to operate the mini-C-arm, on a scale from 1-10.

The structure of the focus group is presented in Table 1. During the focus group, two orthopedic foot and ankle surgeons created their own visualizations of their ideal situation of the use of perioperative fluoroscopy. These results were then discussed. The four foot and ankle operation assistants were interviewed one-on-one. The time involved per interview was typically about fifteen minutes. The interviews were largely unstructured, but questions were asked concerning the ideal situation of the use of perioperative fluoroscopy. Participants were instructed to create their ideal perioperative fluoroscopic scenario.

Table 1. Focus Group Elements, Methods, and Aims.

Focus Group Element	Method	Aim
Introduction	The focus group started with a short presentation of perioperative fluoroscopic imaging during foot/ankle surgeries.	To evoke thoughts on the use of perioperative fluoroscopy in hallux valgus corrections
Composition of ideal scenario	Individually, participants were instructed to create their ideal perioperative fluoroscopic scenario. With the use of a map of the Operation Room (OR) and printed OR components.	To gain insight in the participants ideal situation of the use of perioperative fluoroscopy with the mini-C-arm.
Discussion	The different compositions of the ideal scenario were shown to the participants to start a discussion on the ideal scenario.	To define placement of OR components.

2.3.3 Functional requirements obtaining perioperative fluoroscopic images

Based on the information collected from the observational study, questionnaire, focus group, and interviews, specific requirements were formulated for the development of a protocol for the use of perioperative fluoroscopy during surgical hallux valgus corrections. The use of perioperative fluoroscopy should:

- generate fluoroscopic images that correlate with the postoperative fluoroscopic images.
 - Apply pressure on the foot to simulate weight-bearing as in the postoperative fluoroscopic images.
 - Place at least half of the foot on the mini-C-arm detector.
- fit into the workflow of surgical hallux valgus corrections:
 - Using perioperative fluoroscopy should be As Low As Reasonable Achievable (ALARA) to ensure safety. This will make it possible to obtain fluoroscopic images with less radiation exposure to the patient and surgical staff.
 - Using perioperative fluoroscopy should be timeliness to ensure efficiency. This will enable faster image acquisition and mini-C-arm positioning.
 - Using the protocol of perioperative fluoroscopy should be effective. The use of perioperative fluoroscopy is more effective when the protocol maintained the sterility, fitted into the limited space of the operation room, and was easy to perform.

Using these requirements, a protocol for the use of perioperative fluoroscopy during surgical hallux valgus corrections was made (Appendix A).

2.3.4 Protocol evaluation: a pilot study

A pilot study was conducted to make an inventory of how the developed protocol functions in terms of safety, efficiency, and effectiveness. Three surgical hallux valgus corrections without using the perioperative fluoroscopy protocol were observed and compared against three surgical hallux valgus corrections using the protocol. The frequency of image acquisitions and the total dose area product (DAP) in cGy cm² were documented. The total DAP for the surgical hallux valgus corrections without and with using the protocol were compared to get an impression of the safety of the developed protocol. The safer use of perioperative fluoroscopy was suggested by a lower total DAP. The time it takes from positioning the C-arm until the image acquisition was documented and the time per image acquisition was calculated for the six surgical hallux valgus corrections. The time per image acquisition for the surgical hallux valgus corrections without and with using the protocol were compared to get an impression of the efficiency of the developed protocol. The more efficient use of perioperative fluoroscopy was suggested by a lower time per image acquisition. The HVA and IMA were measured on both the peri- and postoperative images by a technical physician (JiveX Review 5.2.0.22 (Alphatron Medical Systems B.V.)). To determine whether following the developed protocol is more effective, a small consensus meeting was held to test the opinion on the use of the protocol.

2.4 Results

The mean perioperative HVA was $11.5^\circ \pm 5.9^\circ$ and IMA $5.0^\circ \pm 1.8^\circ$ compared to a mean postoperative HVA of $11.4^\circ \pm 4.5^\circ$ ($p = 0.946$) and IMA $6.9^\circ \pm 1.9^\circ$ ($p = 0.008$) (Table 2). These results show that there is a statistically significant increase in the postoperative measured IMA compared with the perioperative measured IMA. There is, however, not a significant difference in the perioperative and postoperative measured HVA.

The interobserver repeatability of the peri- and postoperative fluoroscopic measurements ranged from 0.617 to 0.893 (Table 3). The intraobserver repeatability of the peri- and postoperative fluoroscopic measurements ranged from 0.778 to 0.960.

Table 2. Correlation of the peri- and postoperative HVA and IMA measurements by the technical physician.

	HVA	IMA
Perioperative measurement	$11.5^\circ \pm 5.9^\circ$	$5.0^\circ \pm 1.8^\circ$
Postoperative measurement	$11.4^\circ \pm 4.5^\circ$	$6.9^\circ \pm 1.9^\circ$
p-value	0.946	0.008*

* Significant at 5% level.

Abbreviations: HVA = Hallux Valgus Angle, IMA = Intermetatarsal Angle

Table 3. Interobserver and intraobserver reliabilities of fluoroscopic measurements.

Reliability, ICC (95%)	Interobserver	Intraobserver
HVA		
Perioperative	0.617 (0.123-0.870)	0.960 (0.867-0.988)
Postoperative	0.893 (0.683-0.967)	0.885 (0.651-0.966)
IMA		
Perioperative	0.767 (0.213-0.934)	0.778 (0.405-0.930)
Postoperative	0.861 (0.038-0.970)	0.908 (0.725-0.972)

Abbreviations: HVA = Hallux Valgus Angle, IMA = Intermetatarsal Angle

Not using the protocol resulted in a total DAP ranging from 0.2701 cGy cm² to 0.3585 cGy cm² (Table 4). The total DAP utilizing the protocol ranged from 0.2046 cGy cm² to 1.5060 cGy cm². In addition, the time per image acquisition not using the protocol ranged from 10.3 sec to 13.4 sec. Utilizing the protocol resulted in a time per image acquisition ranging from 3.4 to 12 sec. The measured perioperative HVA and IMA without protocol ranged from 4.5° to 10.5° and 2.9° to 5.4°, compared to a perioperative HVA and IMA ranging from 5.2° to 21.3° and 4.7° to 6.6° with protocol. The measured postoperative HVA and IMA without protocol ranged from 8.1° to 11.4° and 6.4° to 7.9° compared to a postoperative HVA and IMA ranging from 8.1° to 22.2° and 5.5° to 8.0° with protocol.

Table 4. Observations and HVA and IMA measurements by the technical physician during three surgical hallux valgus corrections using the perioperative fluoroscopy protocol and three without protocol.

	Frequency	Total DAP (cGy cm ²)	Positioning time (sec)	Time per image acquisition (sec)	Perioperative		Postoperative	
					HVA	IMA	HVA	IMA
Without protocol								
Operation 1	4	0.2701	41	10.3	7.0°	5.4°	8.1°	7.5°
Operation 2	3	0.2082	36	12	10.5°	2.9°	11.4°	6.4°
Operation 3	5	0.3585	67	13.4	4.5°	3.4°	11.4°	7.9°
With protocol								
Operation 4	4	0.3207	33	8.3	8.4°	4.7°	8.1°	5.5°
Operation 5	3	0.2046	36	12	21.3°	6.6°	22.2°	7.4°
Operation 6	20	1.5060	67	3.4	5.2°	5.8°	8.2°	8.0°

Abbreviations: DAP = Doses Area Product

The small consensus meetings revealed the opinions on the use of the protocol. The mini-C-arm could be moved to the ideal position with just one motion while maintaining sterility. Therefore, using the protocol was thought to be quicker. The protocol was easy to perform since the mini-C-arm could be moved to the ideal position with just one motion. However, the mini-C-arm should be rotated with a tighter turn during surgical hallux valgus corrections of the left foot (Figure 4). This was sometimes more difficult. By positioning the mini-C-arm on the side of the operating room with the most space, the protocol considered the limited space in the operation room.

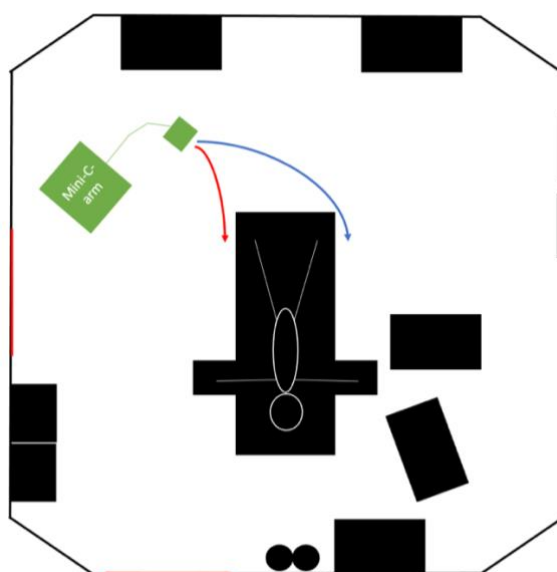


Figure 4. Illustration of the positioning of the mini-C-arm in the operation room. The mini-C-arm rotates with a tighter turn (red arrow) during surgical hallux valgus corrections of the left foot compared to the right foot (blue arrow).

2.5 Discussion

Despite the small sample size, the HVA measurements of the observational study suggest that the peri- and postoperative fluoroscopic images without the use of a protocol correlate. The postoperative measured IMA had a statistically significant increase compared to the perioperative measured IMA ($p = 0.008$). The IMA measurements suggest that there is no correlation between the peri- and postoperative fluoroscopic images, despite the small sample size. However, the mean value of the postoperative measured IMA remained within the limits of a successful correction (IMA $< 9^\circ$).²¹ These findings may suggest that weight-bearing has a statistically significant influence on the measured IMA. According to several publications, weight-bearing widens the forefoot as the medial ray moves through the tarsometatarsal joint, increasing the IMA by 1.5° to 2.6° .²²⁻²⁵ This may explain the statistically significant increase in the postoperative IMA that was found in this study. Because of this, the perioperative fluoroscopy protocol specifies that pressure must be administered to the foot to mimic weight-bearing and better match the postoperative image.

The fluoroscopic measurements are operator-dependent,²⁶ as confirmed by the results of this study: there was no ICC > 0.90 both intra- and inter-observer. However, there was at least a good repeatability in almost all the measurements. What is notable is that the perioperatively measured IMA has lower inter- and intraobserver repeatability (ICC 0.767 and 0.778) than the postoperative IMA (ICC 0.861 and 0.908). The lower repeatability can be explained by the not complete perioperative images of the foot. In some cases, the first and second metatarsal bones are not entirely visible on the perioperative images. Because of this, the perioperative fluoroscopy protocol specifies that at least half of the foot must be placed on the mini-C-arm detector.

The moderate interobserver reliability of the perioperative measured HVA can be explained by the very different HVA measurements of the first patient (6.5° and 25.1°). Since the orthopedic foot and ankle surgeon and the technical physician conducted their measurements independently without being aware of the other measurements, no direct explanation of this difference was discovered. However, it is believed that the measured HVA of 25.1° was inaccurate. If this measurement is not included in the statistical analysis, the perioperative measured HVA becomes highly repeatable with ICC > 0.90 (ICC 0.961; 95% CI, 0.866-0.989).

Based on the fluoroscopic measurements, it is challenging to determine if the current peri- and postoperative images without the use of a protocol correlate due to its operator-dependent component. However, it is thought that the current perioperative image without the use of a protocol does not correlate with the postoperative image, based on the IMA measurements that showed good repeatability. This resulted in the specific requirement that the use of perioperative fluoroscopy should generate fluoroscopic images that correlate with the postoperative fluoroscopic images. Therefore, the perioperative fluoroscopy protocol specifies that pressure must be administered to the foot to mimic weight-bearing, and at least half of the foot must be placed on the mini-C-arm detector. However, this effect may need to be further evaluated.

Based on the information collected from the observational study and the physician-centered experiences explored through the questionnaire, focus group, and interviews with six medical professionals, specific requirements were formulated for the development of the protocol. This indicates that the development of the protocol has received a lot of attention by involving all relevant stakeholders. To explore all physician-centered experiences with perioperative fluoroscopy, multiple tools per participant (questionnaire and focus group or interview) were employed due to the small number of relevant stakeholders ($n=6$). This allowed the collection of enough information to formulate specific requirements for the development of the protocol. The questionnaire, focus group, and interviews were essential for collecting the various viewpoints of the six medical professionals. For example, it was revealed that the orthopedic foot and ankle surgeons are more concerned with moving the mini C-arm to the optimal position, whilst the operation assistants tends to focus more on everything related to using the C-arm (for example: sterility and the safe use of fluoroscopy). When creating the protocol, it was crucial to take this information into account. Thus, the focus group, interviews, and questionnaire revealed all the information necessary for the protocol development, despite the fact that there were only a few stakeholders. Therefore, this method of collecting data was preferred.

A pilot study was conducted to make an inventory of how the developed protocol functions in terms of safety, efficiency, and effectiveness. The DAP was used to measure the amount of radiation released by the mini-C-arm, as it is a recommended method of comparing radiation usage during fluoroscopic procedures and may be used to assess dose-reduction strategies.²⁷ The results may suggest that the use of the developed protocol was not safer because the highest total DAP (ranging from 0.2046 cGy cm^2 to 1.5060 cGy cm^2) was higher compared to the surgical hallux valgus corrections without protocol (ranging from 0.2701 cGy cm^2 to 0.3585 cGy cm^2). However, the six hallux valgus corrections cannot be used to draw a conclusion about the safety of the protocol that was developed. The protocol should be tested during more surgical hallux valgus corrections to draw

meaningful conclusions about the safety of the protocol. The highest total DAP (1.5060 cGy cm²) was documented during operation six. This can be explained by the high frequency of image acquisitions (n=20) compared to the other operations. The orthopedic foot and ankle surgeon performing operation six always employs more fluoroscopy than the orthopedic foot and ankle surgeon performing the other operations. When looking to the total DAP per procedure, Guyonette et al. reported a mean DAP per procedure of 0.8 cGy cm².²⁸ Although following the protocol may not be suggested as safer, the total DAP lays below this reported mean DAP per procedure, with the exception of operation six.

Using the protocol was more efficient since the time per image acquisition (ranging from 3.4 to 12 sec.) was lower compared to surgical hallux valgus corrections without protocol (10.3 sec to 13.4 sec.). The decrease in time per image acquisition was not immediately anticipated because of the learning curve associated with using the protocol, which could initially lead to a longer time per image acquisition. Even quicker image acquisition and mini-C-arm positioning might be possible with more familiarity with the protocol.

The measured peri- and postoperative IMA ranges are closer together during surgical hallux valgus corrections with protocol (perioperative IMA ranging from 4.7° to 6.6° and postoperative IMA ranging 5.5° to 8.0°) than during surgical hallux valgus corrections without protocol (perioperative IMA ranging from 2.9° to 5.4° and postoperative IMA ranging 6.4° to 7.9°). This may suggest that the peri- and postoperative fluoroscopic images with the use of the protocol correlate. However, the six hallux valgus corrections cannot be used to draw a conclusion about the effect of the protocol on the correlation of the peri- and postoperative images. The protocol should be tested during more surgical hallux valgus corrections to draw meaningful conclusions about the effect of the developed protocol on the correlation between peri- and postoperative images.

The protocol was more effective since it maintained the sterility, fitted into the limited space of the operation room, was easy to perform, and using the protocol was thought to be quicker. Consequently, it is likely that the protocol will be used in the future. However, because the mini-C-arm needed to be rotated with a tighter turn during surgical hallux valgus corrections of the left foot, it was more challenging to transfer the mini-C-arm to the appropriate position. Sharpening the angle at which the detector arm of the mini-C-arm is positioned enables a rotation with a wider turn, resolving this problem.

This study has several limitations. First, the peri- and postoperative images were not blinded and randomized during the observational study. The HVA and IMA measurements started with the peri- and postoperative image of patient one and ended with the peri- and postoperative image of patient twelve. The technical physician was unexperienced in measuring the HVA and IMA. As a result, the angular measurements of patient twelve may have been more precise than those of patient one because of the learning curve. Secondly, the observational study suggest that there is no correlation between the current peri- and postoperative images based on a small sample size. Therefore, the power of the test might be too low to identify meaningful differences in the data. To address the correlation between the peri- and postoperative images, a bigger sample size is necessary. Thirdly, the pilot study uses only six surgical hallux valgus corrections performed by two different orthopedic foot and ankle surgeons. More surgical hallux valgus corrections should be considered, and comparisons should be made per orthopedic foot and ankle surgeon, to draw meaningful conclusions about the safety, efficiency, and effectiveness of the developed protocol. The strength of this study is that to the best of our knowledge, this is the first study which has developed and evaluated a protocol for the use of perioperative fluoroscopy during surgical hallux valgus corrections.

Finally, the presented work represents the preliminary step towards the safe, efficient, and effective use of perioperative fluoroscopy during surgical hallux valgus corrections. Future research must focus on the effect of the developed protocol on the correlation between peri- and postoperative images and the further evaluation of the safety, efficiency, and effectiveness of the developed protocol. Considering these findings, further protocol modifications might be required.

2.6 Conclusion

This study conducted an observational study, where the results suggested that the current perioperative image during surgical hallux valgus corrections does not correlate with the postoperative image. Based on the information collected from this observational study, a questionnaire, focus group, and interviews, specific requirements were formulated for the development of a protocol for the use of perioperative fluoroscopy during surgical hallux valgus corrections. A small pilot study was conducted to make an inventory of how the developed protocol functions in terms of safety, efficiency, and effectiveness. The implementation of the protocol suggest that the use of perioperative fluoroscopy becomes more efficient and effective. This may improve the performances of the orthopedic foot and ankle surgeon, which could improve the outcomes of the surgical

correction of hallux valgus. Future research must focus on the effect of the developed protocol on the correlation between peri- and postoperative images and the further of the safety, efficiency, and effectiveness of the developed protocol. Considering these findings, further protocol modifications might be required.

2.7 References

- 1 Jia, J.; Li, J.; Qu, H.; Li, M.; Zhang, S.; Hao, J.; Gao, X.; Meng, X.; Sun, Y.; Hakonarson, H.; Zeng, X.; Xia, Q.; Li, J. New insights into hallux valgus by whole exome sequencing study. *Exp Biol Med (Maywood)*. 2021;246(14):1607-1616, doi:10.1177/15353702211008641.
- 2 Nix, S.; Smith, M.; Vicenzino, B. Prevalence of hallux valgus in the general population: a systematic review and meta-analysis. *J Foot Ankle Res*. 2010;3:1-9, doi:10.1186/1757-1146-3-21.
- 3 Heineman, N.; Liu, G.; Pacicco, T.; Dessouky, R.; Wukich, D.K.; Chhabra, A. Clinical and imaging assessment and treatment of hallux valgus. *Acta Radiol*. 2019;61(1):56-66, doi:10.1177/0284185119847675.
- 4 Ferreyra, M.; Núñez-Samper, M.; Viladot, R.; Ruiz, J.; Isidro, A.; Ibañez, L. What do we know about hallux valgus pathogenesis? Review of the different theories. *J Foot Ankle* 2020;14(3):223-230, doi:10.30795/jfootankle.2020.v14.1202.
- 5 Gawande, K.B.; Mungikar, S.; Hotwani, R.; Ingle, S.; Kulkarni, C.A. Prevalence of Hallux Valgus in Normal Individuals. *J. Med. Pharm. Allied Sci*. 2021;10(4):3138-3141, doi:10.22270/jmpas.V10I4.1263.
- 6 Saad, A.; Lyengar, K.P.; Fitzpatrick, J.; Azoopardi, C.; Panchal, H.; Botchu, R. The Linear Hallux Valgus Offset– A novel way to measure Hallux Valgus. *J Clin Orthop Trauma*. 2022;30, doi:10.1016/j.jcot.2022.101898.
- 7 Kakwani, M.; Kakwani, R. Current concepts review of hallux valgus. *J. Arthrosc. Jt. Surg*. 2021;8(3):222-230, doi:10.1016/j.jajs.2021.04.006.
- 8 Wagner, P.; Wagner, E. Role of Coronal Plane Malalignment in Hallux Valgus Correction. *Foot Ankle Clin*. 2019;25:69-77, doi:10.1016/j.fcl.2019.10.009.
- 9 Steadman, J.; Barg, A.; Saltzman, L. First Metatarsal Rotation in Hallux Valgus Deformity. *Foot Ankle Int*. 2021;42(4), doi:10.1177/1071100721997149.
- 10 Elliot, R.; Saxby, T.; Whitehouse, S. Intraoperative imaging in hallux valgus surgery. *Foot Ankle Surg*. 2012;18(1):19-21, doi:10.1016/j.fas.2011.01.006.
- 11 Zambelli, R.; Baumfeld, D. Intraoperative and Postoperative Evaluation of Hallux Valgus Correction What Is Important? *Foot Ankle Clin N Am* 2020;25(1):127-139, doi:10.1016/j.fcl.2019.10.007.
- 12 Sawah, A.; Zemenova, S.; Haque, R.; Ridley, D.; Abboud, R.; Wang, W.; Harrold, F. Forecasting Posttreatment Outcome of Hallux Valgus Surgery Patients. *Foot Ankle int*. 2021;42(9):1144-1152, doi:10.1177/10711007211002498.
- 13 Trnka, H. Managing Complications of Foot and Ankle Surgery: Hallux Valgus. *Foot Ankle Clin*. 2022;27(2):271-285, doi:10.1016/j.fcl.2021.11.015.
- 14 Ezzatvar, Y.; López-Bueno, L.; Fuentes-Aparicio, L.; Dueñas, L. Prevalence and Predisposing Factors for Recurrence after Hallux Valgus Surgery: A Systematic Review and Meta-Analysis. *J Clin Med*. 2021;10(24), doi:10.3390/jcm10245753.
- 15 Price, A.; Hughes, T.; Kurnik, C.; Kurnik, C.; Gavin, K.; Miller, R. Comparison of Intraoperative Fluoroscopy to Postoperative Weight-Bearing Radiographs Obtained 4 to 6 Weeks After Bunion Repair With A Chevron Osteotomy. *J. Orthop. Res*. 2019;8.
- 16 Pentikainen, I.; Ojala, R.; Ohtonen, P.; Piippo, J.; Leppilahti, J. Preoperative radiological factors correlated to long-term recurrence of hallux valgus following distal chevron osteotomy. *Foot Ankle Int*. 2014;35(12):1262-1267, doi:10.1177/1071100714548703.
- 17 Boffeli, T.; Mahoney, K. Intraoperative Simulated Weightbearing Lateral Foot Imaging: The Clinical Utility and Ability to Predict Sagittal Plane Position of the First Ray in Lapidus Fusion. *J Foot Ankle Surg*. 2016;55(6):1158-1163, doi:10.1053/j.jfas.2016.06.004.
- 18 De Silva, T.; Punnoose, J.; Uneri, A.; Mahesh, M.; Goerres, J.; Jacobsen, M.; Ketcha, M.; Manbachi, A.; Vogt, S.; Kleinszig, G.; Khanna, A.; Wolinsky, J.; Siwerdsen, J.; Osgood, G. Virtual fluoroscopy for intraoperative C-arm positioning and radiation dose reduction. *J Med Imaging (Bellingham)*. 2018;5(1), doi:10.1117/1.JMI.5.1.015005.
- 19 Shao, Z.; Guan, Y.; Tan, J. Virtual Reality Aided Positioning of Mobile C-Arms for Image-Guided Surgery. *Adv. Mech. Eng*. 2014, doi:10.1155/2014/943025.
- 20 Koo, T.; Li, M. A guideline of selecting and reporting intraclass correlation coefficients for reliability research. *J Chiropr Med*. 2016;15(2):155-163, doi:10.1016/j.jcm.2016.02.012.
- 21 Piqué-Vidal, C.; Vila, J. A geometric analysis of hallux valgus: correlation with clinical assessment of severity. *J Foot Ankle Res*. 2009, doi:10.1186/1757-1146-2-15.

- 22 Van der Woude, P.; Keizer, S.; Wever-Korevaar, M.; Thomassen, B. Intra- and Interobserver Agreement in Hallux Valgus Angle Measurements on Weightbearing and Non-Weightbearing Radiographs. *Foot Ankle Surg.* 2019;58(4):706-712.
- 23 Fuhrmann, R.; Layher, F.; Wetzel, W. Radiographic Changes in Forefoot Geometry with Weightbearing. *Foot Ankle Int.* 2003;24(4):326-331, doi:10.1177/107110070302400404.
- 24 Tanaka, Y.; Takakura, Y.; Takaoka, T.; Akiyama, K.; Fujii, T.; Tamai, S. Radiographic Analysis of Hallux Valgus in Women on Weightbearing and Nonweightbearing. *Clin Orthop Relat Res.* 1997;336:186-194, doi:10.1097/00003086-199703000-00026.
- 25 Boszczyk, A.; Kwapisz, S.; Kicinski, M.; Kordasiewicz, B.; Liszka, H. Non-weightbearing compared with weightbearing x-rays in hallux valgus decision-making. *Skeletal Radiol.* 2020;49(9):1441-1447, doi:10.1007/s00256-020-03441-9.
- 26 Carrara, C.; Caravaggi, P.; Belvedere, C.; Leardini, A. Radiographic angular measurements of the foot and ankle in weight-bearing: A literature review. *Foot Ankle Surg.* 2020;26(5):509-517, doi:10.1016/j.fas.2019.07.008.
- 27 Crawley, M.T.; Rogers, A.T. Dose-area product measurements in a range of common orthopaedic procedures and their possible use in establishing local diagnostic reference levels. *Br J Radiol.* 2000;73(871):740-744, doi:10.1259/bjr.73.871.11089466.
- 28 Guyonnet, G.; Mulliez, A.; Fessy, M.; Besse, J. Prospective analysis of intraoperative radiation dose in foot and ankle surgery using mini-C-arm fluoroscopy. Continuous series of 1064 procedures. *Orthop Traumatol Surg Res.* 2021;107(6), doi:10.1016/j.otsr.2021.102994.



Chapter 3

Development of a coordinate system

Chapter 3: Development of a coordinate system

Definition of a Global Coordinate System in the Foot for the Surgical Planning of Forefoot Corrections

Sanne Krakers ^{1,2}, Anil Peters ², Sybrand Homan ², Judith olde Heuvel ² and Gabriëlle Tuijthof ³

¹ Technical Medicine, University of Twente, Enschede, The Netherlands

² Department of Orthopedics, Orthopedisch Centrum Oost Nederland (OCON), Hengelo, The Netherlands

³ Department of Biomechanical Engineering, University of Twente, Enschede, The Netherlands

* This paper has been submitted to the open access journal from MDPI “Biomechanics” for the Special Issue entitled “Personalized Biomechanics and Orthopedics of the Lower Extremities”.

3.1 Abstract

Purpose Forefoot osteotomies to improve the alignment are difficult procedures and can lead to a variety of complications. Preoperative planning in three-dimensions might assist in the successful management of forefoot deformities. The purpose of this study was to develop a global coordinate system in the foot for the planning of forefoot corrections.

Methods Two strategies (CS1 and CS2) were developed for defining a global coordinate system, that meets the criteria of being well defined, robust, highly repeatable, clinical relevant, compatible for foot CT scans, independent of the ankle joint angle, and do not include bones in the forefoot. The absolute angle of rotation was used to quantify repeatability. The anatomical planes of the coordinate systems were visually inspected by an orthopedic surgeon to evaluate the clinical relevancy.

Results The repeatability of CS1 ranged from 0.48° to 5.86°. The definition of CS2 was fully automated and therefore had a perfect repeatability (0°). Clinically relevant anatomical planes were observed with CS2.

Conclusion This study presents an automated method for defining a global coordinate system in the foot according to pre-defined requirements for the planning of forefoot corrections.

Keywords coordinate system – foot – forefoot deformities – hallux valgus – preoperative planning

3.2 Introduction

Surgical reconstruction of forefoot deformities is the most common and a frequently challenging pathologic condition that a foot and ankle surgeon treats.¹ In particular, forefoot corrective osteotomies to improve the alignment are difficult procedures and can lead to a variety of complications (e.g., recurrence of the deformity, and nonunion).²⁻⁴ Preoperative planning in three-dimensions (3D) might assist in successfully managing forefoot deformities. As the primary objective of 3D preoperative planning is to effectively correct the deformity, reduce postoperative morbidity and maintain normal foot biomechanics.^{4,5} This study focuses specifically on hallux valgus because it is a multiplanar deformity defined by medial angulation and pronation of the first metatarsal, making surgical correction particularly difficult.

Hallux valgus is the most common forefoot deformity, affecting 23% of adults aged 18 to 65 years and more than 35% in people over 65 years old.⁶⁻⁹ Hallux valgus can typically be diagnosed through physical examination and standard radiological two-dimensional (2D) imaging, which involves weight-bearing lateral and anteroposterior (AP) images of the foot.¹⁰ However, due to the rotational, multiplanar nature of hallux valgus, it is difficult to describe and quantify hallux valgus accurately and reliably on standard radiological 2D images.^{11,12} Standard 2D radiological images use a 2D projection of a 3D structure as a simplified representation of anatomical information in one plane. As a result, multiplanar deformities cannot be adequately analyzed on each anatomical plane independently since the standard 2D radiological images are not exactly orthogonal, leading to unintentional corrections in untargeted planes.¹³ It would be beneficial to switch to the 3D analysis of hallux valgus to address the errors induced by 2D analysis. Computed tomography (CT) makes it possible to quantify the absolute and relative position and orientation of the bones in the foot and contributes to advanced knowledge of the multiplanar nature of hallux valgus, which might assist with the preoperative planning of hallux valgus corrections.^{14,15}

To do this adequately, it is crucial to define a relevant and robust global coordinate system in the foot for the preoperative planning of hallux valgus corrections. A general reporting standard for local coordinate systems was proposed by the International Society of Biomechanics (ISB) in 2002.¹⁶ The ISB standard is starting to become more widely adopted, however, a consensus method for defining a global coordinate system for the foot has not been established yet. Due to the continuing absence of a standardized method, there have been a number of studies that define their own global coordinate system in the foot (Table 1).^{4,17-21} These coordinate systems have several limitations that cannot be ignored. Firstly, the definitions of the axes are sensitive to operator-dependent accuracy and repeatability.^{14,22} Secondly, they are dependent on the scanned section of the foot or foot posture. Thirdly, they lack unambiguous definition of the origin or axes. Thus, the purpose of this study is to develop a new global coordinate system in the foot for the 3D planning of forefoot corrections.

Table 1. Overview of different studies that defined a global coordinate system in the foot, specifying the accompanying limitations.

Study	Limitations
Cappozo et al. ¹⁷	Operator-dependent accuracy and repeatability
Green et al. ⁴	Dependent on the scanned section of the fibula
Geng et al. ¹⁸	Origin not explicitly defined
Ortolani et al. ¹⁹	Origin not explicitly defined
Yoshioka et al. ²⁰	The ankle joint angle determines the location of the forefoot in the global coordinate system

3.3 Methods

3.3.0 Developing the global coordinate system: the process

To find the global coordinate system in the foot four coordinate system definitions were explored during the development process. This process has contributed to identify the best global coordinate system in the foot. The two coordinate systems with the most varied strategies were discussed in this article, the definitions of the other two coordinate systems are presented in Appendix B.

3.3.1 Requirements to define a global coordinate system

Specific requirements were formulated for the development of a new global coordinate system in the foot based on an expert panel brainstorming session and the limitations of the studies that have defined global coordinate systems in the foot (Table 1),^{4,17-21} the global coordinate system in the foot should:

- be well defined. A well-defined coordinate system include the definition of two axes and the position of the origin.
- be robust. A robust coordinate system constructs the coordinate system consistently using the same definition, regardless of anatomical variations amongst patients (e.g., accessory ossicles).
- be highly repeatable. A highly repeatable coordinate system implies the construction of exactly the same coordinate system within an individual foot if the protocol is repeated. This will enable the same foot orientation in the preoperative planning and independent analysis, regardless of the operator.
- be clinical relevant with recognizable anatomical planes. This is necessary for the clinical interpretation of the deformity. When the virtual AP and lateral views of the coordinate system correspond with the corresponding radiological images, a coordinate system is clinical relevant and has recognizable anatomical planes.
- be compatible for CT scans of the foot. This will make it possible to construct the coordinate system regardless of the scanned section of the tibia and fibula.
- not be sensitive for the ankle joint angle. This will enable the forefoot to be positioned clinically relevantly in the coordinate system, regardless of the ankle joint angle.
- not include bones in the forefoot as they might be deformed.

Using these requirements two strategies were developed for defining a global coordinate system in the foot. The first strategy (CS1) was to use as many points as possible on the 3D foot model. The second strategy (CS2) involved applying as much automatic point selection as possible, while using the points that were the furthest apart from one another.

3.3.2 Study design and subjects

An observational study was conducted at the OCON Centre for Orthopedic Surgery and Sports Medicine, Hengelo, The Netherlands. Inclusion criteria for the study were patients with a hallux valgus deformity who underwent a CT scan for regular care purposes. Exclusion criteria for the study were previous hallux valgus surgery. Data was anonymized and used for the present study unless patients had opted-out for use of their medical data for research purposes. A total of nine feet of nine patients (nine female), with a median age of 30 (17-63) years, and a BMI of 26.2 (18.5-32.5) kg/m² were included.

3.3.3 Data acquisition

CT scans were acquired on a Siemens SOMATOM Definition AS or Siemens SOMATOM Drive (Siemens Healthineers AG, Erlangen, Germany) with the patient in supine position. A splint was used in six patients to create a constant plantigrade foot and neutral ankle position across patients. The splint prevented motion interference and provided the greatest possible replication of stance on a flat surface. The foot CT scans of the other three patients were retrospectively used without a splint.

The CT scans were exported to Materialise's Interactive Medical Image Control System 21.0 (Mimics v21.0, Materialise NV, Leuven, Belgium) in the Digital Imaging and Communications in Medicine (DICOM) format for segmentation. A thresholding tool was used to construct a mask of all pixels with a threshold range of 226 to 3071 Hounsfield Units and the resulting segmentation mask was then manually edited to eliminate holes. Each bone in the segmentation masks was rendered to form a 3D structure, and all bones together formed a 3D model showing the relative positions of the segmented bones in space. The Mimics program files were then converted to 3D binary formatted stereolithography (STL) files. These files were imported to 3-Matic software (Materialise NV, Leuven, Belgium) to construct the two global coordinate systems.

3.3.4 Coordinate system definitions

This study used the direction definitions of the x- (pointing to the right), y- (pointing anteriorly), and z-axis (pointing cranially) to form axes that were clinical applicable, despite the ISB recommendations for an anteriorly pointed x-axis, cranially pointed y-axis, and a z-axis pointed to the right.¹⁶

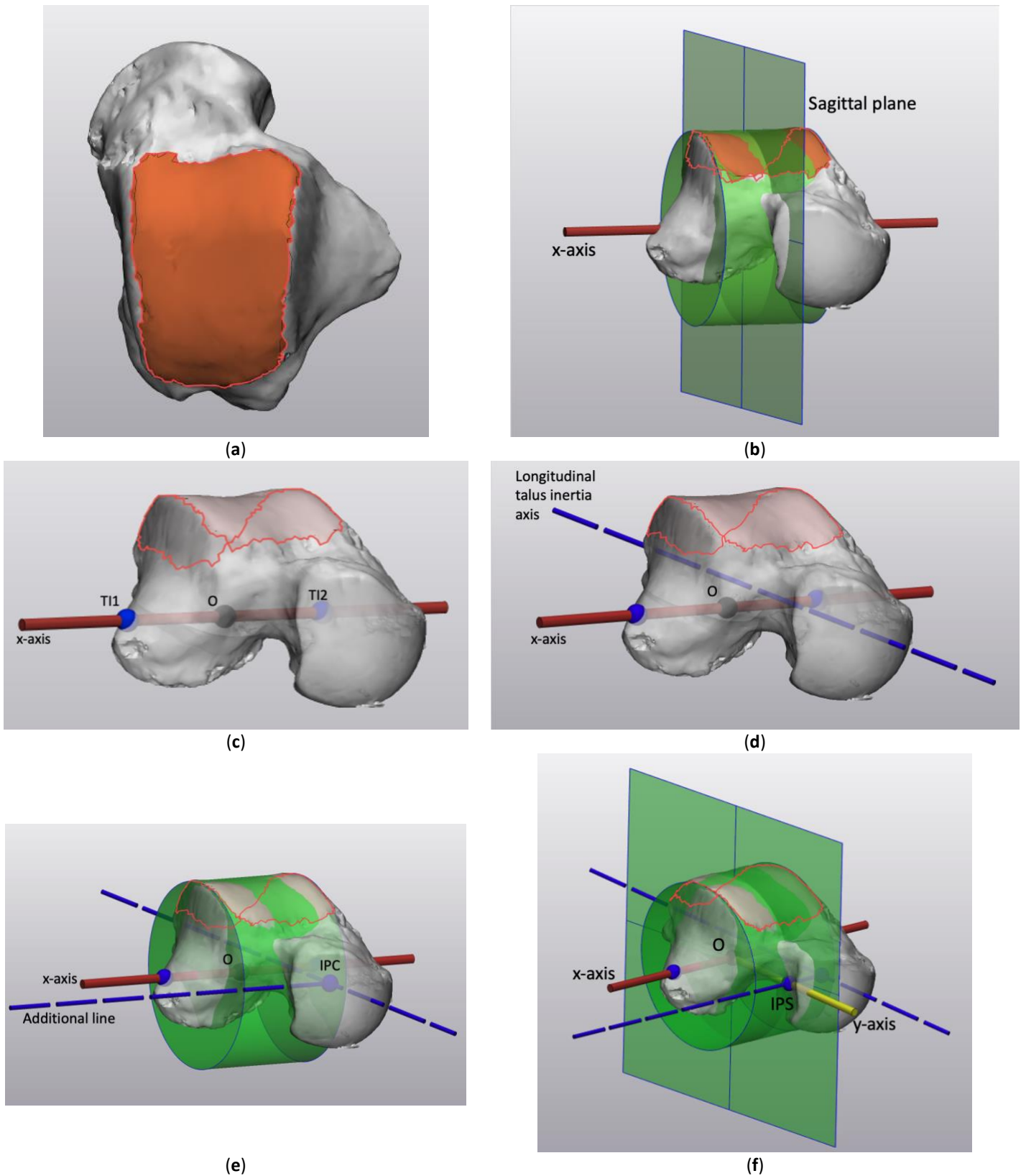


Figure 1. The construction of CS1: (a) Axial view of the talus with the drawing of the facies superior of the trochlea tali; (b) Illustration of the talus with the cylinder fitted on the identified facies superior of the trochlea tali defining the direction of the x-axis (red line), as the normal vector to a sagittal plane; (c) Illustration of the talus and the Origin, as the midpoint of the talar intersections (T11 and T12) of the axis of the cylinder, without the fitted cylinder and sagittal plane; (d) Illustration of the talus and its longitudinal inertia axis without the fitted cylinder and sagittal plane; (e) Illustration of the talus and its longitudinal inertia axis intersecting the cylinder (IPC) without the sagittal plane. An additional parallel to the x-axis was created; (f) Illustration of the talus with the y-axis running from the Origin (O) to the intersection point of the additional line with the sagittal plane (IPS).

The talus was used in the construction of CS1 due to its preservation throughout a broad spectrum of forefoot deformities and its availability in foot CT scans. This will develop a robust coordinate system that is compatible for CT scans of the foot, not sensitive for the ankle joint angle, and does not include bones in the forefoot. To start the construction of CS1, the facies superior of the trochlea tali was manually drawn (Figure 1a). Through this surface a cylinder was fitted with its longitudinal axis defining the direction of the x-axis, as the normal vector to a sagittal plane (Figure 1b). The Origin (O) was defined as the midpoint of the talar intersections (TI1 and TI2) of the axis of the cylinder (Figure 1c). The y-axis was defined as follows. First the longitudinal talus inertia axis was generated (Figure 1d) and at the intersection point with the cylinder (IPC), an additional line parallel to the x-axis was created (Figure 1e). The y-axis runs from the Origin to the intersection point of the additional line with a sagittal plane (IPS) (Figure 1f). The z-axis was orthogonal to the x- and y-axis (Figure 2).

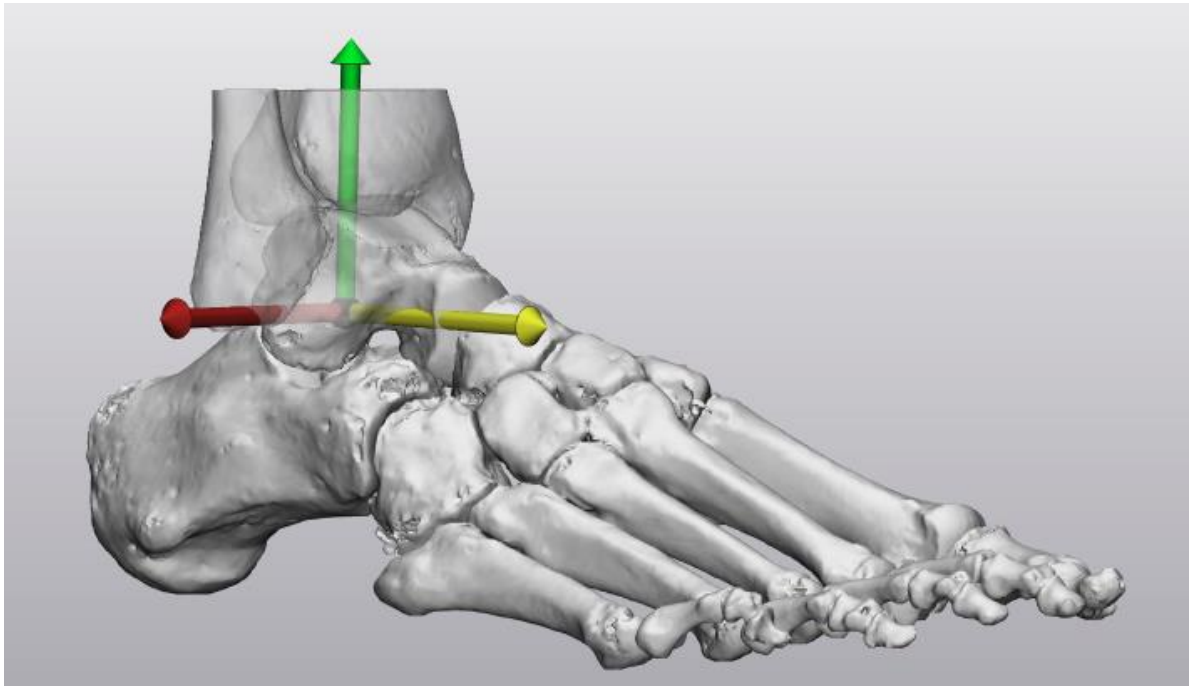


Figure 2. The axes of the global coordinate system of CS1 centered at the origin: x-axis (red), y-axis (yellow), z-axis (green).

The construction of CS2 was a completely automated strategy using the talus and the three weight-bearing points on the calcaneus and first and fifth metatarsal heads, due to its preservation throughout a broad spectrum of forefoot deformities and availability in foot CT scans. This will develop a robust coordinate system that is compatible for CT scans of the foot, not sensitive for the ankle joint angle, and do not include bone in the forefoot. To start the construction of CS2, the most caudal point of the first metatarsal-sesamoid complex (M1), fifth metatarsal (M5), and calcaneus (C) were automatically selected in the original CT scan orientation (Figure 3a). These three weight-bearing points were used to construct a ground plane (Figure 3b). The normal vector of the ground plane defined the direction of the z-axis (Figure 3c). The inertia axes of the talus were generated, with their intersection point serving as the Origin (O) (Figure 3d). To ensure an orthogonal coordinate system, the longitudinal talus inertia axis was projected on the ground plane defining the direction of the y-axis (Figure 3e). The normal vector and the projected longitudinal talus inertia axis were translated towards the Origin to form the z- and y-axis (Figure 3f). The x-axis was orthogonal to the z- and y-axis (Figure 4).

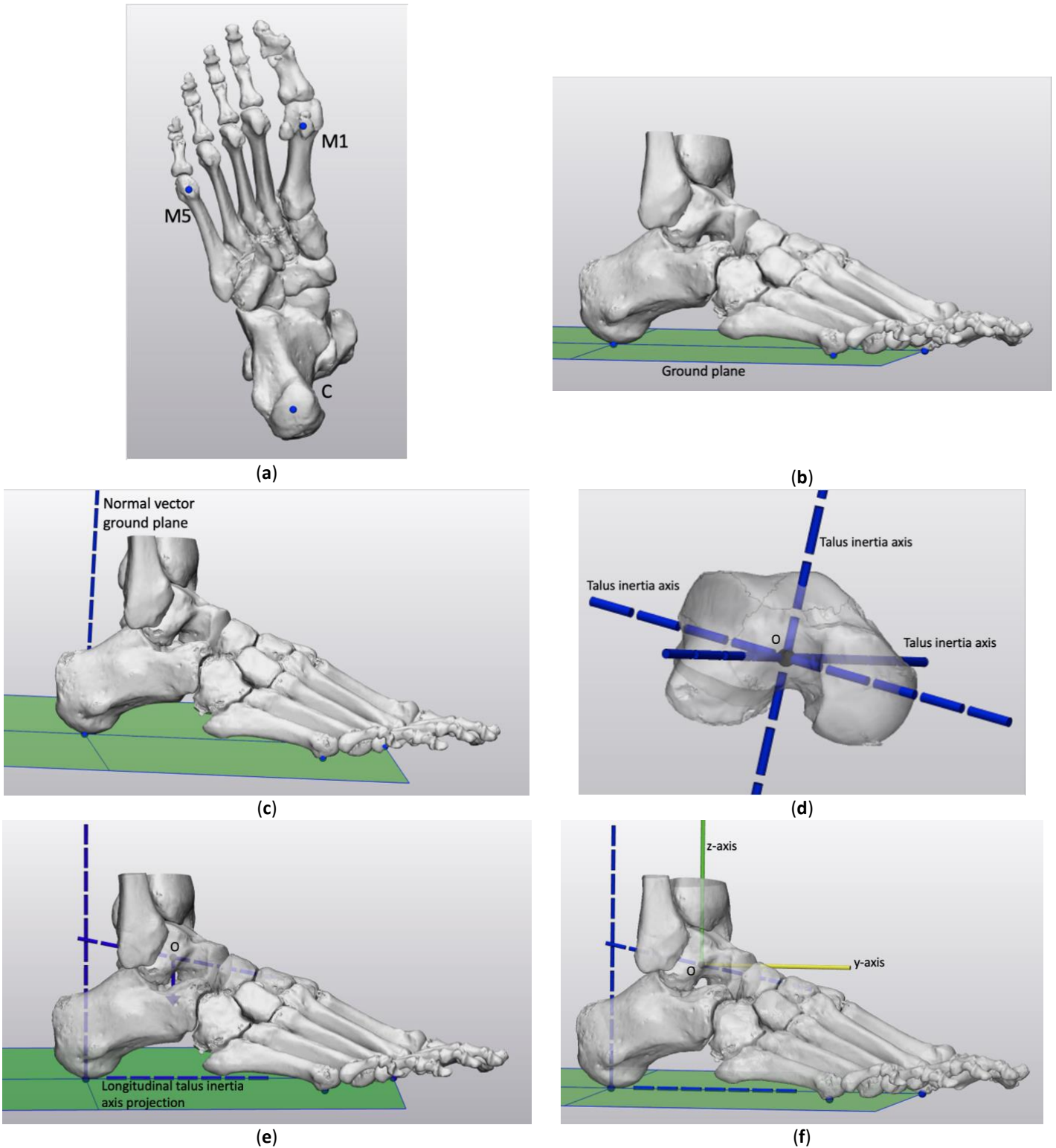


Figure 3. The construction of CS2: (a) Posterior-anterior view of the foot with the three automatic selected weight-bearing points: the most caudal point of the first metatarsal-sesamoid complex (M1), fifth metatarsal (M5), and calcaneus (C) in the original CT scan orientation; (b) Illustration of the foot with the ground plane based on the three weight-bearing points; (c) Illustration of the foot with the normal vector of the ground plane defining the direction of the z-axis; (d) Illustration of the inertia axes of the talus with its the intersection point serving as the Origin (O); (e) Illustration of the foot with the projection of the longitudinal talus inertia axis on the ground plane, defining the direction of the y-axis; (f) Illustration of the foot with the normal vector and projected longitudinal talus inertia axis translated towards the Origin to form the z- and y-axis.

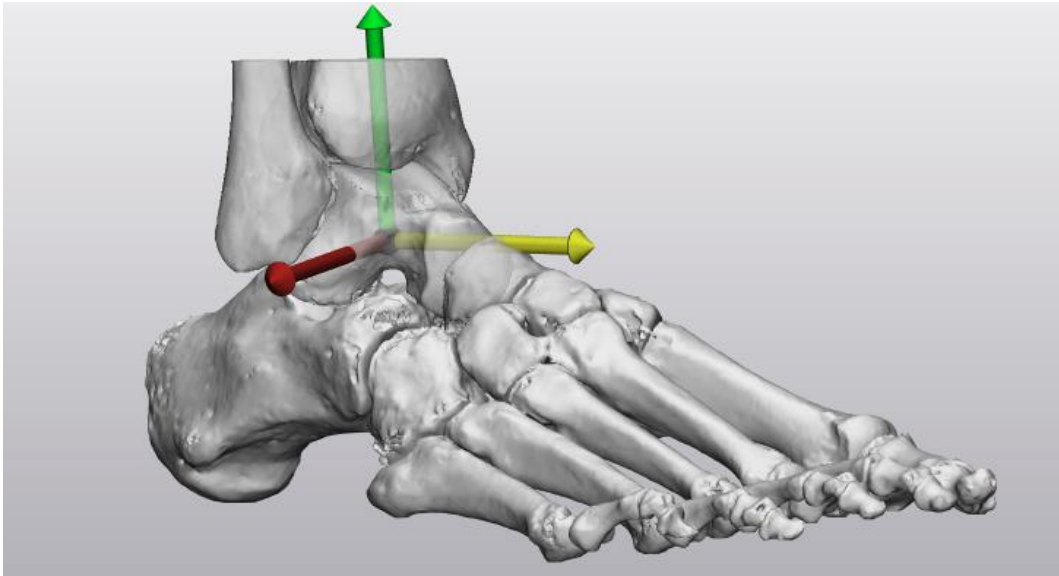


Figure 4. The axes of the global coordinate system of CS2 centered at the origin: x-axis (red), y-axis (yellow), z-axis (green).

3.3.5 Coordinate system evaluation

The developed coordinate systems comply with the requirements that the global coordinate system in the foot should be well defined, be robust, be compatible for CT scans of the foot, not be sensitive for the ankle joint angle, and not include bones in the forefoot. The repeatability and clinical relevancy of the global coordinate systems in the foot were evaluated.

Evaluation of repeatability was assessed as follows. Two different operators constructed the coordinate systems of the six splinted feet independently, using the different strategies. The operators were a technical physician and an orthopedic surgeon (OS). The operators were both familiar with foot anatomy and the technical physician with the employed software. The technical physician repeated the construction of each coordinate system two times for each foot with an interval of one week (TP1 and TP2). The absolute angle of rotation was used to quantify repeatability, it describes the smallest angle of rotation between the repeated coordinate system construction of the technical physician (TP1 and TP2) and for the two operators (TP1 and OS) (Figure 5). The amount of rotation around each axis required to align two coordinate systems was depicted using the axis with angle magnitude. This was calculated for the repeated construction of the technical physician (TP1 and TP2) and for the two operators (TP1 and OS).

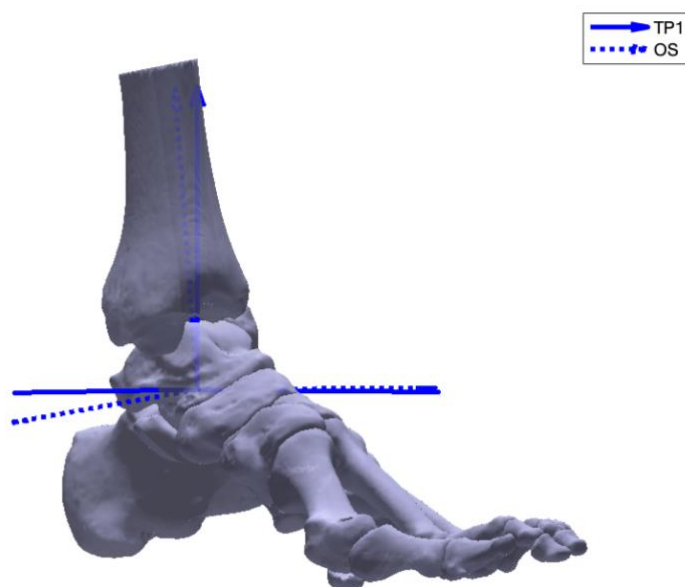


Figure 5. The absolute angle of rotation describing the smallest angle of rotation between the first coordinate system construction of the technical physician (TP1) and the orthopedic surgeon (OS).

Evaluation of clinical relevancy was assessed by generation of virtual weight-bearing AP and lateral images for the nine 3D foot models (Figure 6). Based on the first coordinate system construction of the technical physician, the view straight at the xy- and yz-plane represented the virtual AP and lateral image. These virtual images represents the conventional radiological images, which are used as a reference frame to interpret the virtual images. Orthopedic surgeons were asked if they could use the virtual images for the clinical interpretation of the deformity. The coordinate system was clinically relevant and had recognizable anatomical planes if the virtual images corresponded with the corresponding conventional radiological images. The virtual images of the three 3D foot models without a splint allowed the assessment of the clinical relevancy without the use of a splint in the CT scan.

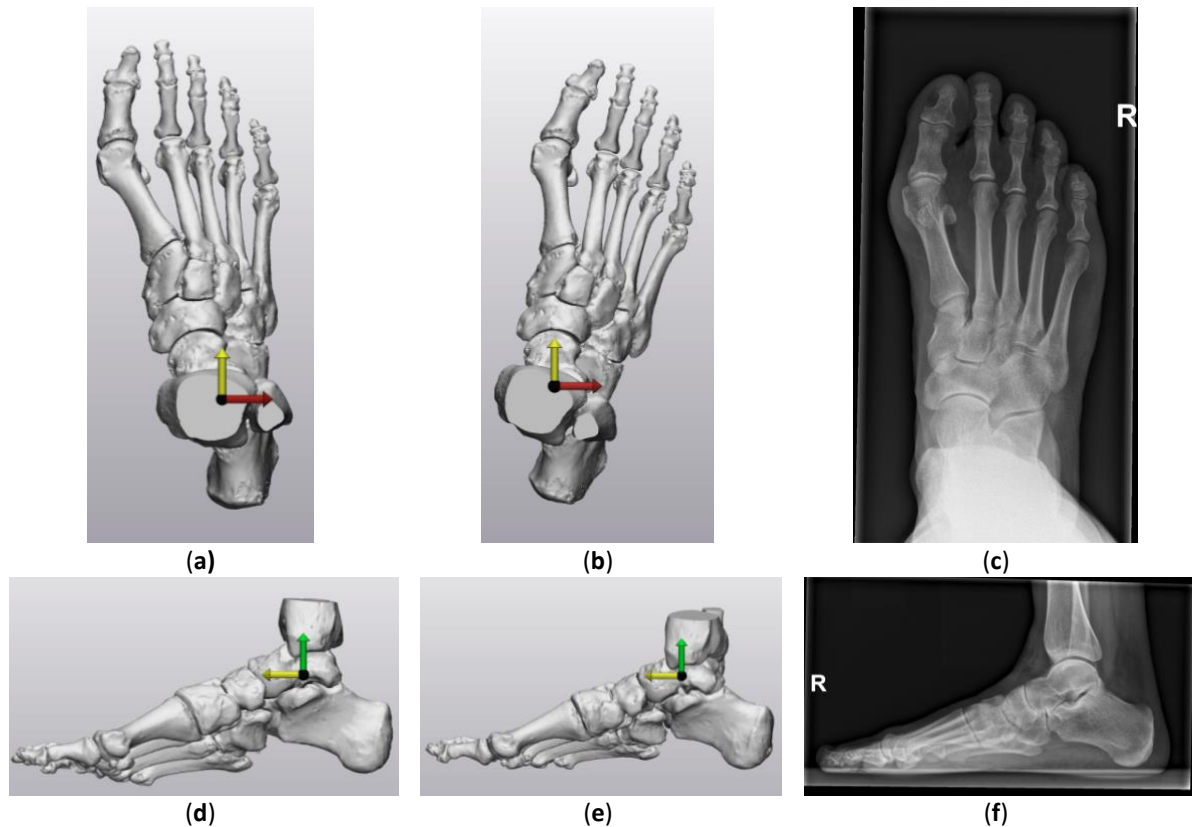


Figure 6. CS1 and CS2 virtual anteroposterior (AP) and lateral image of Patient 2 compared to the corresponding conventional AP and lateral radiological image. For the exact generation of the virtual image, see the body text: (a) CS1 virtual AP image; (b) CS2 virtual AP image; (c) Corresponding conventional AP radiological image; (d) CS1 virtual lateral image; (e) CS2 virtual lateral image; (f) Corresponding conventional lateral radiological image.

3.4 Results

CS1 intraobserver repeatability ranged from 0.48° to 2.12° (Table 2). The interobserver repeatability of CS1 ranged from 0.92° to 5.86°. CS2 was automated and therefore had an intra- and interobserver repeatability of 0°. More specific details on the amount of rotation around each axis necessary to align the two coordinate systems can be found in Table 3. Variation in orientation of the x-, y-, and z-axis was found for each patient in CS1. Each patient had a different axis that required the most rotation to align TP1 and TP2 or OS. For CS2, there was no deviation in orientation of the three axes between TP1 and TP2 or TP1 and OS for any of the patients.

Table 2. The absolute angle of rotation between the first (CS1) and second coordinate system (CS2) definition of the technical physician (TP1 and TP2) and between TP1 and the coordinate system definition of the orthopedic surgeon (OS).

Absolute angle of rotation	Patient 1	Patient 2	Patient 3	Patient 4	Patient 5	Patient 6	Mean (SD)
CS1							
TP1 – TP2	1.66°	0.48°	0.86°	1.48°	2.12°	1.75°	1.39° (0.61°)
TP1 - OS	2.10°	1.30°	0.92°	1.35°	4.43°	5.86°	2.66° (2.01°)
CS2							
TP1 – TP2	0°	0°	0°	0°	0°	0°	0° (0°)
TP1 - OS	0°	0°	0°	0°	0°	0°	0° (0°)

Table 3. The axis with angle magnitude between the first (CS1) and second coordinate system (CS2) definition of the technical physician (TP1 and TP2) and between TP1 and the coordinate system definition of the orthopedic surgeon (OS).

Axis with angle magnitude		Patient 1	Patient 2	Patient 3	Patient 4	Patient 5	Patient 6
CS1							
TP1 – TP2	x-axis	0.28°	0.10°	0.40°	1.26°	-0.56°	-0.12°
	y-axis	-0.34°	-0.44°	-0.42°	0.69°	-2.00°	-1.59°
	z-axis	1.60°	-0.16°	0.63°	-0.36°	-0.46°	0.72°
TP1 - OS	x-axis	0.50°	-1.1°	-0.40°	0.82°	0.36°	0.88°
	y-axis	-2.00°	-0.08°	-0.23°	0.75°	-4.03°	-5.69°
	z-axis	0.38°	-0.72°	-0.79°	0.76°	-1.81°	1.12°
CS2							
TP1 – TP2	x-axis	0°	0°	0°	0°	0°	0°
	y-axis	0°	0°	0°	0°	0°	0°
	z-axis	0°	0°	0°	0°	0°	0°
TP1 - OS	x-axis	0°	0°	0°	0°	0°	0°
	y-axis	0°	0°	0°	0°	0°	0°
	z-axis	0°	0°	0°	0°	0°	0°

The virtual AP and lateral image of CS1 and CS2 compared to the corresponding AP and lateral radiological images of Patient 2 are depicted in Figure 6. Two orthopedic surgeons indicated that the virtual AP and lateral images of CS1 did not correspond to the conventional radiological images of the foot, as the foot appears to be inclined and in endorotation. Both surgeons indicated that the virtual images of CS2 were the most recognizable and correspond to the conventional weight-bearing AP and lateral radiological images of the foot. However, the foot does not lay exactly straight in line in the virtual AP image of CS2. The virtual AP and lateral image of CS1 and CS2 compared to the corresponding radiological images of the three 3D foot models without a splint are depicted in Appendix C. Both orthopedic surgeons indicated that the virtual images of CS2 were the most recognizable and correspond to the conventional weight-bearing radiological images when not using a splint.

3.5 Discussion

The definition of CS2 was preferred because it meets all the requirements for the development of a new global coordinate system in the foot. CS2 includes the definition of two axes and the position of the origin, resulting in a well defined coordinate system. In addition, construction of CS2 uses the talus and three weight-bearing points of the foot due to its preservation throughout a broad spectrum of forefoot deformities and availability in foot CT scans. This creates a robust coordinate system that is constructed consistently using the same definition regardless of anatomical variations. The analysis demonstrated that the automated strategy, CS2, exhibits a high level of repeatability, both inter- and intra-operator. This repeatability is attributed to the minimal intervention required from the operator during the process of defining the coordinate system. This will enable independent analysis of each foot in the same coordinate system, regardless of the operator as it always creates the same coordinate system. The correspondence between the virtual AP and lateral images and the weight-bearing AP and lateral radiographic images validates the clinical relevance of CS2, as it aligns with identifiable anatomical planes. Consequently, the quantification of the absolute and relative position and orientation of the foot bones can be effectively communicated in a clear and consistent manner using this coordinate system. Moreover, the construction of CS2 is completed using standard foot CT scans and therefore altering the parameters to extend the scanning area is not necessary. As a result, radiation exposure is not increased. Additionally, the construction of CS2 does not include bones in the forefoot and is not sensitive for the ankle joint angle, allowing the forefoot to be positioned clinically relevant in the coordinate system, regardless of the ankle joint angle. As a result, the definition of CS2 allows geometrical representations of position and orientation of the bones in the foot for the planning of forefoot corrections.

Despite the definition of CS1 being well defined, robust, compatible for foot CT scans, independent of the ankle joint angle, and excluding bones in the forefoot, it was not preferred because of its poor repeatability and clinical relevancy.

Although a number of previous studies proposed a global coordinate system in the foot (Table 1),^{4,17-21} their definitions did not meet the requirements of being well defined, robust, highly repeatable, clinical relevant, compatible for foot CT scans, independent of the ankle joint angle, and excluding bones in the forefoot.

Additionally, to the best of our knowledge this is the first study which has quantified perfect repeatability of the global coordinate system for the foot using the absolute angle of rotation. Conconi et al. previously used the absolute angle of rotation to calculate the rotational variability among local coordinate systems in the foot.¹⁴ However, the largest rotational variability reported by them was 4.2°. The current study quantified this value as poor repeatability given its proximity to the absolute angles of rotation in the definition of CS1. In addition, this value does not match with the largest absolute angle of rotation (0°) found in the definition of CS2. This confirms the perfect repeatability found in this study. Green et al. previously referenced the x- and y-axis against a best fit talar centroidal axis to evaluate the variability of the global coordinate system.⁴ The calculated angles between the axes and the best fit talar centroidal axis both had a standard deviation of 2.36°. The current study also quantified these values as poor repeatability, as it comes close to the found axis with angle magnitudes in the definition of CS1. In addition, these values does not match with the largest axis with angle magnitude (0°) found in the definition of CS2. This also confirms the perfect repeatability found in this study.

This study has several limitations. First, this study is based on only nine 3D foot models of patients with hallux valgus. This limitation is mitigated by the use of the automated method that results in perfect repeatability, but additional evaluation of the clinical relevancy may be required. Secondly, the effect of segmentation on the coordinate system is not evaluated. The inertia axes of the talus are sensitive to bone geometry for axes different from the main one (the longitudinal talus inertia axis).¹⁴ The bone geometry depends on how the CT scan was segmented, to generate the 3D model. Different segmentation software, CT scan parameters, and operator segmentation expertise may result in differences in bone geometry. However, several studies showed a high repeatability and accuracy for the segmentation process using Mimics software.²³⁻²⁸ Although the exact effect of segmentation on the coordinate system is uncertain, it is believed to be negligible. Thirdly, only the weight-bearing condition is simulated in this study. Weight-bearing CT scanners enables imaging of the foot to be done in the natural weight-bearing position. This has the advantage of reduced radiation exposure^{29,30} and it improves the evaluation of forefoot deformities.^{18,31,32} However, the patients in this study could not stand in the CT scanner during image acquisition. The splint provided the greatest possible replication of stance on a flat surface, maintaining a constant plantigrade foot and neutral ankle position across patients. The proposed coordinate system definition of CS2 has also some limitations. First, talus deformities may result in different orientations of its inertia axes, affecting the coordinate system. Since, forefoot deformities were the focus of this study, the morphology of the hindfoot was assumed to be more or less normal. Secondly, the coordinate system may also be affected by the foot position in the CT scanner because of the use of the automatic point selection in the original CT scan orientation. The foot position determines the most caudal automatic selected points on the first metatarsal-sesamoid complex, fifth metatarsal, and calcaneus (Figure 3a). Consequently, plantarflexion of the ankle in the CT scanner will result in a more distal automatically selected point on the calcaneus compared to Figure 3a. However, a splint solves this problem by creating a constant plantigrade foot and neutral ankle position across patients. The only factor that may have affected the automatic point selection is a skewed positioning of the patient on the table of the CT scanner. This can result in more laterally or medially selected points on the first metatarsal-sesamoid complex, fifth metatarsal, and calcaneus. However, it is believed to have little to no impact on the constructed normal vector of the ground plane. The strength of this study is that to the best of our knowledge, this is the first study which has established and quantified the repeatability and clinical relevancy of two potential global coordinate systems in the foot.

Finally, the presented work represents the preliminary step towards preoperative 3D planning of forefoot corrections. In future endeavors, the proposed coordinate system will be utilized to accurately identify the optimal location and appropriate procedure for correcting forefoot deformities, thus preventing the need for extensive or un-planned surgical interventions. Future research may adopt the proposed coordinate system broadly and reach consensus in order to conduct meaningful comparisons between studies.

3.6 Conclusion

This study presented an automated method for defining a well defined, robust, highly repeatable, clinical relevant, compatible for foot CT scans, independent of the ankle joint angle, and not include bones in the forefoot global coordinate system in the foot for the preoperative planning of forefoot corrections. A high repeatability is achieved by the automated method since it does not rely on manual selected landmarks or fitting of spheres to the bone surfaces. Using this automated method will make it easier to quantify the absolute and relative position and orientation of the bones in the foot and contributes to advanced knowledge of the foot morphology. This could provide more information of the multiplanar nature of hallux valgus, which might assist with the preoperative planning of hallux valgus corrections.

3.7 References

- 1 Zelen, C.M. Advances in forefoot surgery. *Clin Podiatr Med Surg.* 2013;30(3):13-14, doi:10.1016/j.cpm.2013.05.002.
- 2 Femino, J.E.; Mueller, K. Complications of Lesser Toe Surgery. *Clin Orthop Relat Res.* 2001;391:72-88, doi:10.1097/00003086-200110000-00009.
- 3 Sammarco, G.J.; Idusuyi, O.B. Complications after surgery of the hallux. *Clin Orthop Relat Res.* 2001;391:59-71, doi:10.1097/00003086-200110000-00008.
- 4 Green, C.; Fitzpatrick, C.; Fitzpatrick, D.; Stephens, M.; Quinlan, W.; Flavin, R. Definition of Coordinate System for Three-Dimensional Data Analysis in the Foot and Ankle. *Foot Ankle Int.* 2011;32(2):193-199, doi:10.3113/FAI.2011.0193.
- 5 Maestro, M.; Besse, J.L.; Ragusa, M.; Berthonnaud, E. Forefoot morphotype study and planning method for forefoot osteotomy. *Foot Ankle Clin.* 2003;8(4):695-710, doi:10.1016/s1083-7515(03)00148-7.
- 6 Jia, J.; Li, J.; Qu, H.; Li, M.; Zhang, S.; Hao, J.; Gao, X.; Meng, X.; Sun, Y.; Hakonarson, H.; Zeng, X.; Xia, Q.; Li, J. New insights into hallux valgus by whole exome sequencing study. *Exp Biol Med (Maywood).* 2021;246(14):1607-1616, doi:10.1177/15353702211008641.
- 7 Nix, S.; Smith, M.; Vicenzino, B. Prevalence of hallux valgus in the general population: a systematic review and meta-analysis. *J Foot Ankle Res.* 2010;3:1-9, doi:10.1186/1757-1146-3-21.
- 8 Heineman, N.; Liu, G.; Pacicco, T.; Dessouky, R.; Wukich, D.K.; Chhabra, A. Clinical and imaging assessment and treatment of hallux valgus. *Acta Radiol.* 2019;61(1):56-66, doi:10.1177/0284185119847675.
- 9 Ferreyra, M.; Núñez-Samper, M.; Viladot, R.; Ruiz, J.; Isidro, A.; Ibañez, L. What do we know about hallux valgus pathogenesis? Review of the different theories. *J Foot Ankle* 2020;14(3):223-230, doi:10.30795/jfootankle.2020.v14.1202.
- 10 Kuhn, J.; Alvi, F. Hallux Valgus. StatPearls. Treasure Island (FL). Available online: <https://www.ncbi.nlm.nih.gov/books/NBK553092/> (accessed on 30 June 2023).
- 11 Gutekunst, D.J.; Liu, L.; Ju, T.; Prior, F.W.; Sinacore, D.R. Reliability of clinically relevant 3D foot bone angles from quantitative computed tomography. *J Foot Ankle Res.* 2013;6:1-8, doi:10.1186/1757-1146-6-38.
- 12 Welck, M.J.; Al-Khudairi, N. Imaging of Hallux Valgus How to Approach the Deformity. *Foot Ankle Clin.* 2018;23:183-192, doi:10.1016/j.fcl.2018.01.002.
- 13 Schweizer, A.; Fürnstahl, P.; Harders, M.; Székely, G.; Nagy, L. Complex Radius Shaft Malunion: Osteotomy with Computer-Assisted Planning. *Hand (N Y).* 2010;5(2):171-178, doi:10.1007/s11552-009-9233-4.
- 14 Conconi, M.; Pompili, A.; Sancisi, N.; Leardini, A.; Durante, S.; Belvedere, C. New anatomical reference systems for the bones of the foot and ankle complex: definitions and exploitation on clinical conditions. *J Foot Ankle Res.* 2021;14:1-13, doi:10.1186/s13047-021-00504-5.
- 15 Ozturk, A.M.; Suer, O.; Coban, I.; Ozer, M.A.; Govsa, F. Three-Dimensional Printed Anatomical Models Help in Correcting Foot Alignment in Hallux Valgus Deformities. *Indian J Orthop.* 2020;54:199-209, doi:10.1007/s43465-020-00110-w.
- 16 Wu, G.; Siegler, S.; Allard, P.; Kirtley, C.; Leardini, A.; Rosenbaum, D.; Whittle, M.; D'Lima, D.D.; Cristofolini, L.; Witte, H.; Schmid, O.; Stokes, I. ISB recommendation on definitions of joint coordinate system of various joints for the reporting of human joint motion—part I: ankle, hip, and spine. *J Biomech.* 2002;35(4):543-548, doi:10.1016/s0021-9290(01)00222-6.
- 17 Cappozzo, A.; Catani, F.; Della Croce, U.; Leardini, A. Position and orientation in space of bones during movement: anatomical frame definition and determination. *Clin Biomech (Bristol, Avon).* 1995;10(4):171-178, doi:10.1016/0268-0033(95)91394-t.
- 18 Geng, X.; Wang, C.; Ma, X.; Wang, X.; Huang, J.; Zhang, C.; Xu, J.; Yang, J. Mobility of the first metatarsal-cuneiform joint in patients with and without hallux valgus: in vivo three-dimensional analysis using computerized tomography scan. *J Orthop Surg Res.* 2015;10:1-7, doi:10.1186/s13018-015-0289-2.
- 19 Ortolani, M.; Leardini, A.; Pavani, C.; Scicolone, S.; Girolami, M.; Bevoni, R.; Lullini, G.; Durante, S.; Berti, L.; Belvedere, C. Angular and linear measurements of adult flexible flatfoot via weight-bearing CT scans and 3D bone reconstruction tools. *Sci Rep.* 2021;11:1-13, doi:10.1038/s41598-021-95708-x.
- 20 Yoshioka, N.; Ikoma, K.; Kido, M.; Imai, K.; Maki, M.; Arai, Y.; Fujiwara, H.; Tokunaga, D.; Inoue, N.; Kubo, T. Weight-bearing three-dimensional computed tomography analysis of the forefoot in patients with flatfoot deformity. *J Orthop Sci.* 2016;21:154-158, doi:10.1016/j.jos.2015.12.001.

- 21 Modenese, L.; Renault, J.B. Automatic generation of personalised skeletal models of the lower limb from three-dimensional bone geometries. *J Biomech.* 2021;116:1-10, doi:10.1016/j.jbiomech.2020.110186.
- 22 Brown, K.M.; Bursley, D.E.; Arneson, L.J.; Andrews, C.A.; Ludewig, P.M.; Glasoe, W.M. Consideration of digitization precision when building local coordinate axes for a foot model. *J Biomech.* 2009;42:1263-1269, doi:10.1016/j.jbiomech.2009.03.013.
- 23 Moerenhout, B.A.M.M.L.; Gelaude, F.; Swennen, G.R.J.; Casselman, J.W.; Van der Sloten, J.; Mommaerts, M.Y. Accuracy and repeatability of cone-beam computed tomography (CBCT) measurements used in the determination of facial indices in the laboratory setup. *J Craniomaxillofac Surg.* 2009;37(1):18-23, doi:10.1016/j.jcms.2008.07.006.
- 24 Van den Broeck, J.; Vereecke, E.; Wirix-Speetjens, R.; Vander Sloten, J. Segmentation accuracy of long bones. *Med Eng Phys.* 2014;36(7):949-953, doi:10.1016/j.medengphy.2014.03.016.
- 25 Giudice, A.L.; Ronsivalle, V.; Grippaudo, C.; Lucchese, A.; Muraglie, S.; Lagravère, M.O.; Isola, G. One Step before 3D Printing—Evaluation of Imaging Software Accuracy for 3-Dimensional Analysis of the Mandible: A Comparative Study Using a Surface-to-Surface Matching Technique. *Materials (Basel).* 2020;13(12):1-15, doi:10.3390/ma13122798.
- 26 Mandolini, M.; Brunzini, A.; Facco, G.; Mazzoli, A.; Forcellese, A.; Gigante, A. Comparison of Three 3D Segmentation Software Tools for Hip Surgical Planning. *Sensors (Basel).* 2022;22(14):1-16, doi:10.3390/s22145242.
- 27 Bertolini, M.; Luraghi, G.; Belicchi, I.; Migliavacca, F.; Colombo, G. Evaluation of segmentation accuracy and its impact on patient-specific CFD analysis. *Int J Interact Des Manuf.* 2022;16:545-556, doi:10.1007/s12008-021-00802-z.
- 28 Abdullah, J.Y.; Abdullah, A.M.; Hadi, H.; Husein, A.; Rajion, Z.A. Comparison of STL skull models produced using open-source software versus commercial software. *Rapid Prototyp J.* 2019;25(10):1585-1591, doi:10.1108/RPJ-08-2018-0206.
- 29 Godoy-Santos, A.L.; Bernasconi, A.; Bordalo-Rodrigues, M.; Lintz, F.; Lôbo, C.F.T.; De Cesar Netto, C. Weight-bearing cone-beam computed tomography in the foot and ankle specialty: where we are and where we are going - an update. *Radiol Bras.* 2021;54(3):177-184, doi:10.1590/0100-3984.2020.0048.
- 30 Lintz, F.; Beaudet, P.; Richardi, G.; Brillhault, J. Weight-bearing CT in foot and ankle pathology. *Orthop Traumatol Surg Res.* 2021;107:1-8, doi:10.1016/j.otsr.2020.102772.
- 31 Fuhrmann, R.; Layher, F.; Wetzel, W. Radiographic Changes in Forefoot Geometry with Weightbearing. *Foot Ankle Int.* 2003;24(4):326-331, doi:10.1177/107110070302400404.
- 32 Tanaka, Y.; Takakura, Y.; Takaoka, T.; Akiyama, K.; Fujii, T.; Tamai, S. Radiographic Analysis of Hallux Valgus in Women on Weightbearing and Nonweightbearing. *Clin Orthop Relat Res.* 1997;336:186-194, doi:10.1097/00003086-199703000-00026.

Chapter 4

Concepts for the 3D quantification
of hallux valgus

Chapter 4: Concepts for the 3D quantification of hallux valgus

4.1 Introduction

Recent systematic reviews of the literature by Barg et al. and Lalevee et al. showed that 10% of patients who underwent surgical hallux valgus corrections were dissatisfied with the results, and that the postoperative recurrence rate of hallux valgus is as high as 64% after at least five years of follow-up.^{1,2} This raises the question how well we understand the extremely complex multifactorial, and multiplanar hallux valgus deformity, as well as its risk factors, pathophysiology, deformity components, treatment goals, and expected outcomes.³

The classic description of hallux valgus has for a long time been an axial plane deformity.⁴ However, hallux valgus is a multiplanar deformity that involves multiple bones and a multitude of soft tissue imbalances. It is not only an axial plane deformity but is also defined by the rotational deformity of the first metatarsal.⁴⁻⁹ Currently, the diagnosis, assessment of the severity, and the surgical treatment planning of hallux valgus are performed using physical examination and standard radiological two-dimensional (2D) imaging.¹⁰ Due to the multiplanar nature of hallux valgus, it is difficult to describe and quantify hallux valgus accurately and reliably on standard radiological 2D images,^{11,12} necessitating a reproducible three-dimensional (3D) quantification of hallux valgus. This chapter explored potential methods for the 3D quantification of hallux valgus in 3-Matic software (Materialise NV, Leuven, Belgium) using the coordinate system and 3D models discussed in “Chapter 3: Development of a coordinate system”.

4.2 Axial plane deformity

The axial plane deformity is defined by medial angulation (varus deviation) of the first metatarsal and lateral (valgus) deviation of the proximal phalanx at the first metatarsophalangeal (MTP) joint (Figure 1).^{4-9,13} Measurements of the axial plane deformity using standard radiological 2D imaging include the Hallux Valgus Angle (HVA) and the Intermetatarsal Angle (IMA).^{8,14} However, it is believed that the alignment can be evaluated with more precision and accuracy using a 3D quantification of the axial plane deformity.

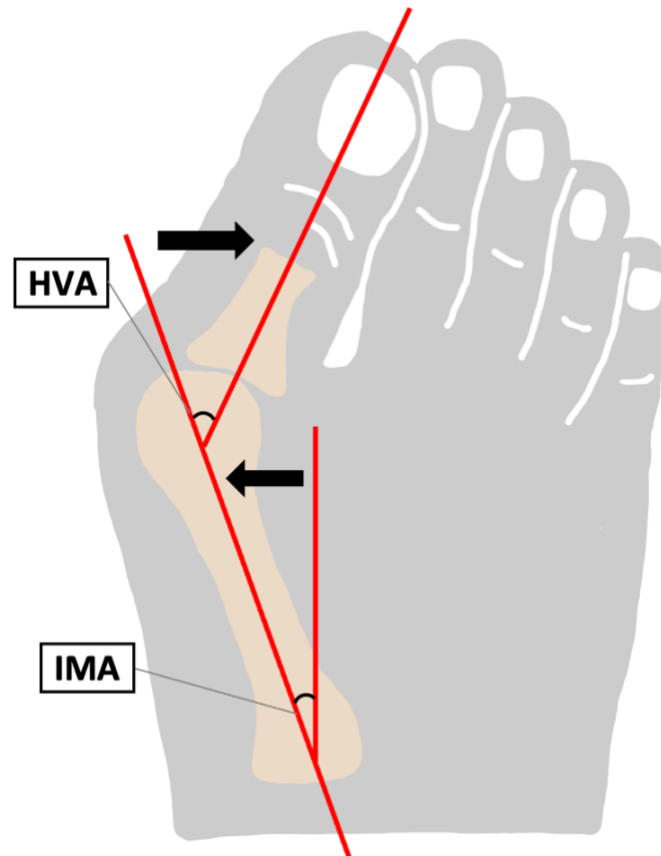


Figure 1. The axial plane deformity in hallux valgus with the varus deviation of the metatarsal and valgus deviation of the proximal phalanx.

For the 3D quantification of the HVA, a first and logic strategy is to copy the 2D strategy into a 3D version. To this end, the longitudinal inertia axes of the first metatarsal and proximal phalanx are used and they can be automatically generated. The HVA is defined as the angle between the projected longitudinal inertia axes of the first metatarsal and proximal phalanx on the ground plane (for the definition see: “Chapter 3: Development of a coordinate system”) (Figure 2). For the 3D quantification of the IMA, the longitudinal inertia axes of the first and second metatarsal are generated. The IMA is defined as the angle between the projected longitudinal inertia axes of the first and second metatarsal on the ground plane (for the definition see: “Chapter 3: Development of a coordinate system”) (Figure 3).

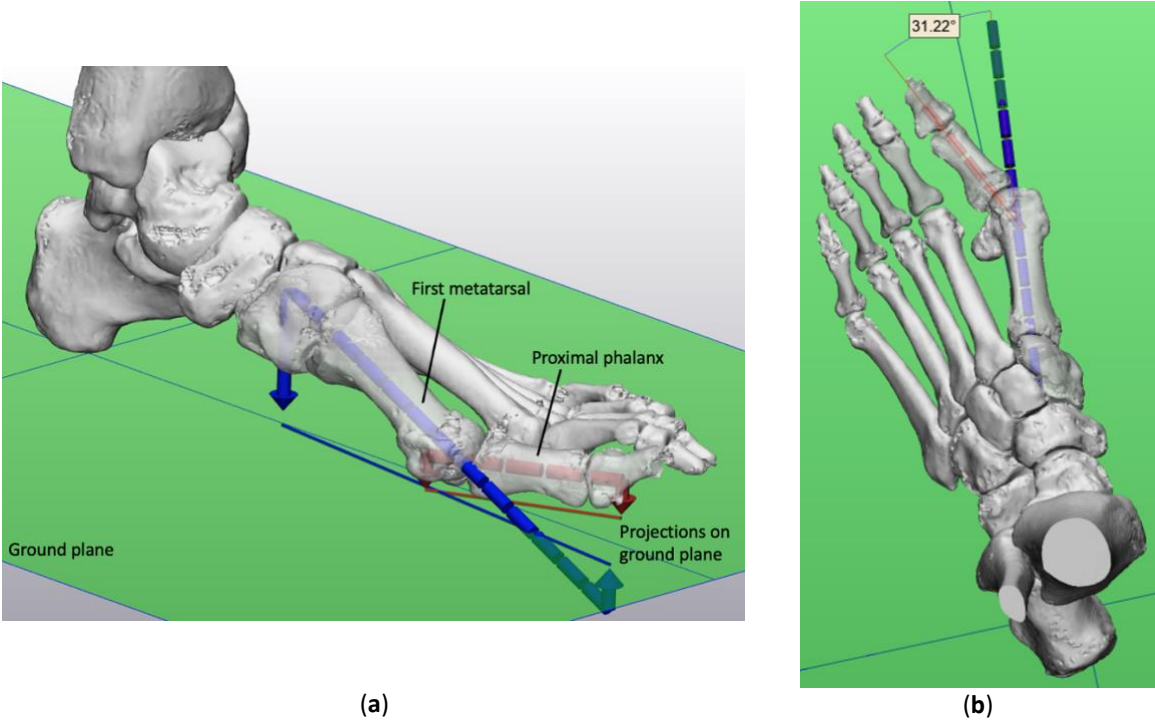


Figure 2. (a) The longitudinal inertia axes of the first metatarsal (blue dashed line) and proximal phalanx (red dashed line) projected on the ground plane (blue and red line); (b) The definition of the HVA on the ground plane.

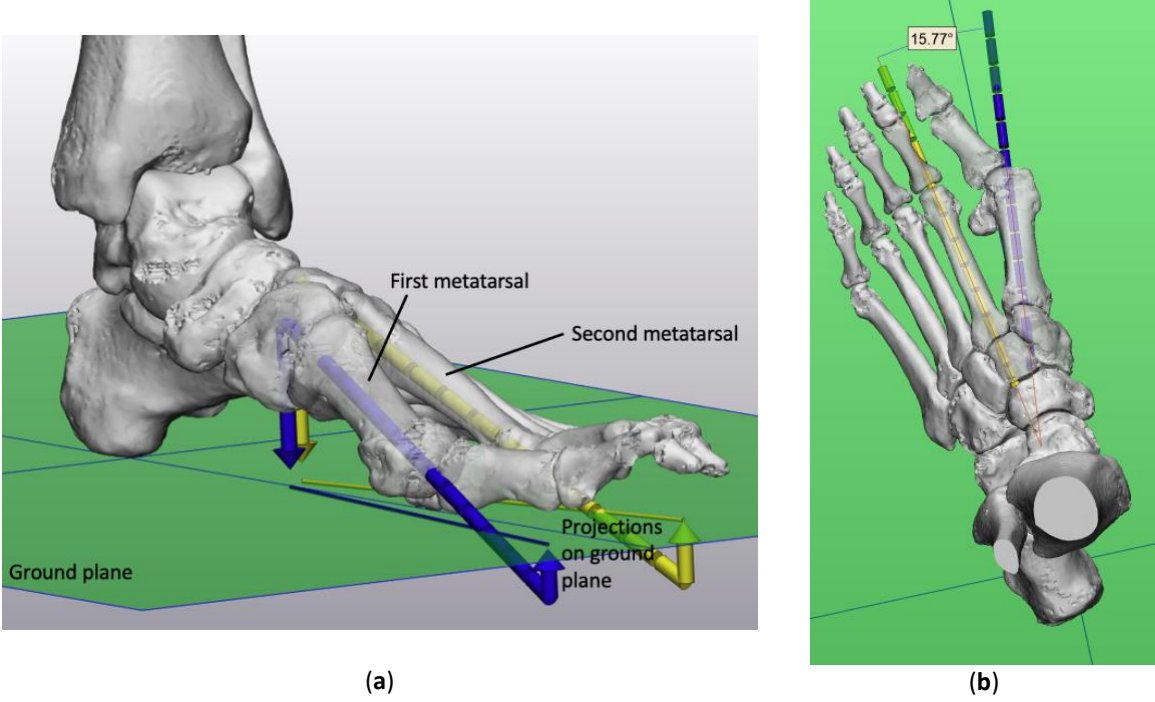


Figure 3. (a) The longitudinal inertia axes of the first metatarsal (blue dashed line) and second metatarsal (yellow dashed line) projected on the ground plane (blue and yellow line); (b) The definition of the IMA on the ground plane.

On the standard radiographic 2D images of the same foot shown in Figure 2 and 3, the orthopedic surgeon measured a HVA of 33.6° and an IMA of 19°. This demonstrates that there is a distinction between the 3D measurements of the HVA (31.2°) and IMA (15.8°) and the standard 2D measurements. These differences may affect the classification of the severity of the hallux valgus deformity and consequently the treatment plan. In this case, a measured IMA of 19° or 15.8° makes the difference between the classification of a severe (IMA > 18°) or moderate (IMA 11-18°) deformity. This leads to a different treatment approach. A proximal osteotomy (e.g. proximal Chevron and proximal wedge osteotomy) is used for more severe deformities and a midshaft osteotomy (e.g. Scarf osteotomy) is indicated for moderate to severe deformities.¹⁵⁻¹⁸ As a result, the measured differences in 2D and 3D may be clinically relevant as it may affect the choice and level of the osteotomy and consequently the outcome of the surgical hallux valgus correction.

4.3 Rotational deformity

The overall rotational deformity in hallux valgus refers to the rotation of the first metatarsal in the coronal plane (i.e., pronation of the first metatarsal).¹⁹ Pronation of the metatarsal occurs when the plantar portion of the first metatarsal faces the second metatarsal (Figure 4). The exact origin of the overall rotational deformity in hallux valgus is not fully understood.^{19,20} Most studies report a gross rotational deformity without specification of where it rotates.²¹ However, the main contributors to the overall rotational deformity in hallux valgus may be^{21,22}:

- Internal bone torsion of the first metatarsal (Figure 5a).
- Rotation at the first tarsometatarsal (TMT 1) joint (Figure 5b).

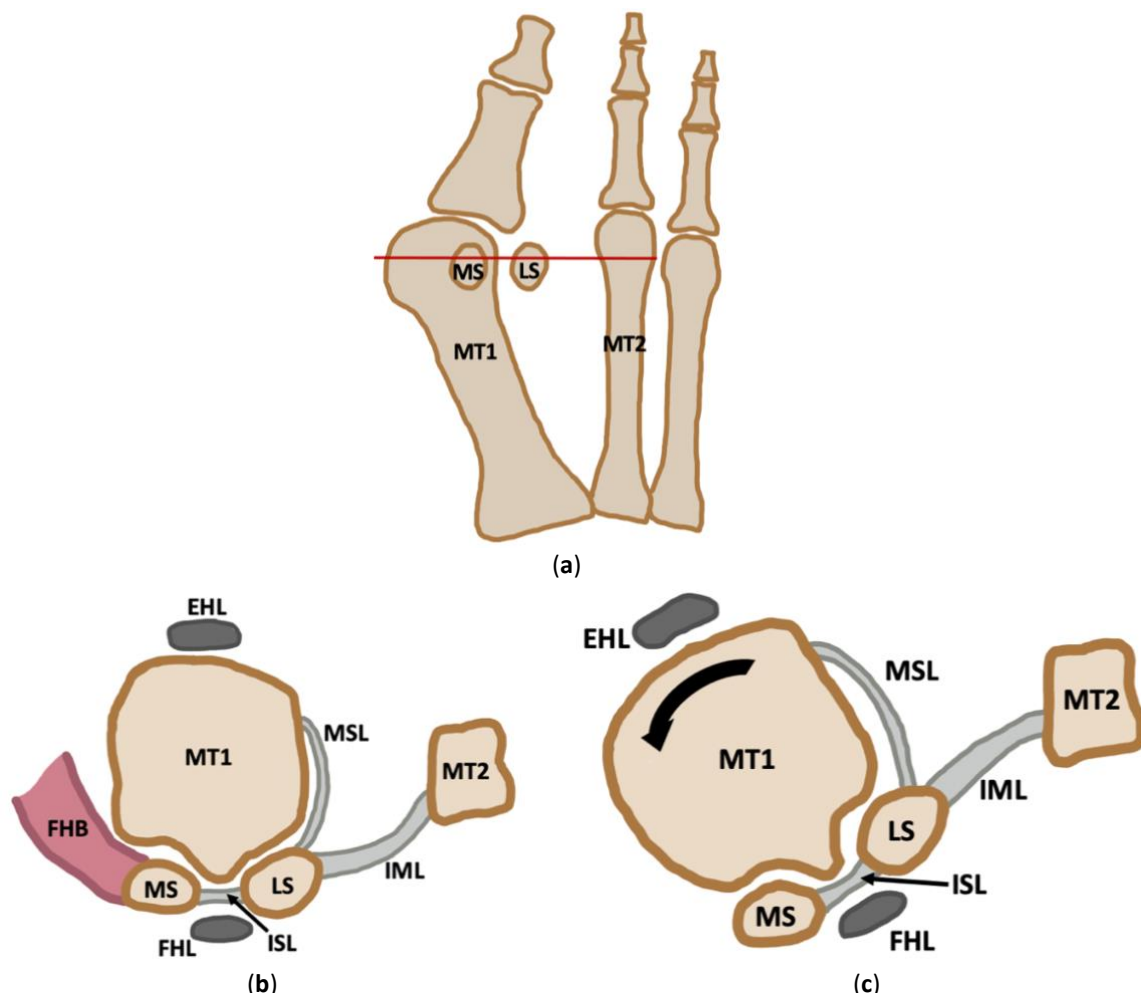


Figure 4. Illustration showing the pronation of the first metatarsal in the coronal plane. (a) Illustration of hallux valgus in the anteroposterior view; (b) Cross-section at the red line in Figure 4a, showing the non-pronated first metatarsal. (c) Cross-section at the red line in Figure 4a, showing the pronated first metatarsal. MT1: first metatarsal. MT2: second metatarsal. MS: medial sesamoid. LS: lateral sesamoid. IML: intermetatarsal ligament. MSL: metatarsosesamoid ligament. EHL: extensor hallucis longus tendon. FHL: flexor hallucis longus tendon. ISL: intersesamoid ligament. FHB: flexor hallucis brevis medial head.

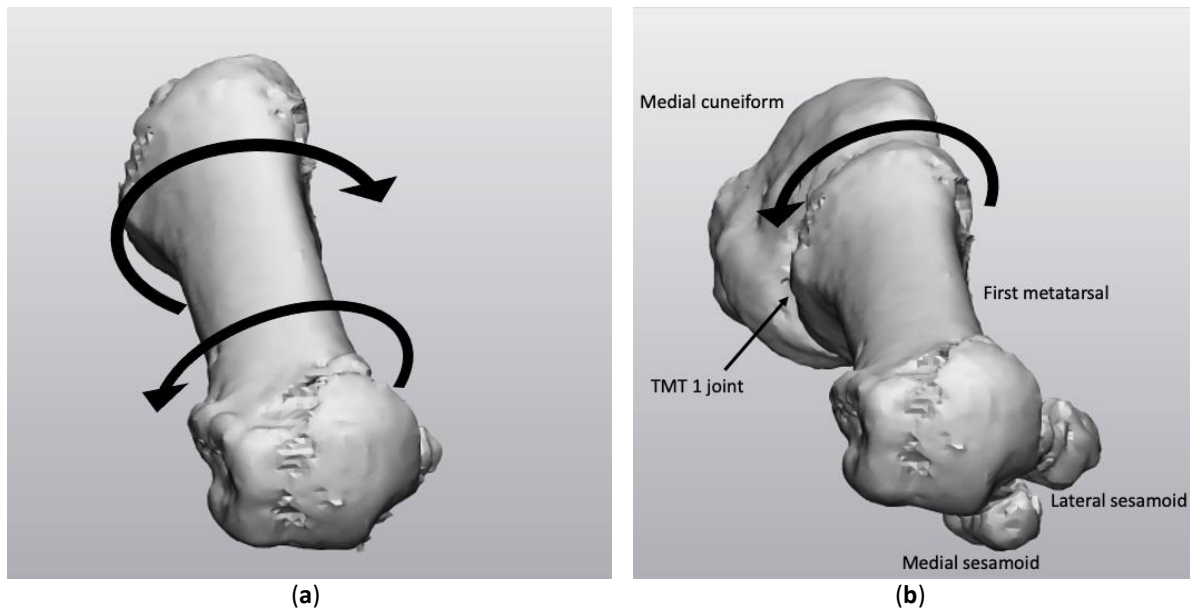


Figure 5. (a) Internal bone torsion of the first metatarsal; (b) Rotation at the first tarsometatarsal (TMT 1) joint.

Several studies have demonstrated that correction of the overall rotational deformity (e.g., by a rotating Lapidus procedure²³) minimized the risk of the common postoperative complication of recurrent hallux valgus.²⁴⁻²⁸ According to the Center Of Rotation of Angulation (CORA) method in deformity corrections,^{21,29} determining the exact deformity site will guide the subsequent surgical procedure. However, the overall rotational deformity is difficult to quantify on standard radiographic 2D imaging,^{24,30} necessitating a reproducible 3D quantification. Identifying the rotational component of the deformity might enable the full correction of hallux valgus.³¹

Not only is it difficult to quantify the overall rotational deformity using standard radiographic 2D imaging, Dutch guidelines also do not take this measurement into account.²³ However, it is possible to estimate the pronation of the first metatarsal in a radiographic weight-bearing anteroposterior (AP) image of the foot. This method uses the shape of the lateral contour of the first metatarsal head to divide pronation in three stages: 10° to 20°, 20° to 30°, > 30° (Table 1).^{4,13} The head takes on a progressively more rounded shape as it pronates due to the metatarsal condyles that become visible laterally. Stage one (10° to 20°) is classified as mild metatarsal pronation. The lateral metatarsal head shape is rounded, but a step from the condyle outline to the joint line can be seen. Stage two (20° to 30°) is classified as moderate metatarsal pronation. The metatarsal head is visible with a not perfectly rounded lateral border that is continuous laterally with the MTP joint (i.e., without any corners or steps in between). Stage three (> 30°) is classified as severe metatarsal pronation. The lateral head contour is completely circular, representing the complete profile of the lateral metatarsal condyle. It is not a logic strategy to copy this 2D method into a 3D version by projecting the contour of the first metatarsal head on the axial plane because it remains difficult to determine the exact degree of pronation.

Table 1. Estimation of the first metatarsal pronation in radiographic weight-bearing anteroposterior images of the foot.

Stage	0	1	2	3
Classification	-	Mild	Moderate	Severe
Rotation Range	0°	10° - 20°	20° - 30°	>30°
Lateral Head Shape	Sharp	Irregular	Rounded	Circular
Lateral Condyle Visibility	Not Visible	Notable	Observable	Apparent
Lateral Articular Surface Continuity	Non	Step-Off	Notched	Smooth
Image Examples				

4.3.1 Internal bone torsion of the first metatarsal

The internal bone torsion of the first metatarsal, the twisting of the first metatarsal about its longitudinal inertia axis, may be the main contributor to the overall rotational deformity in hallux valgus (Figure 5a).^{21,22} Wei et al. and Ota et al. introduced two 3D measurement methods to quantify the torsion of the first metatarsal head with respect to the proximal articular surface.^{21,32} By combining and altering these two methods, a new 3D measurement method is introduced using two vectors (Vector A and Vector B) to assess the internal bone torsion of the first metatarsal.

Vector A is created at the first metatarsal head. To start the construction of Vector A, the first metatarsal is viewed in the sagittal (yz-) plane of the coordinate system (Figure 6a). A plane is created perpendicular to this view by manually selecting two points proximal to the metatarsal head (Figure 6b), to separate the metatarsal head from the rest of the metatarsal at the position of the plane (Figure 6c). A cylinder is fitted through the first metatarsal head with its longitudinal axis defining Vector A (Figure 6d). To create a cylinder that fits through the first metatarsal head alone, the metatarsal head must be separated using the plane.

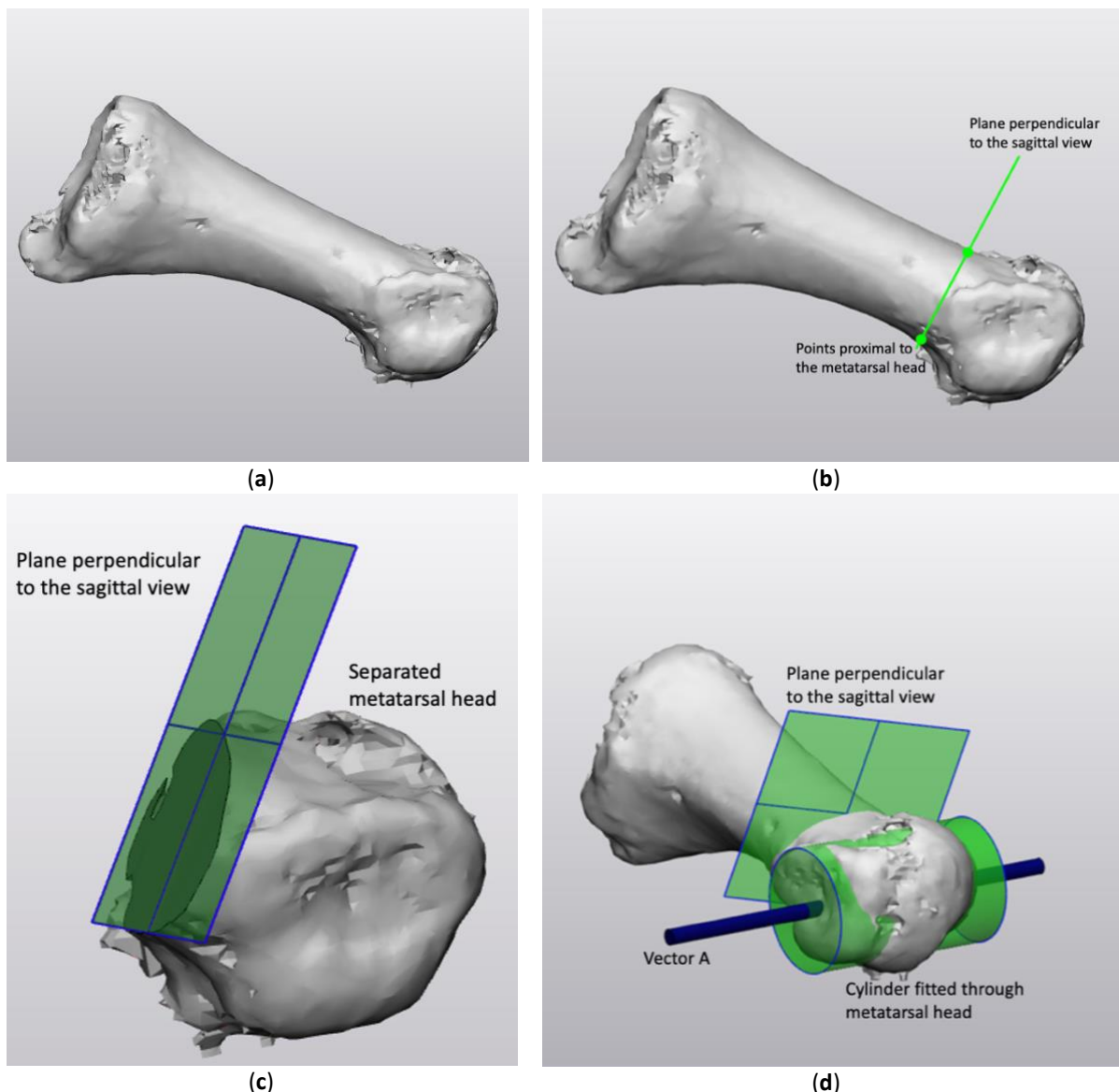


Figure 6. The construction of Vector A: (a) The first metatarsal in the sagittal view; (b) The plane constructed proximal to the first metatarsal head perpendicular to the sagittal view; (c) The separated metatarsal head; (d) The cylinder fitted through the first metatarsal head with its longitudinal axis defining Vector A.

Vector B is created at the proximal articular surface of the first metatarsal. To start the construction of Vector B, the longitudinal first metatarsal inertia axis is generated as the normal vector to a plane (Figure 7a). This plane is moved manually along the longitudinal axis to the location just beneath the proximal articular surface (Figure 7b). The proximal articular surface is then separated from the rest of the metatarsal at the position of the plane (Figure 7c). The most superior and inferior point of the proximal articular surface were automatically selected in the coordinate system orientation. Vector B is created connecting the most superior and inferior point on the proximal articular surface (Figure 7d).

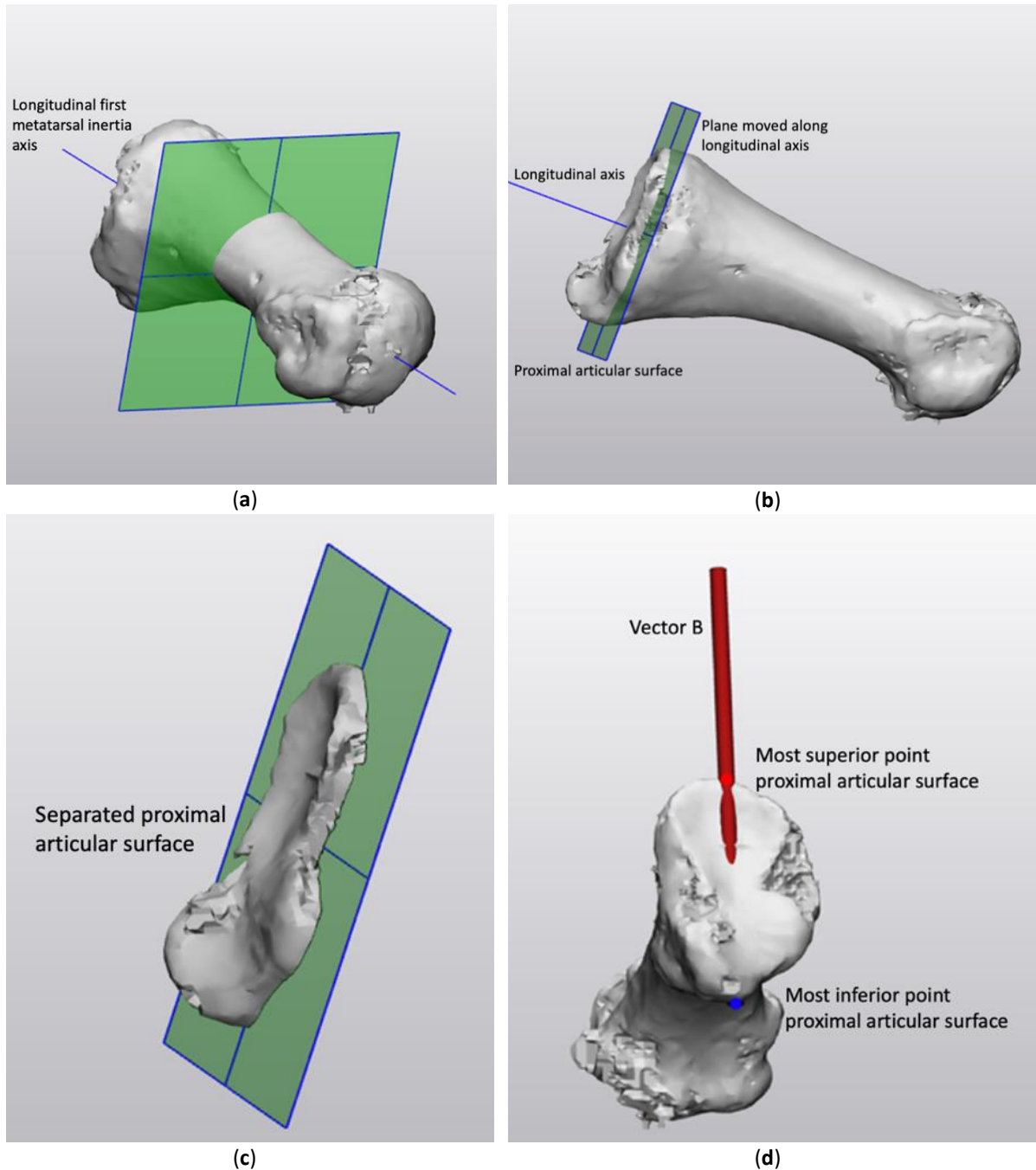


Figure 7. The construction of Vector B: (a) The longitudinal first metatarsal inertia axis as the normal vector to a plane; (b) The plane moved along the longitudinal axis towards the proximal articular surface; (c) The separated proximal articular surface of the first metatarsal; (d) The line connecting the automatically selected most superior and inferior point on the proximal articular surface defining Vector B.

The internal bone torsion angle of the first metatarsal is defined as the angle in the coronal plane between Vector A and Vector B minus 90° (Figure 8). In this case, the internal bone torsion angle of the first metatarsal is $101.8^\circ - 90^\circ = 11.8^\circ$. The three stages of pronation described by the 2D method to estimate the pronation of the first metatarsal may be used to quantify this angle. Based on these stages, this case will be quantified as mild metatarsal pronation (Table 1). It is advised that the internal bone torsion angle of the first metatarsal be reduced to less than 10° during preoperative planning of the hallux valgus correction. However, this needs further research.

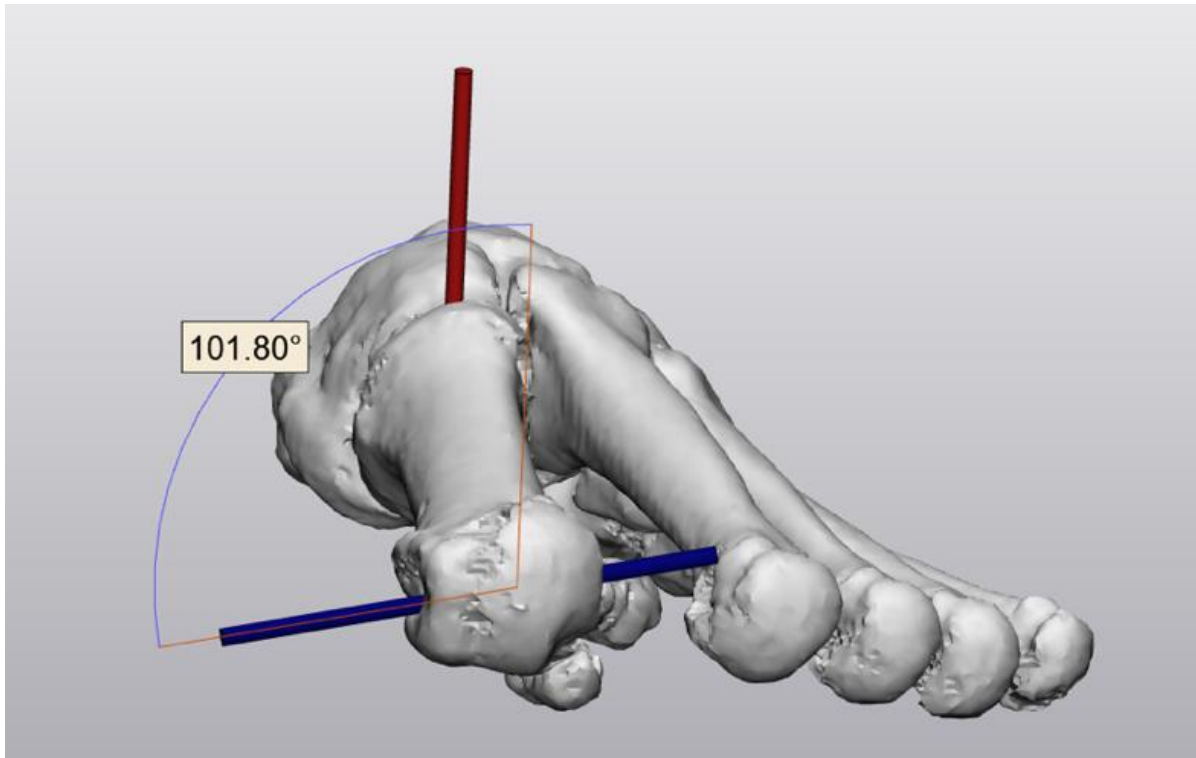


Figure 8. The definition of the angle between Vector A and Vector B in the coronal plane. The internal bone torsion angle of the first metatarsal: $101.8^\circ - 90^\circ = 11.8^\circ$.

4.3.2 Rotation at the TMT 1 joint

The rotation at the TMT 1 joint may also be the main contributor to the overall rotational deformity in hallux valgus (Figure 5b).^{21,22} Wei et al. introduced a 3D measurement method to quantify the rotation at the TMT 1 joint.²¹ By altering this method, a new 3D measurement method is introduced using two vectors (Vector B and Vector C) to assess the rotation at the TMT 1 joint.

Vector B is created at the proximal articular surface of the first metatarsal and its construction is described in “Chapter 4.3.1: Internal bone torsion”. Vector C is created at the distal end of the medial cuneiform. To start the construction of Vector C, the distal articular surface of the medial cuneiform is manually drawn (Figure 9a). Through this surface a plane is fitted (Figure 9b). This plane is moved manually along its normal vector to the location just beneath the distal articular surface (Figure 9c). The distal articular surface is then separated from the rest of the medial cuneiform at the position of the plane (Figure 9d). A plane is constructed in the middle of the distal articular surface, perpendicular to the coronal view by manually selecting two points (Figure 9e). Vector C is created connecting the automatically selected most lateral points on the superior and inferior distal articular surface of the medial cuneiform (Figure 9f).

The TMT 1 joint rotation angle was defined as the angle in the coronal plane between Vector B and Vector C (Figure 10). In this case, the TMT 1 joint rotation angle is 10.4° .

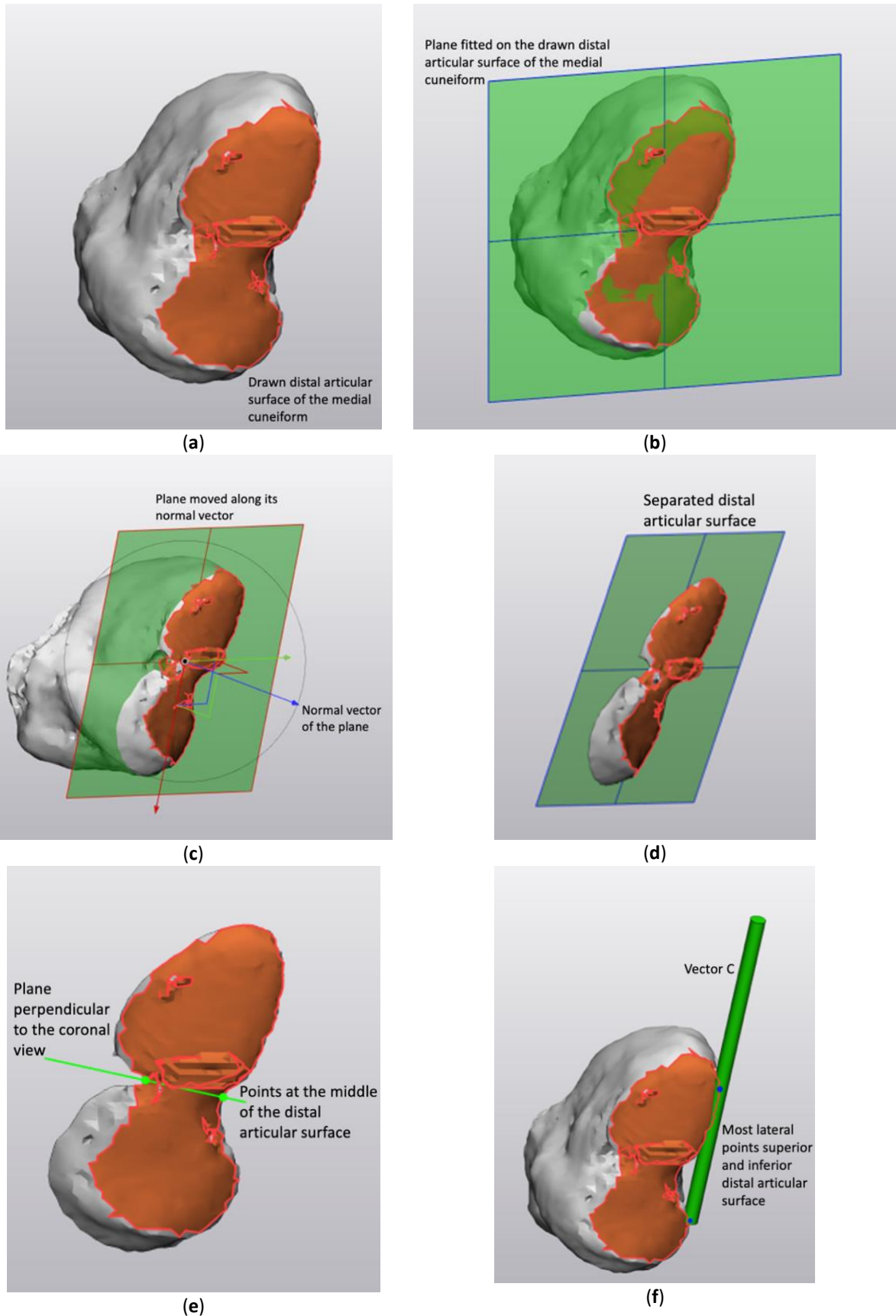


Figure 9. The construction of Vector C: (a) The drawing of the distal articular surface of the medial cuneiform; (b) The plane fitted on the drawing of the articular surface; (c) The plane moving along its normal vector towards the distal articular surface; (d) The separated distal articular surface of the medial cuneiform; (e) The plane constructed in the middle of the distal articular surface perpendicular to the coronal view; (f) The line connecting the automatically selected most lateral points on the superior and inferior distal articular surface defining Vector C.

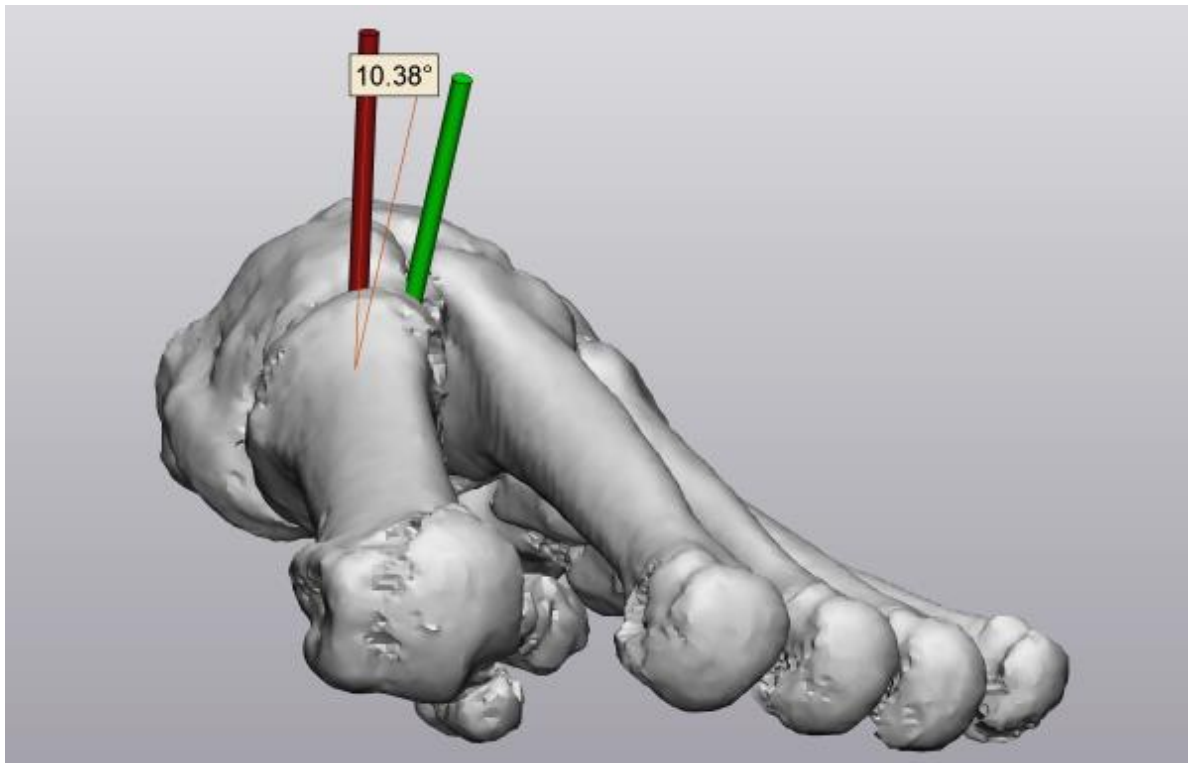


Figure 10. The definition of the TMT joint rotation angle between Vector B and Vector C in the coronal plane.

4.4 Future directions

This chapter explored potential methods for the 3D quantification of hallux valgus. Nevertheless, the 3D quantification need further development and finetuning to take one step further in the pathway to understanding hallux valgus in a 3D environment. Additional work is needed in several aspects of the deformity, such as quantification of possible sagittal plane deformities, the quantification of the sesamoid position, and maybe in the quantification of additional axial plane and rotational deformities.

A 3D quantification method can help in a better understanding of the effects of different surgical procedures in hallux valgus corrections. As a result, future research should investigate the effects of different procedures on the alignment. By simulating different procedures in 3-Matic, the effects can be quantified in a 3D environment. This may lead to a better understanding of the effects of each surgical hallux valgus procedure. By simulating every surgical hallux valgus procedure, an overview of the specific effects of each procedure can be created. This overview can be used by the orthopedic surgeon in clinical practice to make a more deliberate decision about the procedure selection. For instance, if two procedures are possible based on the severity of the hallux valgus deformity, the overview may show the desired alignment effect in only one procedure. This may lead to better procedure selection and consequently better surgical outcomes.

Furthermore, an adequate 3D quantification method for hallux valgus may enable the quantification of the deformity with more precision, accuracy and reproducibility compared to measurements on standard radiographic 2D imaging. The extremely complex multifactorial, and multiplanar hallux valgus deformity will be better understood by assessing hallux valgus deformities in clinical practice using a 3D quantification method. With a better understanding of the hallux valgus deformity, the orthopedic surgeon can make a more informed decision on the optimal surgical procedure. This may lead to better surgical outcomes.

Hallux valgus frequently affects the contralateral side; hence it cannot be used as a template during preoperative planning. Due to the possibility to quantify the desired position of the first metatarsal head in 3D, it may result in accurately preoperatively planned corrections in one or multiple planes. How the preoperative planning can be applied in hallux valgus corrections needs to be investigated in future studies.

For example, the IMA may be used as reference in the preoperative planning of hallux valgus corrections. The first metatarsal can be picked up and moved in space (rotated in the axial plane) until the IMA reaches the normal value of $< 9^\circ$ to correct the axial plane deformity (Figure 11). However, the use of the IMA in the preoperative planning of hallux valgus corrections will be complex for patients with metatarsus adductus. Metatarsus

adductus is an axial plane deformity characterized by adduction of all of the metatarsals (Figure 12).³³⁻³⁵ The prevalence of metatarsus adductus has been reported to be between 29% and 35% in patients with hallux valgus.³⁴ The IMA will not provide an accurate representation of the severity of the hallux valgus deformity because all of the metatarsals are adducted. This will narrow the gap between the first and second metatarsal. Future research should look into the effects of metatarsus adductus for the preoperative planning of hallux valgus corrections.

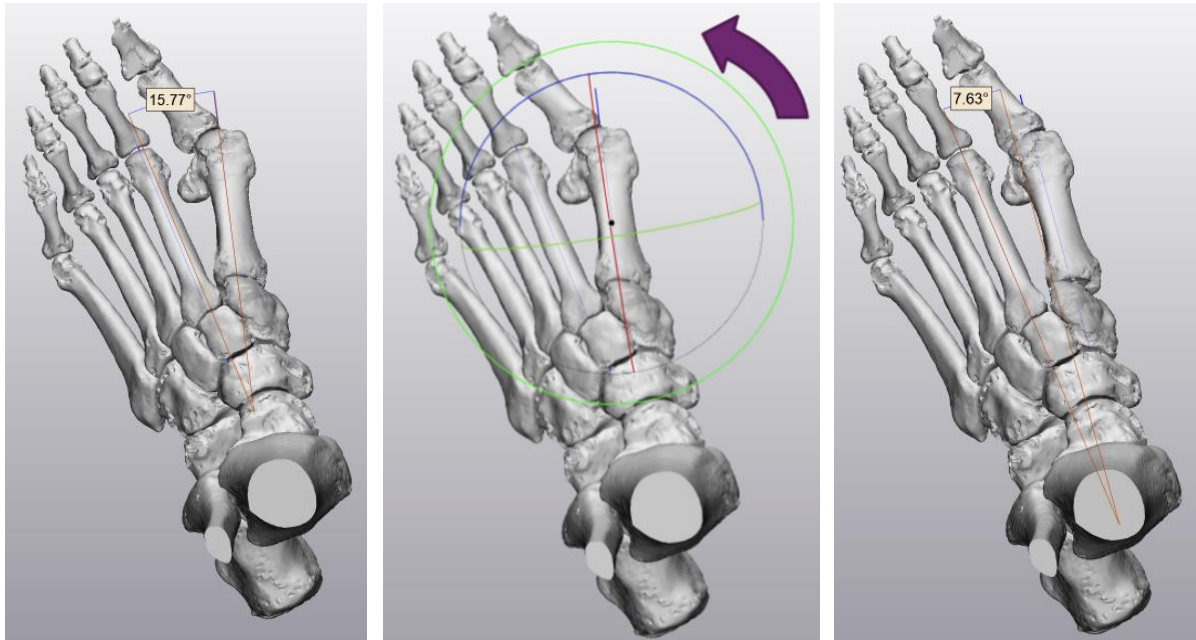


Figure 11. The use of the IMA in the surgical planning of hallux valgus corrections.



Figure 12. Illustration of hallux valgus with metatarsus adductus.

4.5 References

- 1 Barg, A.; Harmer, J.R.; Presson, A.P.; Zhang, C.; Lackey, M.; Saltzman, C.L. Unfavorable outcomes following surgical treatment of hallux valgus deformity: a systematic literature review. *J Bone Joint Surg Am.* 2018;100(18):1563-1573, doi:10.2106/JBJS.17.00975.
- 2 Lalevee, M.; de Cesar Netto, C.; ReSurg; Boubllil, D.; Coillard, J.Y. Recurrence rates with longer-term follow-up after hallux valgus surgical treatment with distal metatarsal osteotomies: a systematic review and meta-analysis. *Foot Ankle Int.* 2023;44(3):210-222, doi:10.1177/10711007231152487.
- 3 de Cesar Netto, C. From 2D to 3D: Understanding Hallux Valgus Deformity. *Foot Ankle Int.* 2023, doi:10.1177/10711007231180573.
- 4 Wagner, P.; Wagner, E. Role of Coronal Plane Malalignment in Hallux Valgus Correction. *Foot Ankle Clin.* 2019;25:69-77, doi:10.1016/j.fcl.2019.10.009.
- 5 Jia, J.; Li, J.; Qu, H.; Li, M.; Zhang, S.; Hao, J.; Gao, X.; Meng, X.; Sun, Y.; Hakonarson, H.; Zeng, X.; Xia, Q.; Li, J. New insights into hallux valgus by whole exome sequencing study. *Exp Biol Med (Maywood).* 2021;246(14):1607-1616, doi:10.1177/15353702211008641.
- 6 Gawande, K.B.; Mungikar, S.; Hotwani, R.; Ingle, S.; Kulkarni, C.A. Prevalence of Hallux Valgus in Normal Individuals. *J. Med. Pharm. Allied Sci.* 2021;10(4):3138-3141, doi:10.22270/jmpas.V10I4.1263.
- 7 Nix, S.; Smith, M.; Vicenzino, B. Prevalence of hallux valgus in the general population: a systematic review and meta-analysis. *J Foot Ankle Res.* 2010;3:1-9, doi:10.1186/1757-1146-3-21.
- 8 Saad, A.; Lyengar, K.P.; Fitzpatrick, J.; Azoopardi, C.; Panchal, H.; Botchu, R. The Linear Hallux Valgus Offset— A novel way to measure Hallux Valgus. *J Clin Orthop Trauma.* 2022;30, doi:10.1016/j.jcot.2022.101898.
- 9 Kakwani, M.; Kakwani, R. Current concepts review of hallux valgus. *J. Arthrosc. Jt. Surg.* 2021;8(3):222-230, doi:10.1016/j.jajs.2021.04.006.
- 10 Kuhn, J.; Alvi, F. Hallux Valgus. StatPearls. Treasure Island (FL). Available online: <https://www.ncbi.nlm.nih.gov/books/NBK553092/> (accessed on 30 June 2023).
- 11 Gutekunst, D.J.; Liu, L.; Ju, T.; Prior, F.W.; Sinacore, D.R. Reliability of clinically relevant 3D foot bone angles from quantitative computed tomography. *J Foot Ankle Res.* 2013;6:1-8, doi:10.1186/1757-1146-6-38.
- 12 Welck, M.J.; Al-Khudairi, N. Imaging of Hallux Valgus How to Approach the Deformity. *Foot Ankle Clin.* 2018;23:183-192, doi:10.1016/j.fcl.2018.01.002.
- 13 Hirschfeld, E.W.; Hirschfeld, P.W. in *Foot and Ankle Disorders* (Springer Cham, 2022).
- 14 Heineman, N.; Liu, G.; Pacicco, T.; Dessouky, R.; Wukich, D.K.; Chhabra, A. Clinical and imaging assessment and treatment of hallux valgus. *Acta Radiol.* 2019;61(1):56-66, doi:10.1177/0284185119847675.
- 15 Lin, J.; Bustillo, J. Surgical treatment of hallux valgus: a review. *Curr. opin. orthop.* 2007;18(2):112-117, doi:10.1097/BCO.0b013e328082e2b6.
- 16 Bertolo, F.; Pautasso, A.; Cuocolo, C.; Invernizzi, D.; Atzori, F. The Endolog technique for moderate to severe hallux valgus treatment: Clinical and radiographic analysis of 194 patients. *Foot Ankle Surg.* 2021;27(1):46-51, doi:10.1016/j.fas.2020.02.001
- 17 Wagner, E.; Ortiz, C. Osteotomy Considerations in Hallux Valgus Treatment Improving the Correction Power. *Foot Ankle Clin.* 2012;17(3):481-498, doi:10.1016/j.fcl.2012.06.007.
- 18 Smyth, N.; Aiyer, A. Introduction: Why Are There so Many Different Surgeries for Hallux Valgus? *Foot Ankle Clin.* 2018;23(2):171-182, doi:10.1016/j.fcl.2018.01.001.
- 19 Najefi, A.A.; Malhotra, K.; Patel, S.; Cullen, N.; Welck, M. Assessing the Rotation of the First Metatarsal on Computed Tomography Scans: A Systematic Literature Review. *Foot Ankle Int.* 2022;43(1):66-76, doi:10.1177/10711007211020676.
- 20 Cruz, E.P.; Wagner, F.V.; Henning, C.; Sanhudo, J.A.V.; Pagnussato, F.; Galia, C.R.;. Does Hallux Valgus Exhibit a Deformity Inherent to the First Metatarsal Bone? *J Foot Ankle Surg.* 2019;58(6):1210-1214, doi:10.1053/j.jfas.2018.09.031.
- 21 Wei, R.X.; Ko, V.M.C.; Chui, E.C.S.; Fu, B.S.C.; Hung, V.W.Y.; Yung, P.S.H.; Ling, S.K.K. Investigation on the Site of Coronal Deformities in Hallux Valgus. *Sci Rep.* 2023;13(1), doi:10.1038/s41598-023-28469-4.
- 22 Steadman, J.; Barg, A.; Saltzman, L. First Metatarsal Rotation in Hallux Valgus Deformity. *Foot Ankle Int.* 2021;42(4), doi:10.1177/1071100721997149.
- 23 Vereniging., Nederlandse Orthopaedische. Hallux Valgus. Federatie Medisch Specialisten. Available online: https://richtlijndatabase.nl/richtlijn/hallux_valgus/startpagina - hallux_valgus.html (accessed on 9 August 2023).

- 24 Seki, H.; Oki, S.; Suda, Y.; Takeshima, K.; Kokubo, T.; Nagura, T.; Ishii, K. Three-Dimensional Analysis of the First Metatarsal Bone in Minimally Invasive Distal Linear Metatarsal Osteotomy for Hallux Valgus. *Foot Ankle Int.* 2020;41(1):84-93, doi:10.1177/1071100719875222.
- 25 Dayton, P.; Feilmeier, M.; Kauwe, M.; Hirschi, J. Relationship of frontal plane rotation of first metatarsal to proximal articular set angle and hallux alignment in patients undergoing tarsometatarsal arthrodesis for hallux abducto valgus: a case series and critical review of the literature. *J Foot Ankle Surg.* 2013;52(3):348-354, doi:10.1053/j.jfas.2013.01.006.
- 26 DiDomenico, L.A.; Fahim, R.; Rollandini, J.; Thomas, Z.M. Correction of frontal plane rotation of sesamoid apparatus during the Lapidus procedure: a novel approach. *J Foot Ankle Surg.* 2014;53(2):248251, doi:10.1053/j.jfas.2013.12.002.
- 27 Kim, Y.; Kim, J.; Young, K.; Naraghi, R.; Cho, H.; Lee, S. A New Measure of Tibial Sesamoid Position in Hallux Valgus in Relation to the Coronal Rotation of the First Metatarsal in CT Scans. *Foot Ankle Int.* 2015;36(8):944-952, doi:10.1177/1071100715576994.
- 28 Yasuda, T.; Okuda, R.; Jotoku, T.; Shima, H.; Hida, T.; Neo, M. Proximal supination osteotomy of the first metatarsal for hallux valgus. *Foot Ankle Int.* 2015;36(6):696-704, doi:10.1177/1071100715572188.
- 29 Paley, D. in *Principles of Deformity Correction* (Springer, 2005).
- 30 Yamaguchi, S.; Sasho, T.; Endo, J.; Yamamoto, Y.; Akagi, R.; Sato, Y.; Takahashi, K. Shape of the lateral edge of the first metatarsal head changes depending on the rotation and inclination of the first metatarsal: a study using digitally reconstructed radiographs. *J Orthop Sci.* 2015;20(5):868-874, doi:10.1007/s00776-015-0749-x.
- 31 Wagner, E.; Wagner, P. Metatarsal Pronation in Hallux Valgus Deformity: A Review. *J Am Acad Orthop Surg Glob Res Rev.* 2020;4(6), doi:10.5435/JAAOSGlobal-D-20-00091.
- 32 Ota, T.; Nagura, T.; Kokubo, T.; Kitashiro, M.; Ogihara, N.; Takeshima, K.; Seki, H.; Suda, Y.; Matsumoto, M.; Nakamuro, M. Etiological factors in hallux valgus, a three-dimensional analysis of the first metatarsal. *J Foot Ankle Res.* 2017;10, doi:10.1186/s13047-017-0226-1.
- 33 Aiyer, A.A.; Shariff, R.; Ying, L.; Shub, J.; Myerson, M.S. Prevalence of Metatarsus Adductus in Patients Undergoing Hallux Valgus Surgery. *Foot Ankle Int.* 2014;35(12), doi:10.1177/1071100714551022.
- 34 Loh, B.; Chen, J.Y.; Yew, A.K.S.; Chong, H.C.; Yeo, M.G.H.; Tao, P.; Yeo, N.E.M.; Koo, K.; Singh, I.R. Prevalence of Metatarsus Adductus in Symptomatic Hallux Valgus and Its Influence on Functional Outcome. *Foot Ankle Int.* 2015;36(11):1316-1321, doi:10.1177/1071100715595618.
- 35 Lee, J.; Lee, H.S.; Jeong, J.J.; Seo, D.K.; Kee, T.; So, S.; Choi, Y.R. Distal chevron metatarsal osteotomy is a viable treatment option for hallux valgus with metatarsus adductus-multicentre retrospective study. *Int Orthop.* 2021;45(9):2261-2270, doi:10.1007/s00264-021-05117-y.



Chapter 5

General discussion

Chapter 5: General discussion

5.1 General discussion

This thesis focused on the optimization of surgical hallux valgus corrections by 1) obtaining repeatable and consistent perioperative images, and 2) transition the surgical procedure selection based upon a three-dimensional (3D) analysis and planning approach. In Chapter 2, a protocol for the use of perioperative fluoroscopy was developed and evaluated in a pilot study. In Chapter 3, a relevant global coordinate system in the foot was developed, to enable the transition towards a 3D hallux valgus planning approach. In Chapter 4, concepts of the 3D quantification of hallux valgus for future 3D planning were elaborated.

The clinical relevancy of Chapter 2 in this thesis is that the presented protocol enables the efficient and effective use of perioperative fluoroscopy during surgical hallux valgus corrections. Fluoroscopy is frequently used perioperatively to assist the orthopedic surgeon in hardware placement and the assessment of the deformity correction to prevent technical issues and provide good performances of the orthopedic surgeon.¹⁻⁵ This process requires repeatable and consistent perioperative images that correlate with the postoperative fluoroscopic images to visualize the achieved correction accurately. However, obtaining certain fluoroscopic images in a standardized fashion is difficult to achieve in foot and ankle surgery.³ The presented protocol fits into the workflow of the procedure and may obtain perioperative images that correlate with the postoperative images. The implementation of the protocol may improve the performances of the orthopedic surgeon, which could improve the outcomes of the surgical correction of hallux valgus.

Secondly, the clinical relevancy of Chapter 3 in this thesis is that the development of a global coordinate system in the foot enables the transition towards the 3D surgical planning of forefoot corrections. For the quantification of the absolute and relative position and orientation of the bones in the foot, a relevant and robust global coordinate system must be defined. However, due to the continuing absence of a standardized method, there have been a number of studies that defined their own global coordinate system with limitations that cannot be ignored.⁶⁻¹¹ The global coordinate system presented in Chapter 3 represents the preliminary step towards 3D preoperative planning of forefoot corrections. Future studies can be compared in a meaningful way if the proposed coordinate system is widely used. This may increase knowledge of forefoot deformities and revolutionize the treatment of complex multiplanar forefoot deformities, such as hallux valgus. Eventually, this may result in a better surgical procedure selection for hallux valgus corrections, and consequently in more consistently satisfactory, long-term outcomes.

The processes described in this thesis are not only clinically relevant, but also crucial for the optimization of surgical hallux valgus corrections. The developed global coordinate system enables the transition towards the 3D planning of surgical hallux valgus corrections. The implementation of the protocol together with future 3D preoperative planning may eventually lead to improved outcomes of surgical hallux valgus corrections. However, if only 3D preoperative planning of surgical hallux valgus is used in the future, surgical outcomes may still be suboptimal if the perioperative images does not correspond with the postoperative images. So, all the processes described in this thesis were important for the optimization of surgical hallux valgus corrections.

The technical physician is expected to play an important role in the optimization of surgical hallux valgus corrections since it strives to improve diagnostics and therapy through innovative use of technology in healthcare. Additional research for the optimization of surgical hallux valgus corrections, recommended later in the discussion, is expected to be done by a technical physician. The potential research result may contribute to the optimization of surgical hallux valgus corrections.

Besides those presented in Chapter 2, 3, and 4, this thesis has some general limitations that need to be discussed. First, one major factor that the 3D models in this thesis do not include, is the effect of weight-bearing. The used 3D models were acquired using CT scans with the patients in a splint and in supine position to provide the greatest possible replication of stance on a flat surface. However, weight-bearing CT scans (WBCT) have demonstrated significant advances including lower radiation exposure than with conventional CT, the ability to reliably perform standard measurements in a 3D environment, and a more complete and accurate evaluation of the hallux valgus deformity.¹²⁻¹⁹ This enables a better understanding of the positioning of the bones in the foot. Weight-bearing also widens the forefoot as the medial ray moves through the tarsometatarsal joint, increasing the IMA by 1.5° to 2.6°. ²⁰⁻²³ However, it is believed that this increase will be negligible if a sufficient replication of stance on a flat surface can be achieved during the CT scan of the foot. This indicates that when there is a

sufficient replication of stance on a flat surface, the measured Hallux Valgus Angle (HVA) and Intermetatarsal Angle (IMA) values in two-dimensional (2D) are comparable to the measurements in 3D. As a result, even if WBCT had been utilized, the outcomes of Chapters 2,3, and 4 would have been unaffected. In addition, there is a limited availability of WBCT. Further research may be able to use WBCT, however for the time being, conventional CT with sufficient replication of stance on a flat surface is expected to be adequate.

Secondly, despite the combined bony and soft tissue pathology of hallux valgus, the 3D models in this thesis do not incorporate soft tissues. The simulation of soft tissue interactions may be useful in preoperative planned hallux valgus corrections. This is because soft tissue procedures has been advocated as essential by certain authors to achieve satisfactory alignment and reduce the risk of recurrent hallux valgus.²⁴⁻²⁷ It may be possible to gain insights into how to restore the physiological balance of the soft tissues around the first metatarsophalangeal joint by simulating the effect of various osteotomies on soft tissue interactions. However, it is believed that this has no effect on surgical procedure selection. Since the current 3D models do not incorporate soft tissues, the concepts of the 3D quantification of hallux valgus are limited to the rigid deformity. This indicates that while the impact of soft tissue interactions cannot be simulated, osseous interventions can be planned. Even if the 3D models included soft tissues, the outcomes of Chapters 2,3, and 4 would have been unaffected.

While a protocol was developed to obtain repeatable and consistent perioperative images and the coordinate system enabled transition towards a 3D planning approach, more work should be done in the optimization of surgical hallux valgus corrections. Therefore, the following future directions are advised for the optimization of surgical hallux valgus corrections.

First, the concepts of the 3D quantifications of hallux valgus need further development and finetuning. Additional work is needed in several aspects of the deformity, such as quantification of possible sagittal plane deformities, the quantification of the sesamoid position and maybe in the quantification of additional axial plane and rotational deformities. This may enable further understanding of the hallux valgus deformity in a 3D environment, potential resulting in a better procedure selection.

Secondly, the effects of different surgical procedures in hallux valgus corrections needs to be investigated. With better understanding of the effects of different surgical procedure in hallux valgus corrections, future discussions on the choice and level of the osteotomy may be improved. By simulating different procedures in 3-Matic software (Materialise NV, Leuven, Belgium), the effects on the alignment can be quantified in a 3D environment. For example, a Chevron osteotomy can be mimicked by creating cutting planes. These cutting planes can be simulated with the cutting button in 3-Matic, separating the distal and proximal fractures and enabling the distal fragment to be placed laterally. The cutting planes will be altered in the coronal and/or axial plane for each simulation, to simulate multiplanar Chevron osteotomies. The potential methods for the 3D quantification of hallux valgus described in Chapter 4 will be used to quantify the effects on the alignment of each simulated osteotomy. This will potential result in a better understanding of the effects of each surgical hallux valgus procedure and better procedure selection.

Thirdly, future research needs to investigate methods to plan hallux valgus corrections in 3D and how it can be translated to the operating table. It is thought that the possibility to quantify the desired position of the first metatarsal head in 3-Matic software may result in accurately preoperatively planned corrections in one or multiple planes. However, a 3D planning process to achieve accurately planned corrections needs to be developed. When a specific hallux valgus correction is virtually planned, patient specific guides (PSGs) can make it possible to perform the planned correction efficient and accurate (Figure 1).²⁸ PSGs are surgical instruments custom made to perfectly fit onto the bone cortex. Common PSG functions include saw guidance, screw placement, and bone reposition guidance.^{29,30} A PSG can be designed in 3-Matic based on the preoperative planned correction containing a 3D model of the anatomy with indicated osteotomy planes, drilling trajectories, screw placements and/or bone reposition. However, the limited space and smaller incision required for surgical hallux valgus corrections make PSGs difficult to use. Surgical navigation (using augmented reality) can also replicate the planned correction, in contrast to the use of PSGs (Figure 2). Augmented reality makes the superimposition of a hologram to reality possible. It enables visual feedback of the surgical instrument (e.g., saw or K-wires) relative to the planned position, in order to achieve the planned correction. The limited space and smaller incision required for surgical hallux valgus corrections make augmented reality particularly beneficial. However, the technique is expensive and has a learning curve.³¹ Other alternatives may be robotic guided surgery. Robotic techniques have promising applications in orthopedic surgery. However, orthopedic robotic products are currently not focused on the foot.³² Therefore, it is necessary to investigate the best method if future planned hallux valgus corrections need to be translated precisely to the operating table.

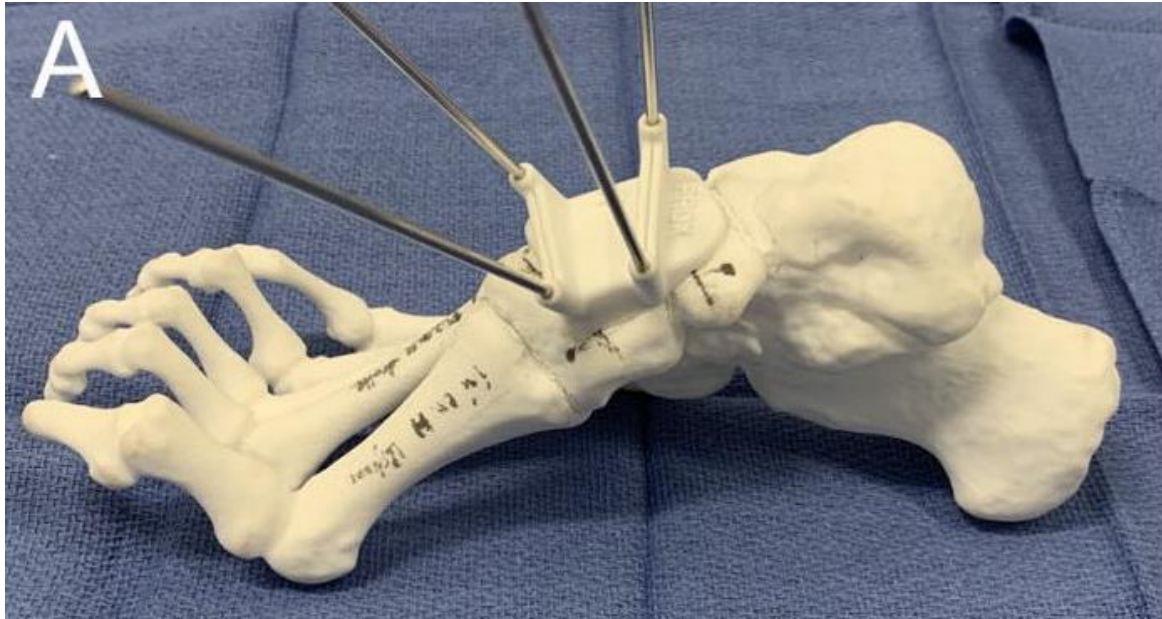


Figure 1. Example of a patient specific guide (PSG) designed by Dagneaux et al. for anterior midfoot tarsectomy.³³



Figure 2. Setup of experiments with augmented reality guided osteotomies in hallux valgus corrections adapted from Viehöfer et al.³¹ Left: Surgeon performing the osteotomy wearing augmented reality glasses. Right: Foot model with overlaying hologram.

Lastly, the ultimate goal of surgical hallux valgus correction optimization should be to identify the personalized correction that would be most effective for each patient. This might be accomplished by creating a digital dynamic twin model for each patient that includes both bones and soft tissues. If this existed, it would be possible to simulate how a surgical procedure would affect not only alignment of the bones, but also the distribution of forces among all relevant anatomical structures. This potential results in an optimized correction to reduce the common postoperative complication of recurrent hallux valgus.

In conclusion, this thesis presented a protocol for the efficient and effective use of perioperative fluoroscopy during surgical hallux valgus corrections that fits into the workflow of the procedure and may obtain perioperative images that correlate with the postoperative images. This may help to prevent technical issues during the procedure and improve the performances of the orthopedic surgeon. The developed global coordinate system in Chapter 3 enables the transition towards the 3D planning of surgical hallux valgus corrections. Although the concepts of the 3D quantifications of hallux valgus need further development and finetuning, a variety of future studies can be started to further optimize surgical hallux valgus corrections. This offers perspective to achieve consistent satisfactory, long-term outcomes.

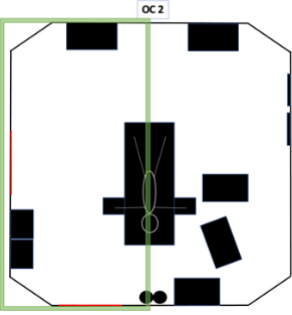
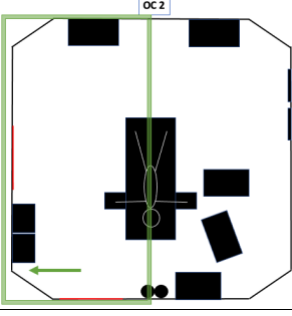

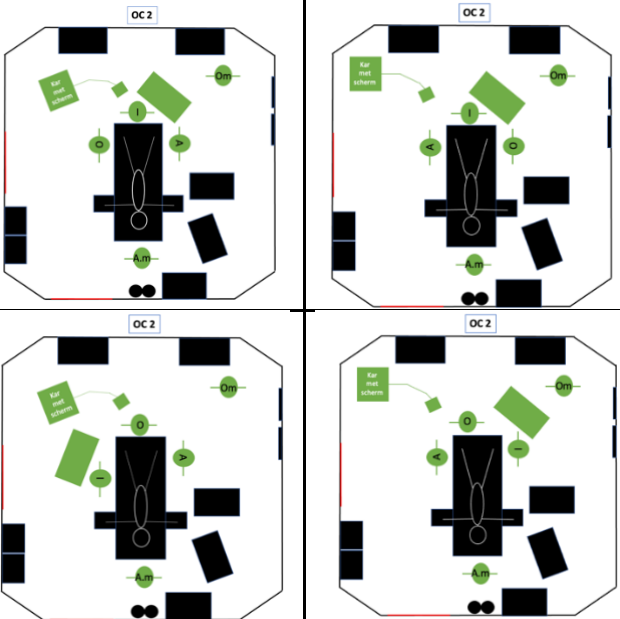
5.2 References

- 1 Saad, A.; Lyengar, K.P.; Fitzpatrick, J.; Azoopardi, C.; Panchal, H.; Botchu, R. The Linear Hallux Valgus Offset– A novel way to measure Hallux Valgus. *J Clin Orthop Trauma*. 2022;30, doi:10.1016/j.jcot.2022.101898.
- 2 Heineman, N.; Liu, G.; Pacicco, T.; Dessouky, R.; Wukich, D.K.; Chhabra, A. Clinical and imaging assessment and treatment of hallux valgus. *Acta Radiol*. 2019;61(1):56-66, doi:10.1177/0284185119847675.
- 3 Elliot, R.; Saxby, T.; Whitehouse, S. Intraoperative imaging in hallux valgus surgery. *Foot Ankle Surg*. 2012;18(1):19-21, doi:10.1016/j.fas.2011.01.006.
- 4 De Silva, T.; Punnoose, J.; Uneri, A.; Mahesh, M.; Goerres, J.; Jacobsen, M.; Ketcha, M.; Manbachi, A.; Vogt, S.; Kleinszig, G.; Khanna, A.; Wolinsky, J.; Siwerdsen, J.; Osgood, G. Virtual fluoroscopy for intraoperative C-arm positioning and radiation dose reduction. *J Med Imaging (Bellingham)*. 2018;5(1), doi:10.1117/1.JMI.5.1.015005.
- 5 Guyonnet, G.; Mulliez, A.; Fessy, M.; Besse, J. Prospective analysis of intraoperative radiation dose in foot and ankle surgery using mini-C-arm fluoroscopy. Continuous series of 1064 procedures. *Orthop Traumatol Surg Res*. 2021;107(6), doi:10.1016/j.otsr.2021.102994.
- 6 Cappozzo, A.; Catani, F.; Della Croce, U.; Leardini, A. Position and orientation in space of bones during movement: anatomical frame definition and determination. *Clin Biomech (Bristol, Avon)*. 1995;10(4):171-178, doi:10.1016/0268-0033(95)91394-t.
- 7 Green, C.; Fitzpatrick, C.; Fitzpatrick, D.; Stephens, M.; Quinlan, W.; Flavin, R. Definition of Coordinate System for Three-Dimensional Data Analysis in the Foot and Ankle. *Foot Ankle Int*. 2011;32(2):193-199, doi:10.3113/FAI.2011.0193.
- 8 Geng, X.; Wang, C.; Ma, X.; Wang, X.; Huang, J.; Zhang, C.; Xu, J.; Yang, J. Mobility of the first metatarsal-cuneiform joint in patients with and without hallux valgus: in vivo three-dimensional analysis using computerized tomography scan. *J Orthop Surg Res*. 2015;10:1-7, doi:10.1186/s13018-015-0289-2.
- 9 Ortolani, M.; Leardini, A.; Pavani, C.; Scicolone, S.; Girolami, M.; Bevoni, R.; Lullini, G.; Durante, S.; Berti, L.; Belvedere, C. Angular and linear measurements of adult flexible flatfoot via weight-bearing CT scans and 3D bone reconstruction tools. *Sci Rep*. 2021;11:1-13, doi:10.1038/s41598-021-95708-x.
- 10 Yoshioka, N.; Ikoma, K.; Kido, M.; Imai, K.; Maki, M.; Arai, Y.; Fujiwara, H.; Tokunaga, D.; Inoue, N.; Kubo, T. Weight-bearing three-dimensional computed tomography analysis of the forefoot in patients with flatfoot deformity. *J Orthop Sci*. 2016;21:154-158, doi:10.1016/j.jos.2015.12.001.
- 11 Modenese, L.; Renault, J.B. Automatic generation of personalised skeletal models of the lower limb from three-dimensional bone geometries. *J Biomech*. 2021;116:1-10, doi:10.1016/j.jbiomech.2020.110186.
- 12 de Carvalho, K.A.M.; Walt, J.S.; Ehret, A.; Tazegul, T.E.; Dibbern, K.; Mansur, N.S.B.; Lalevée, M.; de Cesar Netto, C. Comparison between Weightbearing-CT semiautomatic and manual measurements in Hallux Valgus. *Foot Ankle Surg*. 2022;28(4):518-525, doi:10.1016/j.fas.2022.02.014.
- 13 de Cesar Netto, C.; Richter, M. Use of Advanced Weightbearing Imaging in Evaluation of Hallux Valgus. *Foot Ankle Clin*. 2020;25(1):31-45, doi:10.1016/j.fcl.2019.10.001.
- 14 Collan, L.; Kankare, J.A.; Mattila, K. The biomechanics of the first metatarsal bone in hallux valgus: a preliminary study utilizing a weight bearing extremity CT. *Foot Ankle Surg*. 2013;19(3):155-161, doi:10.1016/j.fas.2013.01.003.
- 15 Welck, M.J.; Singh, D.; Cullen, N.; Goldberg, A. Evaluation of the 1st metatarso-sesamoid joint using standing CT - The Stanmore classification. *Foot Ankle Surg*. 2018;24(4):314-319, doi:10.1016/j.fas.2017.03.005.
- 16 Barg, A.; Bailey, T.; Richter, M.; de Cesar Netto, C.; Lintz, F.; Burssens, A.; Phisitkul, P.; Hanrahan, C.J.; Saltzman, C.L. Weightbearing Computed Tomography of the Foot and Ankle: Emerging Technology Topical Review. *Foot Ankle Int*. 2018;39(3):376-386, doi:10.1177/1071100717740330.
- 17 Richter, M.; Seidl, B.; Zech, S.; Hahn, S. PedCAT for 3D-imaging in standing position allows for more accurate bone position (angle) measurement than radiographs or CT. *Foot Ankle Surg*. 2014;20(3):201-207, doi:10.1016/j.fas.2014.04.004.
- 18 Lintz, F.; de Cesar Netto, C.; Barg, A.; Burssens, A.; Richter, M.; Weight Bearing CT International Study Group. Weight-bearing cone beam CT scans in the foot and ankle. *EFORT Open Rev*. 2018;3(5):278-286, doi:10.1302/2058-5241.3.170066.
- 19 Lôbo, C.F.T.; Bordalo-Rodrigues, M. Weight-Bearing Computed Tomography International Study Group. WEIGHT-BEARING CONE BEAM CT SCANS AND ITS USES IN ANKLE, FOOT, AND KNEE: AN UPDATE ARTICLE. *Acta Ortop Bras*. 2021;29(2):105-110, doi:10.1590/1413-785220212902236939.

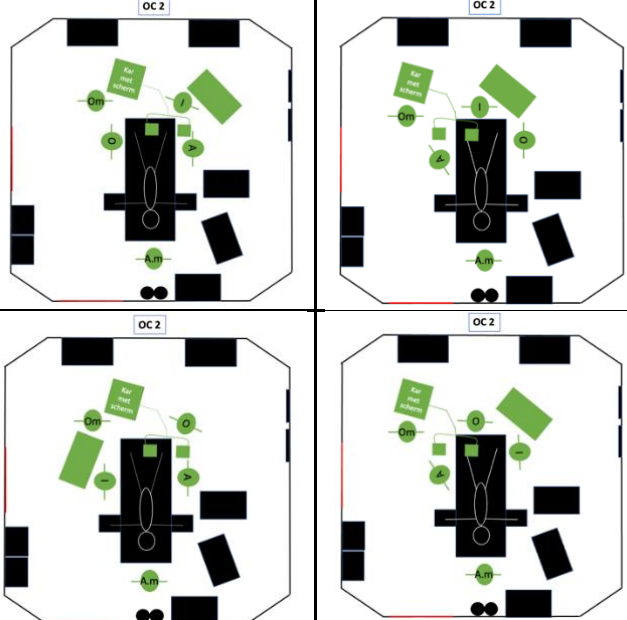
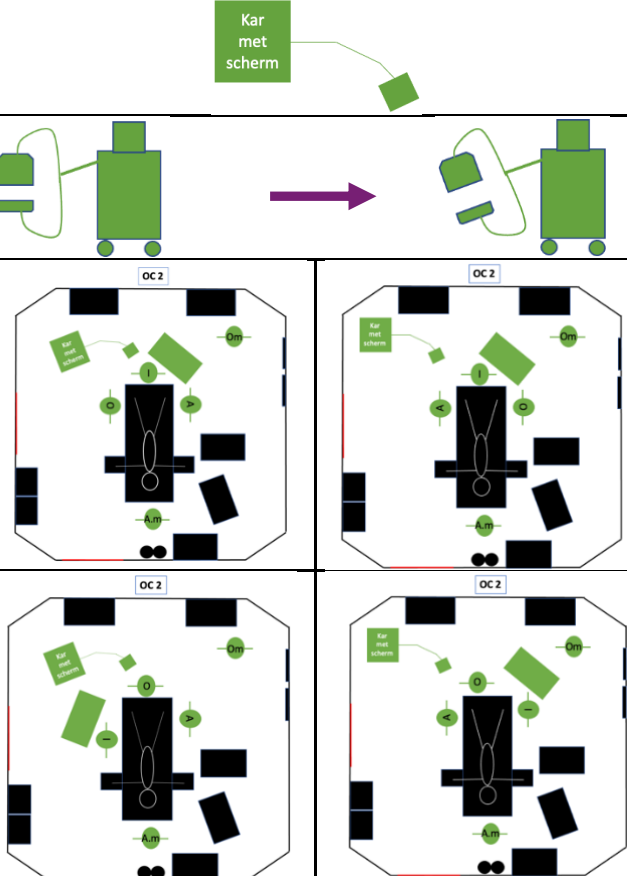
- 20 Van der Woude, P.; Keizer, S.; Wever-Korevaar, M.; Thomassen, B. Intra- and Interobserver Agreement in Hallux Valgus Angle Measurements on Weightbearing and Non-Weightbearing Radiographs. *Foot Ankle Surg.* 2019;58(4):706-712.
- 21 Fuhrmann, R.; Layher, F.; Wetzell, W. Radiographic Changes in Forefoot Geometry with Weightbearing. *Foot Ankle Int.* 2003;24(4):326-331, doi:10.1177/107110070302400404.
- 22 Tanaka, Y.; Takakura, Y.; Takaoka, T.; Akiyama, K.; Fujii, T.; Tamai, S. Radiographic Analysis of Hallux Valgus in Women on Weightbearing and Nonweightbearing. *Clin Orthop Relat Res.* 1997;336:186-194, doi:10.1097/00003086-199703000-00026.
- 23 Boszczyk, A.; Kwapisz, S.; Kicinski, M.; Kordasiewicz, B.; Liszka, H. Non-weightbearing compared with weightbearing x-rays in hallux valgus decision-making. *Skeletal Radiol.* 2020;49(9):1441-1447, doi:10.1007/s00256-020-03441-9.
- 24 Izzo, A.; Vallefucio, S.; Basso, M.A.; Ray, R.; Smeraglia, F.; Cozzolino, A.; Mariconda, M.; Bernasconi, A. Role of lateral soft tissue release in percutaneous hallux valgus surgery: a systematic review and meta-analysis of the literature. *Arch Orthop Trauma Surg.* 2022;143(7):3997-4007, doi:10.1007/s00402-022-04693-x.
- 25 Schneider, W. Distal soft tissue procedure in hallux valgus surgery: biomechanical background and technique. *Int Orthop.* 2013;37(9):1669 - 1675, doi:10.1007/s00264-013-1959-5.
- 26 Augoyard, R.; Largey, A.; Munoz, M.A.; Canovas, F. Efficacy of first metatarsophalangeal joint lateral release in hallux valgus surgery. *Orthop Traumatol Surg Res.* 2013;99(4):425-431, doi:10.1016/j.otsr.2013.01.009.
- 27 Seo, J.H.; Lee, H.S.; Choi, Y.R.; Park, S.H. Distal chevron osteotomy with lateral release for moderate to severe hallux valgus patients aged sixty years and over. *Int Orthop.* 2020;44(6):1099-1105, doi:10.1007/s00264-020-04562-5.
- 28 Wirth, S.H.; Espinose, N. The Use of Virtual Planning and Patient-specific Guides to Correct Complex Deformities of the Foot and Ankle. *Foot Ankle Clin.* 2020;25(2):257-268, doi:10.1016/j.fcl.2020.02.004.
- 29 Popescu, D.; Laptoiu, D. Rapid prototyping for patient-specific surgical orthopaedics guides: A systematic literature review. *Proc Inst Mech Eng H.* 2016;230(6):495-515, doi:10.1177/0954411916636919.
- 30 Popescu, D.; Laptoiu, D. Design and 3D printing customized guides for orthopaedic surgery – lessons learned. *Rapid Prototyp J.* 2018;24(5):901-913, doi:10.1108/RPJ-05-2017-0099.
- 31 Viehöfer, A.F.; Wirth, S.H.; Zimmermann, S.M.; Jaberg, L.; Dennler, C.; Fürnstahl, P.; Farshad, M. Augmented reality guided osteotomy in hallux Valgus correction. *BMC Musculoskelet Disord.* 2020;21, doi:10.1186/s12891-020-03373-4.
- 32 Li, C.; Wang, L.; Perka, C.; Trampuz, A. Clinical application of robotic orthopedic surgery: a bibliometric study. *BMC Musculoskelet Disord.* 2021;22(1), doi:10.1186/s12891-021-04714-7.
- 33 Dagneaux, L.; Canovas, F. 3D Printed Patient-Specific Cutting Guide for Anterior Midfoot Tarsectomy. *Foot Ankle Int.* 2020;41(2):211-215, doi:10.1177/1071100719882723.

Appendix

Appendix A: Protocol for the use of perioperative fluoroscopy during surgical hallux valgus corrections

Stappen	Afbeeldingen		Verantwoordelijkheden B= beslissen, U= uitvoeren
	Rechtervoet	Linkervoet	
1. Plaatsen C-boog Plaats de C-boog aan de <u>linkerzijde</u> van de operatiekamer.			U: operatieassistenten
2. Opstarten C-boog Stop de stekker van de C-boog in het dichtstbijzijnde stopcontact en start C-boog verder op.			U: omloop
3. Zet C-boog in startvorm Zorg dat de detector en röntgenbuis in een flauwe C bocht is verbonden met de kar. Op de afbeeldingen zijn de bovenaanzichten van de C-boog te zien.			U: omloop
4. Plaats C-boog in startpositie Nadat de opdektafel de operatiekamer is binnengereden, plaats de C-boog op de juiste startpositie. Zorg dat de detector en röntgenbuis van de C-boog in het plenum staat. Op de afbeeldingen zijn per voet de twee situaties weergegeven die passen bij de operatie aanpak van de twee orthopeden.			U: omloop
5. Steriel afdekken C-boog Dek de C-boog steriel af met de daar bijbehorende hoes.			U: omloop en instrumenterende

<p>6. Indraaien C-boog Wanneer een röntgenopname moet worden gemaakt, draait de omloop de C-boog in.</p> <p>De omloop duwt de C-boog vanuit de kar in een flauwe c-bocht richting de operatietafel met de detector op de hoogte van de operatietafel. De assistent kan hierin helpen door de C-boog bij de steriele hoes aan te pakken.</p> <p>Zorg hierbij dat orthopeed het scherm goed kan zien en houd de steriliteit in acht.</p>			<p>B: orthopeed U: omloop, assistent</p>
<p>7. Draai detector en röntgenbuis Draai de detector en röntgenbuis met ongeveer 20 tot 30 graden.</p>			<p>U: instrumenterende</p>
<p>8. Maken AP opname De assistent of orthopeed laat de voet aan de zijkant van de tafel hangen en plaatst de voorvoet in het midden van de detector.</p> <p>De omloop drukt op het voetpedaal om de röntgenopname te maken.</p> <p>Als de gewenste röntgenopname is gemaakt plaatst de assistent of orthopeed de voet terug op de operatietafel.</p> <p>Als het maken van een goede röntgenopname niet gaat, wordt aangeraden om gebruik te maken van de laser op de C-boog.</p> <p>Probeer bij het maken van de AP opnames om zo min mogelijk van positie te ruilen en houd de steriliteit in acht.</p>			<p>B: orthopeed U: assistent, omloop, orthopeed</p>
<p>9. C-boog in laterale opname positie De omloop trekt de C-boog bij de kar iets van de operatietafel vandaan. De assistent zet de detector en röntgenbuis weer in de neutrale positie en draai hierna de C-arm om een laterale opname te kunnen maken.</p> <p>De omloop duwt vanuit de kar de detector en röntgenbuis boven de operatietafel. De assistent kan hierin helpen door de C-boog bij de steriele hoes aan te pakken.</p>			<p>U: omloop, assistent</p>

<p>10. Maken laterale opname De assistent of orthopeed plaatst de voet tegen het midden van de detector aan.</p> <p>De omloop drukt op het voetpedaal om de röntgenopname te maken.</p> <p>Als het maken van een goede röntgenopname niet gaat, wordt aangeraden om gebruik te maken van de laser op de C-boog.</p> <p>Probeer bij het maken van de laterale opnames om zo min mogelijk van positie te ruilen en houd de steriliteit in acht.</p>		<p>B: orthopeed U: assistent, omloop, orthopeed</p>
<p>11. Zet C-boog terug in startvorm en uitdraaien De omloop trekt de C-boog bij de kar iets van de operatietafel vandaan. De assistent zet de detector en röntgenbuis weer in de neutrale positie. Draai de detector en röntgenbuis met ongeveer 20 tot 30 graden.</p> <p>De omloop plaatst de C-boog weer op de juiste startpositie. Zorg dat de detector en röntgenbuis van de C-boog in het plenum blijft staan.</p>		<p>U: omloop, assistent</p>
<p>12. Herhaal stap 6 t/m 10 bij nieuwe röntgenopnames</p>		<p>B: orthopeed U: assistent, omloop, orthopeed</p>

Appendix B: Definitions of two different coordinate systems

The two coordinate systems with the most varied strategies were discussed in “Chapter 3: Development of a coordinate system”, the definitions of the other two coordinate systems (CS3 and CS4) are presented in this section.

To start the construction of CS3, the facies superior of the trochlea tali was manually drawn (Figure 1a). Through this surface a cylinder was fitted with its longitudinal axis intersecting a point on the medial talus (MT). The cylinder was translated along its longitudinal axis towards the most prominent point on the lateral talus (MLT). The line connecting MT and MLT defines the direction of the x-axis, as the normal vector to a sagittal plane (Figure 1b). The Origin (O) was defined as the midpoint between MT and MLT (Figure 1c). The y-axis was defined as follows. First the longitudinal talus inertia axis was generated (Figure 1d) and at the intersection point with the cylinder (IPC), an additional line parallel to the x-axis was created (Figure 1e). The y-axis runs from the Origin to the intersection point of the additional line with a sagittal plane (IPS) (Figure 1f). The z-axis was orthogonal to the x- and y-axis (Figure 2).

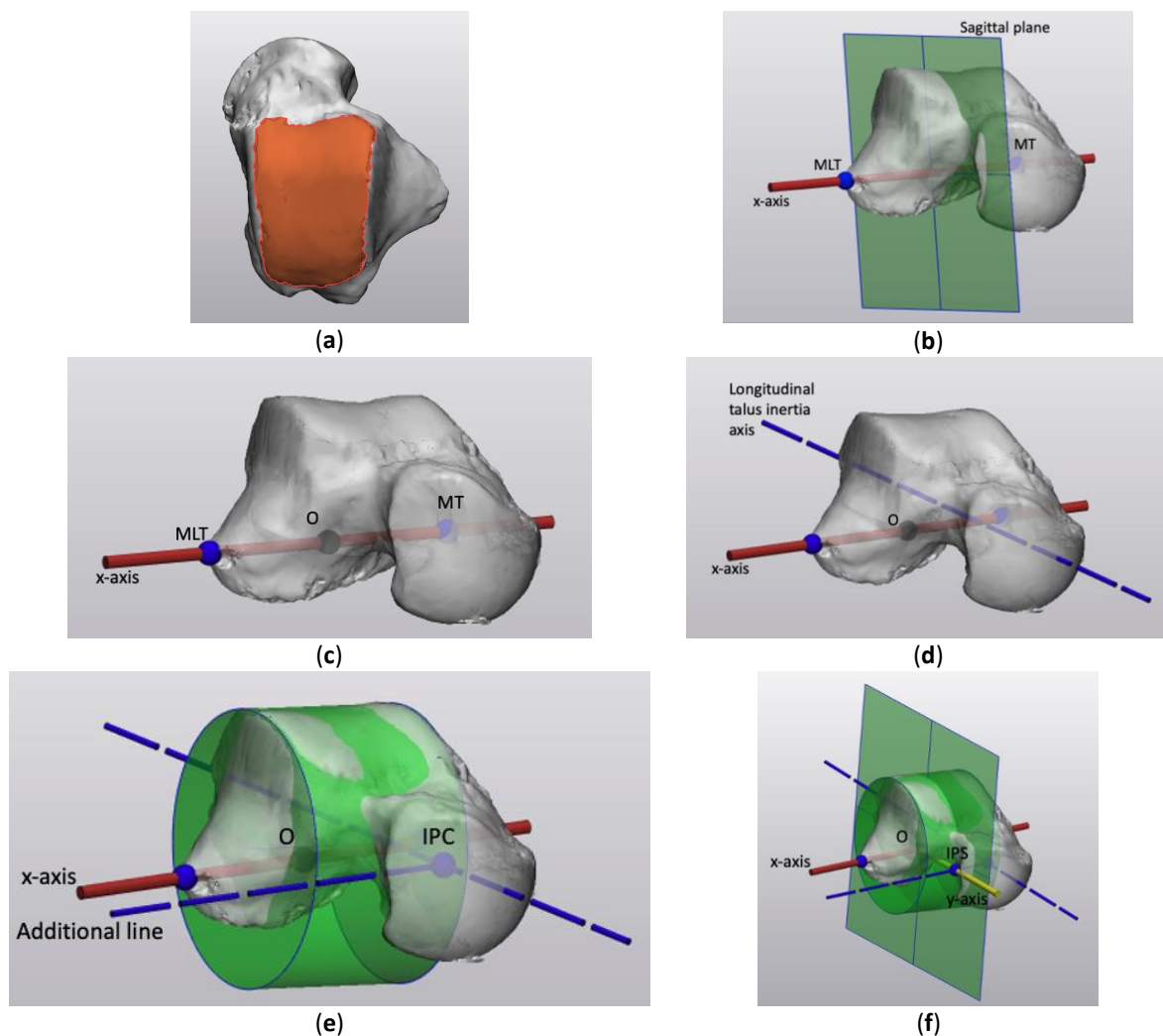


Figure 1. The construction of CS3: (a) Axial view of the talus with the drawing of the facies superior of the trochlea tali; (b) Illustration of the talus with the line connecting the point on the medial talus (MT) and most lateral point on the talus (MLT) defining the direction of the x-axis (red line), as the normal vector to a sagittal plane; (c) Illustration of the talus and the Origin, as the midpoint of MT and MLT, without the fitted cylinder and sagittal plane; (d) Illustration of the talus and its longitudinal inertia axis without the fitted cylinder and sagittal plane; (e) Illustration of the talus and its longitudinal inertia axis intersecting the cylinder (IPC) without the sagittal plane. An additional parallel to the x-axis was created; (f) Illustration of the talus with the y-axis running from the Origin (O) to the intersection point of the additional line with the sagittal plane (IPS).

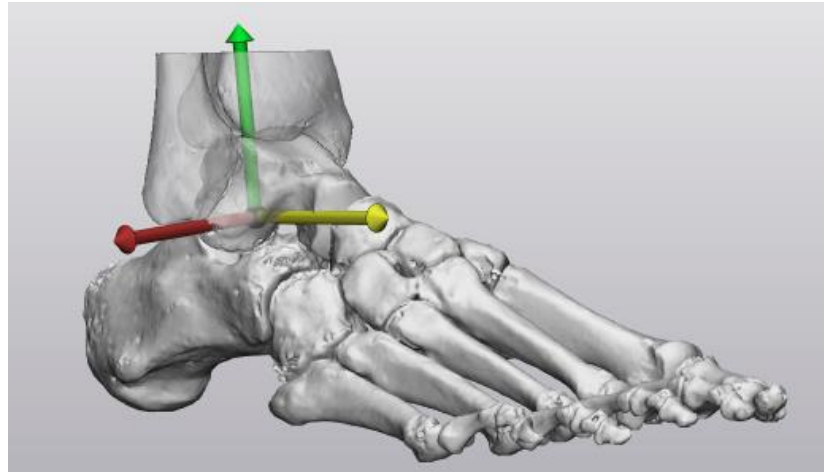


Figure 2. The axes of the global coordinate system of CS3 centered at the origin: x-axis (red), y-axis (yellow), z-axis (green).

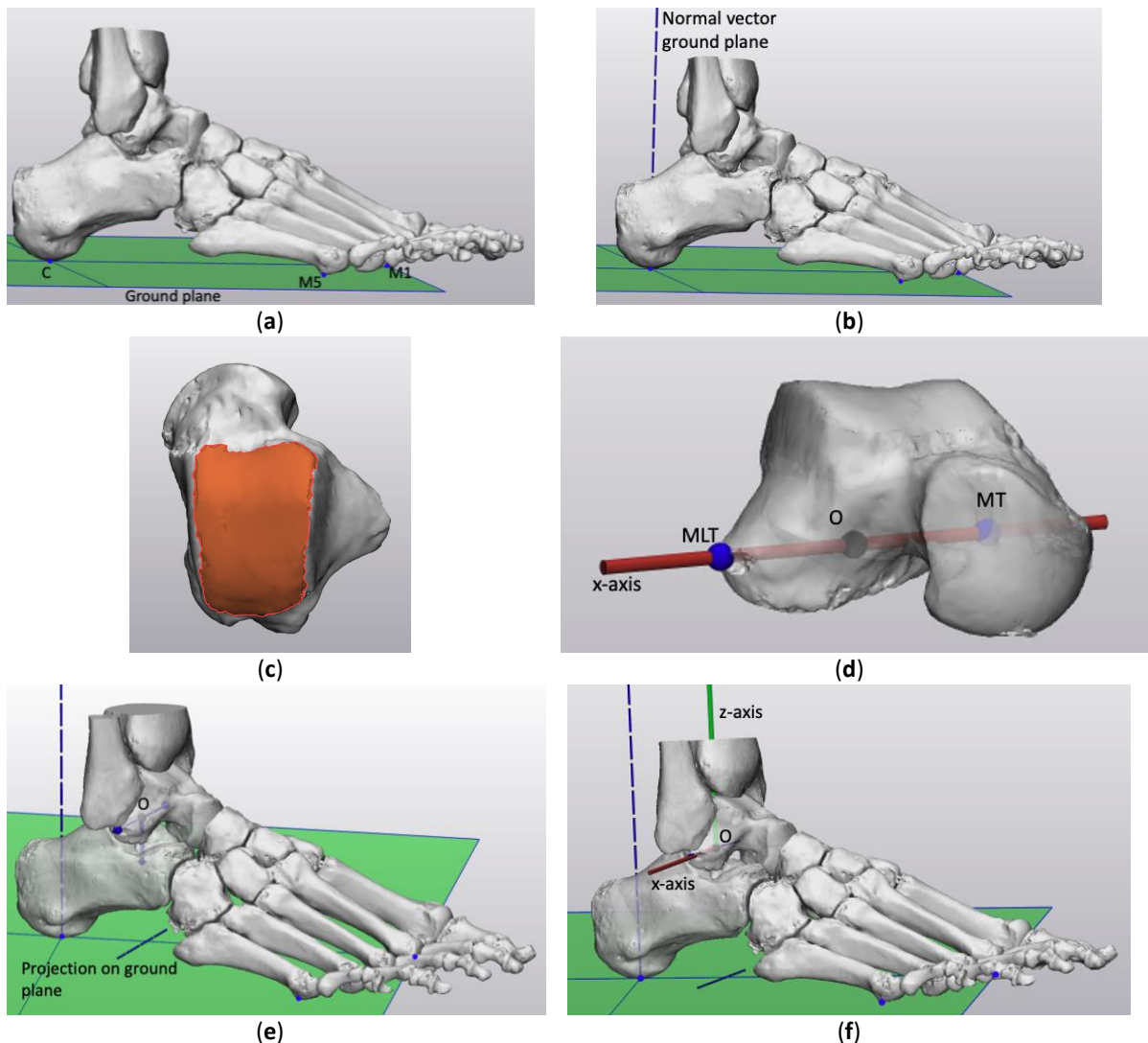


Figure 3. The construction of CS3: (a) Illustration of the foot with the ground plane based on the most caudal point of the first metatarsal-sesamoid complex (M1), fifth metatarsal (M5), and calcaneus (C) in the original CT scan orientation; (b) Illustration of the foot with the normal vector of the ground plane defining the direction of the z-axis; (c) Axial view of the talus with the drawing of the facies superior of the trochlea tali; (d) Illustration of the talus and the Origin, as the midpoint of the point on the medial talus (MT) and the most prominent point on the lateral talus (MLT); (e) Illustration of the foot with the projection of the line connecting MT and MLT on the ground plane, defining the direction of the x-axis; (f) Illustration of the foot with the normal vector and projected line connecting MT and MLT translated towards the Origin to form the z- and x-axis.

To start the construction of CS4, the most caudal point of the first metatarsal-sesamoid complex (M1), fifth metatarsal (M5), and calcaneus (C) were automatically selected in the original CT scan orientation. These three weight-bearing points were used to construct a ground plane (Figure 3a). The normal vector of the ground plane defined the direction of the z-axis (Figure 3b). The x-axis was defined as follows. First the facies superior of the trochlea tali was manually drawn (Figure 3c). Through this surface a cylinder was fitted with its longitudinal axis intersecting a point on the medial talus (MT). The cylinder was translated along its longitudinal axis towards the most prominent point on the lateral talus (MLT). The Origin (O) was defined as the midpoint between MT and MLT (Figure 3d). To ensure an orthogonal coordinate system, the line connecting MT and MLT was projected on the ground plane defining the direction of the x-axis (Figure 3e). The normal vector and the projected line connecting MT and MLT were translated towards the Origin to form the z- and x-axis (Figure 3f). The y-axis was orthogonal to the z- and x-axis (Figure 4).

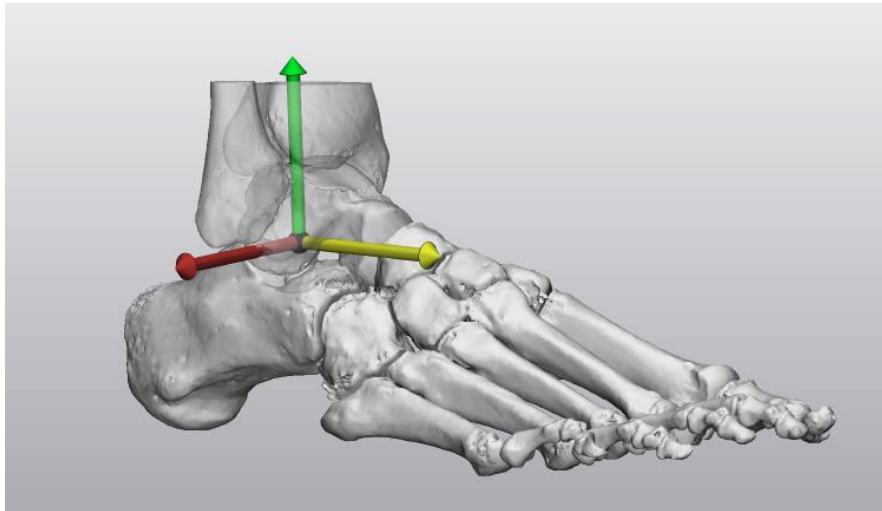


Figure 4. The axes of the global coordinate system of CS4 centered at the origin: x-axis (red), y-axis (yellow), z-axis (green).

Appendix C: CS1 and CS2 of the three 3D foot models without a splint

Figure 1 and 2 depicts the virtual AP and lateral images of CS1 and CS2 compared to the corresponding radiographic images of the three 3D foot models without a splint.

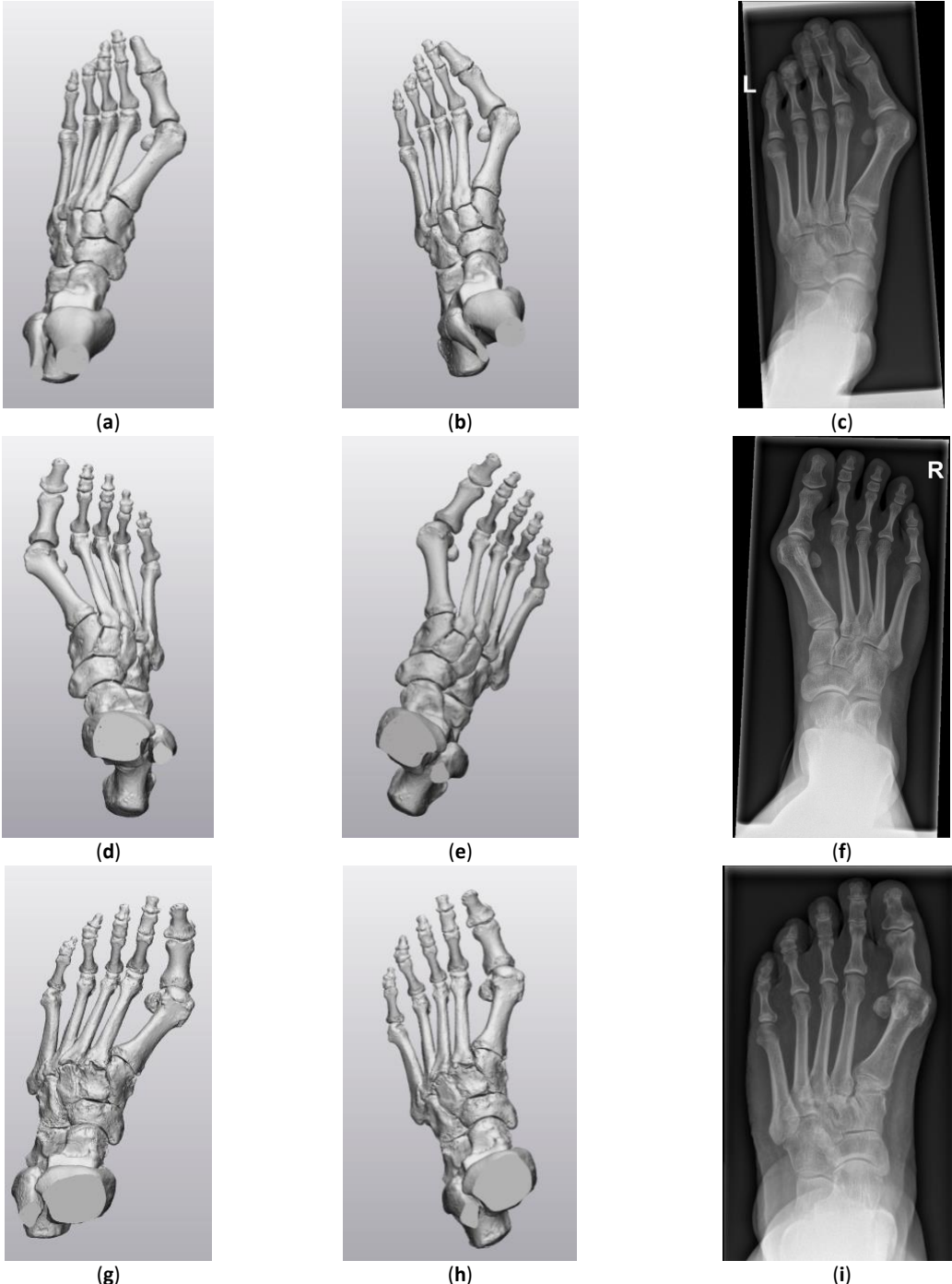


Figure 1. CS1 and CS2 virtual anteroposterior (AP) images of the three 3D foot models without a splint compared to the corresponding conventional AP radiographic image: (a) Foot model one virtual AP image CS1; (b) Foot model one virtual AP image CS2; (c) Corresponding conventional AP radiographic image; (d) Foot model two virtual AP image CS1; (e) Foot model two virtual AP image CS2; (f) Corresponding conventional AP radiographic image; (g) Foot model three virtual AP image CS1; (h) Foot model three virtual AP image CS2; (i) Corresponding conventional AP radiographic image.

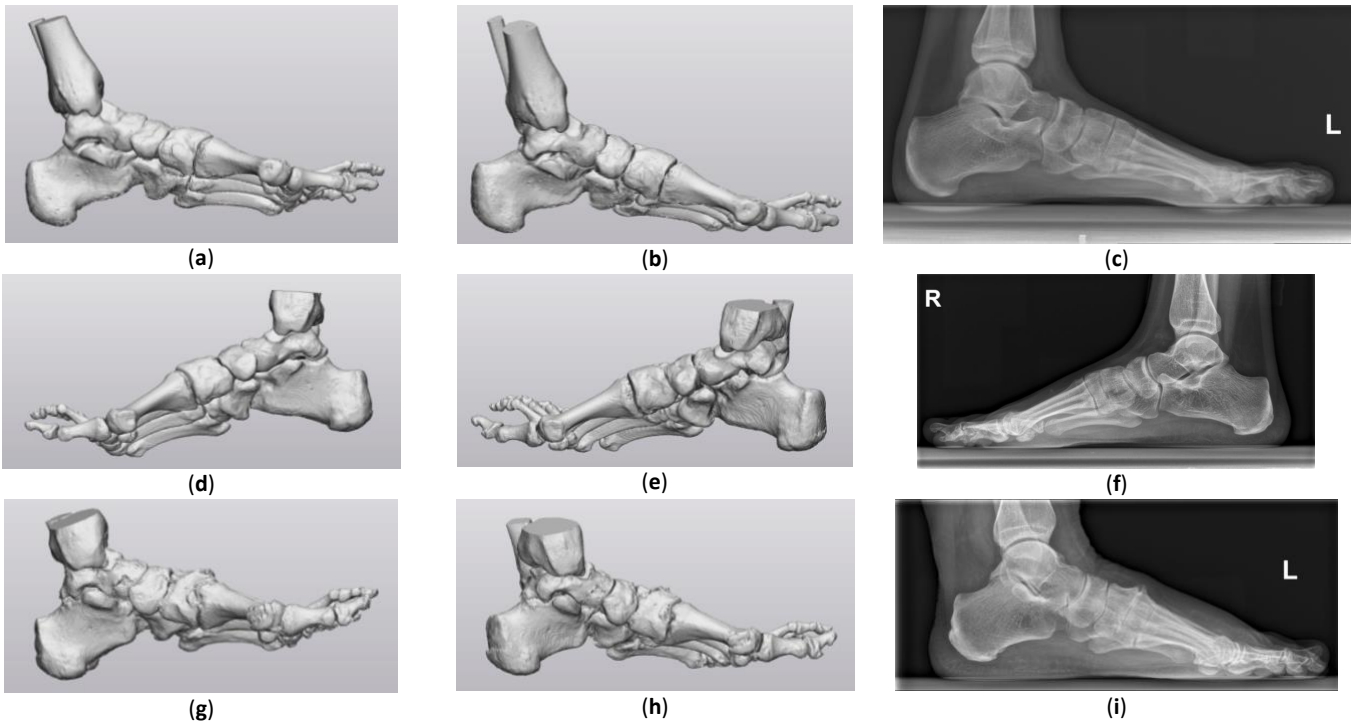


Figure 2. CS1 and CS2 virtual lateral image of the three 3D foot models without a splint compared to the corresponding conventional lateral radiographic image: (a) Foot model one virtual lateral image CS1; (b) Foot model one virtual lateral image CS2; (c) Corresponding conventional lateral radiographic image; (d) Foot model two virtual lateral image CS1; (e) Foot model two virtual lateral image CS2; (f) Corresponding conventional lateral radiographic image; (g) Foot model three virtual lateral image CS1; (h) Foot model three virtual lateral image CS2; (i) Corresponding conventional lateral radiographic image.

